

SyNPL: Synthetic Notch pluripotent cell lines to monitor and manipulate cell interactions *in vitro* and *in vivo*

Mattias Malaguti[‡], Rosa Portero Migueles, Jennifer Annoh, Daina Sadurska*, Guillaume Blin and Sally Lowell[‡]

ABSTRACT

Cell-cell interactions govern differentiation and cell competition in pluripotent cells during early development, but the investigation of such processes is hindered by a lack of efficient analysis tools. Here, we introduce SyNPL: clonal pluripotent stem cell lines that employ optimised Synthetic Notch (SynNotch) technology to report cell-cell interactions between engineered ‘sender’ and ‘receiver’ cells in cultured pluripotent cells and chimaeric mouse embryos. A modular design makes it straightforward to adapt the system for programming differentiation decisions non-cell-autonomously in receiver cells in response to direct contact with sender cells. We demonstrate the utility of this system by enforcing neuronal differentiation at the boundary between two cell populations. In summary, we provide a new adaptation of SynNotch technology that could be used to identify cell interactions and to profile changes in gene or protein expression that result from direct cell-cell contact with defined cell populations in culture and in early embryos, and that can be customised to generate synthetic patterning of cell fate decisions.

KEY WORDS: Cell interaction, SynNotch, Pluripotent stem cells, Cell engineering, Patterning

INTRODUCTION

During embryogenesis, pluripotent cells undergo a series of cell fate decisions that are controlled by interactions between epiblast cells, their early differentiated derivatives and the surrounding extra-embryonic tissues (Arnold and Robertson, 2009; Nowotschin and Hadjantonakis, 2010; Rossant and Tam, 2009). The transcriptional changes that accompany exit from pluripotency and differentiation into specific cell types have been extensively characterised, and the long-range signals that control these changes are now well understood (De Los Angeles et al., 2015; Kinoshita and Smith, 2018; Pera and Tam, 2010; Posfai et al., 2021; Tam and Loebel, 2007). Less is known about how early developmental decisions are influenced by direct interactions of cells with their neighbours. Cell-cell interactions play a key role in development (Dias et al., 2014; Gurdon, 1987; Johnson and Ziomek, 1983; Schultz, 1985), but

until recently there has been a paucity of molecular and technological tools available to study these processes in detail in relevant settings (Nishida-Aoki and Gujral, 2019; Yang et al., 2021).

Quantitative image analysis can be used to identify and infer the effect of neighbours on the properties of cells of interest in fixed samples (Blin et al., 2018; Fischer et al., 2020; Forsyth et al., 2021; Toth et al., 2018). We have recently developed a software suite for automated neighbour identification during live imaging (Blin et al., 2019), which provides researchers with a further dimension to study the effects of cell-cell interactions on cell fate decisions. Although live image analysis provides high-resolution visual information, this approach is labour intensive and only leads to neighbour identification *a posteriori*.

The field of synthetic developmental biology (Davies, 2017; Ebrahimkhani and Ebisuya, 2019; Ho and Morsut, 2021; Santorelli et al., 2019; Schlissel and Li, 2020) seeks to understand the mechanisms of patterning and cell differentiation through the engineering of genetic circuits (Cachat et al., 2016; Matsuda et al., 2015; Sekine et al., 2018). By re-engineering the Notch/Delta signalling cascade (Fig. 1A), Lim and colleagues generated a synthetic circuit capable of reporting and manipulating cell-cell interactions in real time (Morsut et al., 2016). A ‘sender’ cell presenting an extracellular membrane-bound antigen of interest is recognised by a ‘receiver’ cell expressing a chimaeric Synthetic Notch (SynNotch) receptor, which is composed of an extracellular antigen-recognition domain, an intracellular synthetic effector domain and the Notch1 core transmembrane domain containing proteolytic cleavage sites (Fig. 1B-D). The modularity of SynNotch circuitry makes it possible to interrogate and manipulate the effects of interactions between cell types of interest.


SynNotch technology has been used for monitoring cell-cell interactions, generating synthetic patterns, generating synthetic morphogen gradients, inducing contact-mediated gene editing and generating custom antigen receptor T-cells (Cho et al., 2018; Choe et al., 2021; He et al., 2017; Huang et al., 2020; Roybal et al., 2016; Sgodda et al., 2020; Toda et al., 2018, 2020; Wang et al., 2021). SynNotch technology has been established in *Drosophila* (He et al., 2017) as well as in immortalised cell lines and differentiated cell types, but its potential in the study of mammalian developmental events remains largely untapped.

Mouse embryonic stem cells (ESCs) can be differentiated into any cell type *in vitro*, can give rise to chimaeric embryos and can be used to establish transgenic mouse lines (Bradley et al., 1984; Evans and Kaufman, 1981; Martin, 1981). Adapting the SynNotch system for use in mouse ESCs would therefore permit monitoring and manipulation of cell-cell interactions in a developmental context both *in vivo* and *in vitro*. The original system designed by Morsut et al. (2016) used lentiviral transduction of immortalised and primary cell lines, where transgene expression was driven from the retroviral SFFV promoter. Lentiviral transduction can lead to multiple copy transgene integration in mouse ESCs (Pfeifer et al., 2002), and the

Centre for Regenerative Medicine, Institute for Stem Cell Research, School of Biological Sciences, University of Edinburgh, 5 Little France Drive, Edinburgh EH16 4UU, UK.

*Present address: Sir William Dunn School of Pathology, University of Oxford, Oxford, OX1 3RE, UK

[‡]Authors for correspondence (mattias.malaguti@ed.ac.uk; sally.lowell@ed.ac.uk)

 M.M., 0000-0003-4392-7183; J.A., 0000-0002-7163-7899; D.S., 0000-0001-7139-7314; G.B., 0000-0002-9295-237X; S.L., 0000-0002-4018-9480

This is an Open Access article distributed under the terms of the Creative Commons Attribution License (<https://creativecommons.org/licenses/by/4.0>), which permits unrestricted use, distribution and reproduction in any medium provided that the original work is properly attributed.

Handling Editor: James Briscoe

Received 24 September 2021; Accepted 13 May 2022

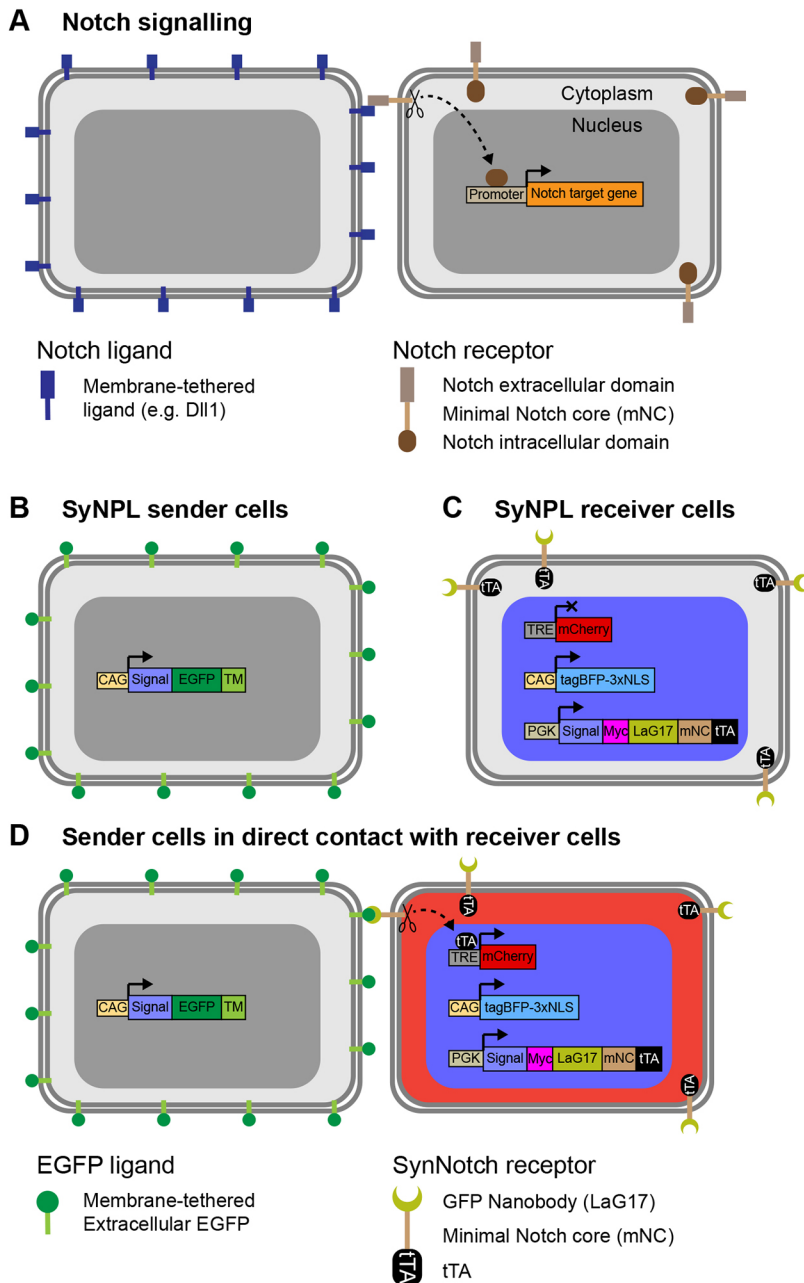


Fig. 1. Diagram of SynNotch cell-cell interaction reporter ES cells. (A) Interaction between a membrane-tethered ligand and the Notch receptor extracellular domain leads to the cleavage of the Notch core transmembrane domain, which contains proteolytic cleavage sites. In turn, this leads to the release of the Notch intracellular domain from the membrane, allowing it to translocate to the nucleus and drive transcription of target genes. (B) SyNPL sender cells express membrane-tethered extracellular EGFP from a ubiquitous promoter. (C) SyNPL receiver cells contain a *TRE-mCherry* transgene, express *tagBFP-3xNLS* from a ubiquitous promoter and express a SynNotch receptor from a ubiquitous promoter. The SynNotch receptor comprises an extracellular LaG17 anti-GFP nanobody, the core transmembrane region of Notch1 and an intracellular tTA. (D) Upon interaction of the EGFP on a sender cell with the SynNotch receptor, the Notch1 core domain is cleaved, releasing the tTA, which can translocate into the nucleus, bind the TRE element and drive *mCherry* transcription.

SFFV promoter is prone to silencing in mouse pluripotent cells and their derivatives (Herbst et al., 2012; Pfaff et al., 2013; Wu et al., 2011), making this system suboptimal for mouse ESCs.

In this study, we made several adaptations to the original SynNotch system (Morsut et al., 2016) to establish clonal modular SynNotch pluripotent cell lines (SyNPL). We characterised the SyNPL system by monitoring interactions between EGFP-expressing sender cells and mCherry-inducible receiver cells *in vitro*, then showed that this system can report interactions between neighbouring cells *in vivo* in chimaeric mouse embryos, that it can be used for synthetic patterning and that its modular design can be exploited to conveniently manipulate cell-cell interactions and drive contact-mediated synthetic cell fate engineering.

RESULTS

Design of SyNPL ESCs

We adapted the SynNotch system, which was previously established through viral transduction of immortalised mouse L929 fibroblasts

and K562 erythroleukaemic cells (Morsut et al., 2016), for use in mouse ESCs. In this system, sender cells are labelled with membrane-tethered extracellular EGFP (Fig. 1B). Receiver cells constitutively express a SynNotch receptor composed of an anti-GFP nanobody (LaG17) (Fridy et al., 2014), the mouse Notch1 minimal transmembrane core (Uniprot: Q01705, residues 1427-1752) and a tetracycline transactivator (tTA) (Gossen and Bujard, 1992), and contain a tetracycline response element (TRE) promoter capable of driving *mCherry* expression in response to tTA binding (Fig. 1C). Interaction of EGFP on sender cells with the anti-GFP nanobody on receiver cells leads to cleavage of the Notch1 core, releasing the tTA, which can translocate to the nucleus, bind to the TRE promoter and drive *mCherry* expression (Fig. 1D). In addition, we constitutively labelled receiver cells with a tagBFP-3xNLS construct (Fig. 1C,D) to conveniently identify them by fluorescence microscopy and flow cytometry, even in the absence of a contact-dependent mCherry signal.

Our aims when adapting the SynNotch system were to generate ESC lines with low cell-cell variability, robust and sustained transgene expression, and a modular design to allow convenient transgene exchange. In order to avoid cell-cell variability, we generated clonal cell ESC lines with stable genomic integration of the SynNotch system components, delivering transgenes by electroporation rather than lentiviral transduction (Boggs et al., 1986; Charrier et al., 2011; Pfeifer et al., 2002; Smithies et al., 1985). We sought to ensure uniform levels of transgene expression by screening clonal lines and/or targeting transgenes to specific genomic locations, and by replacing the silencing-prone SFFV retroviral promoter used by Morsut et al. (2016) with CAG (Niwa et al., 1991) or mouse *Pgk1* (McBurney et al., 1991) promoters, which have been extensively characterised in mouse ESCs (Chen et al., 2011; Hong et al., 2007). Finally, we introduced modularity to our system by generating a ‘landing platform’ master cell line to allow recombination-mediated cassette exchange (RMCE) of transgenes of interest.

Generation of extracellular membrane-tethered EGFP-expressing sender ESCs

We first generated clonal sender cell lines expressing membrane-tethered extracellular EGFP. The CAG and mouse *Pgk1* promoters are both silencing-resistant promoters commonly used to drive ubiquitous transgene expression in ESCs (Herbst et al., 2012; Liew et al., 2007). We asked which of these promoters can generate

sender cells with strong and uniform expression of membrane EGFP. We also explored whether EGFP molecules with HA and Myc protein tags can retain ‘sender’ function in pluripotent cells.

We electroporated mouse ESCs with four alternative sender constructs, containing either CAG or mouse *Pgk1* promoters driving expression of either untagged or HA- and Myc-tagged EGFP fused to a membrane-tethering domain (Fig. 2A-D). We isolated and expanded 64 clonal lines derived from stable genomic integration of the four constructs, and screened them by flow cytometry, analysing median EGFP intensity (Fig. 2E,F), percentage of EGFP-positive cells (Fig. 2G,H) and EGFP distribution (Figs S1, S2). Both CAG and *Pgk1* promoters drive high uniform expression of EGFP, and, as expected, there is considerable variability in EGFP expression between clonal lines.

We selected one untagged EGFP sender clone (CmGP1) and one HA- and Myc-tagged EGFP sender clone (CHmGMP19), exhibiting high, uniform and similar levels of EGFP expression (Fig. 2I) for further analysis. For both clones, the pattern of EGFP expression was consistent with membrane localisation, and, in the case of the HA- and Myc-tagged CHmGMP19 clone, the pattern of HA and Myc expression coincided with that of EGFP (Fig. 2J).

Generation of a safe harbour site landing pad master ESC line

To facilitate convenient and repeated modification of the genome, we generated a clonal ESC line carrying a ‘landing pad’ targeted to the *Rosa26* locus, a safe harbour site in the mouse genome

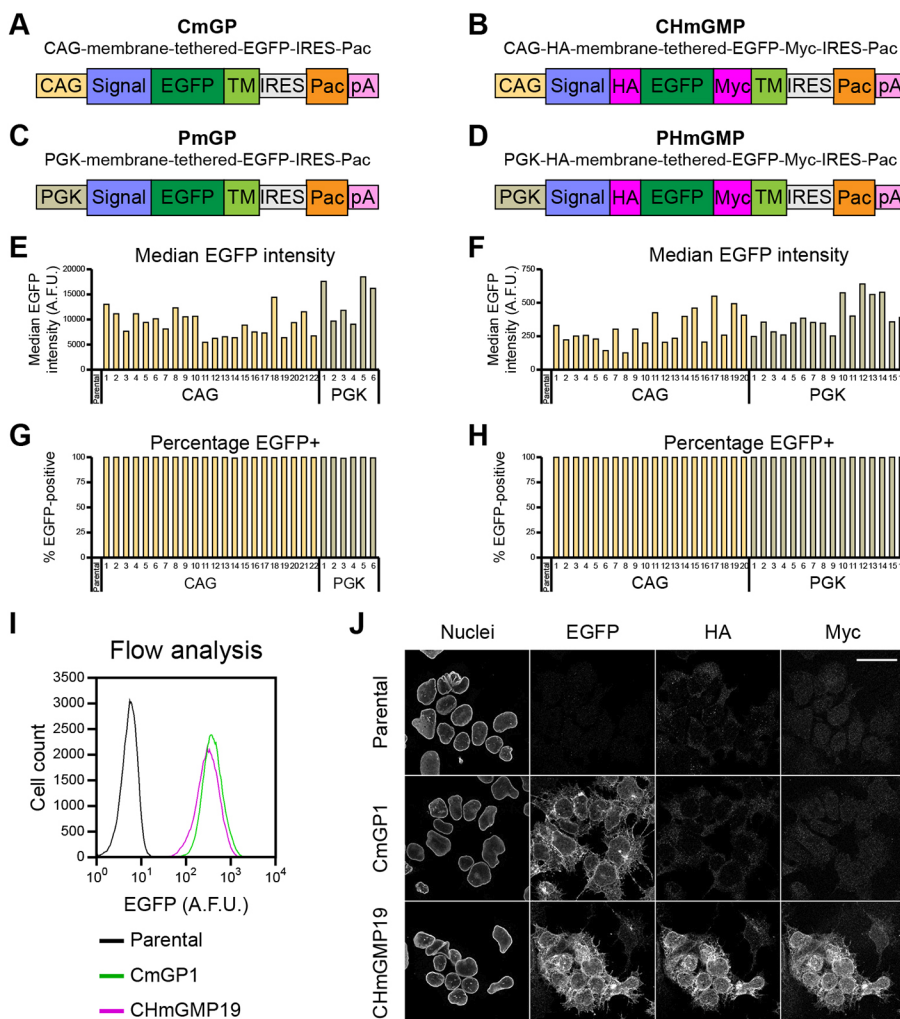


Fig. 2. Screening of clonal sender ESC lines.

(A-D) Diagram of the constructs used to generate EGFP sender cell lines. (E) Median EGFP intensity and (G) percentage of EGFP-positive cells in untagged EGFP sender cells. Parental wild-type cells are included as a negative control. Five-thousand cells were analysed for each clone. (F) Median EGFP intensity and (H) percentage of EGFP-positive cells in HA- and Myc-tagged EGFP sender cells. Parental wild-type cells are included as a negative control. Fifteen-thousand cells were analysed for each clone. Analyses were performed separately from those in E, median intensities are not directly comparable. $n=1$ in E-H. (I) Comparison of EGFP distributions in parental wild-type cells, CmGP clone 1 (CmGP1) and CHmGMP clone 19 (CHmGMP19) sender cells. Eighty-five thousand cells were analysed for each sample. Data are from a single experiment, representative of nine biological replicates. (J) Immunofluorescence of parental wild-type, CmGP1 and CHmGMP19 sender cells. Scale bar: 30 μ m. Nuclei are indicated by lamin B1 staining. A.F.U.: arbitrary fluorescence units.

(Friedrich and Soriano, 1991). This landing pad contains a splice acceptor, the *Neo* (G418/geneticin resistance) gene and a CAG promoter driving expression of *mKate2-3xNLS*, which encodes a red fluorescent protein with no evident phenotypic effect in mouse embryos (Malaguti et al., 2013; Shcherbo et al., 2009). This entire cassette is flanked by two *attP50* sites, which allows for ϕ C31 integrase-mediated recombination with cassettes flanked by two *attB53* sites (Huang et al., 2009; Tosti et al., 2018) (Fig. S3A). After confirming insertion at the correct genomic locus (Fig. S3B), we verified that all cells express high and uniform levels of *mKate2-3xNLS* (Fig. S3C,D). We named this cell line EM35.

An 'all-in-one' design fails to generate fully functional mCherry inducible receiver cells

We first asked whether it is possible to target all transcriptional units required for receiver cell activity to the *Rosa26* landing pad in EM35 ESCs, and whether this would lead to the generation of functional receiver ESCs. Design and characterisation of the resulting cell lines is explained in detail in the supplementary Materials and Methods and Figs S4-S9. Briefly, mCherry could, as expected, be induced by subpopulations of tagBFP-positive receiver cells in response to interaction with EGFP-positive sender cells, but this receiver cell design was hampered by variable levels of tagBFP, variable inducibility of mCherry and low levels of the SynNotch receptor. We conclude that the SynNotch receptor construct and *TRE-mCherry* cassette can function as expected in ESCs, but further modifications to the design are required to obtain a reliable contact-reporting system.

A multi-step design produces fully functional mCherry-inducible receiver ESCs

We hypothesised that two independent events may be affecting mCherry inducibility in 'all-in-one-locus' receiver cells (Figs S4-S9). First, *mCherry* and *tagBFP* transgenes may have been lost due to mitotic recombination (Stern, 1936) or errors in replication at similar DNA sequences in close proximity (*Pgk1* promoters and *bGHPA* signals). Second, the SynNotch receptor may not be expressed at high enough levels (Fig. S9).

We circumvented potential loss of DNA by physically separating the three transcriptional units through random genomic integration of the SynNotch receptor and *tagBFP-3xNLS* cassettes, and by removing identical DNA sequences. To increase levels of SynNotch receptor and obtain uniform levels of tagBFP-3xNLS, we added an internal ribosome entry site (IRES) followed by *Ble* (zeocin resistance gene) downstream of the SynNotch receptor sequence, and an IRES followed by *Hph* (hygromycin B resistance gene) downstream of the *tagBFP-3xNLS* sequence (Fig. 3A).

We first randomly integrated the SynNotch receptor construct into the genome of EM35 landing pad ESCs (Fig. S10A). We selected two clones (35SRZ9 and 35SRZ86) with high, uniform Myc expression (Fig. S10B). The levels of Myc in these clones were higher than those in receiver cells generated with an all-in-one design (clones SNCB+4 and SNCB-6) and higher than those in Myc-tagged sender cells (CHmGMP19) (Fig. S10C). We then randomly integrated the *tagBFP-3xNLS* transgene into the genome of these two clones (Fig. S10D). We selected one clone for each parental line with high uniform expression of tagBFP-3xNLS (PSNB-A clone 10, PSNB-B clone 3) (Fig. S10E,F). We renamed these lines PSNB (parental SynNotch tagBFP) clones A and B, respectively.

Next, we performed RMCE at the *Rosa26* landing pad in PSNB cells to replace the *mKate2* transgene with one of three

constructs: the *TRE-mCherry* cassette present in the SCNB construct, a *tetO-mCherry* cassette with more tTA-binding sequences elements in the inducible promoter (to test whether this led to improved mCherry induction) or an empty vector cassette to generate tagBFP-positive mKate2- and mCherry-negative control cell lines (Fig. S11A). We verified that integration of the empty vector cassette led to loss of mKate2 expression, and used these control cell lines to confirm that tagBFP signal was able to unambiguously identify receiver cells (Fig. 3B,C, Fig. S11B).

We then asked whether the new receiver cell lines containing inducible mCherry cassettes expressed mCherry in response to co-culture with sender cells. We screened 27 clones for tagBFP and mCherry expression by culturing them in the presence or absence of sender cells for 24 h (Fig. S11C-G). We observed that all genetically identical clones behaved very similarly, suggesting we were not experiencing silencing or loss of DNA. Clones containing the larger *tetO-mCherry* cassette exhibited high levels of mCherry leakiness in the absence of sender cells. Co-culture with sender cells led to mCherry induction, but the distributions in the presence and absence of sender cells overlapped significantly (Fig. S11D,F,G). Clones containing the smaller *TRE-mCherry* cassette exhibited mCherry leakiness in the absence of sender cells; however, co-culture with sender cells led to an increase in mCherry expression to levels that displayed minimal overlap with those seen in cells cultured in the absence of sender cells (Fig. S11C,E,G). Leakiness in the absence of sender cells could be reduced, but not abolished, by treatment of cells with the γ -secretase inhibitor DAPT (which inhibits cleavage of the SynNotch receptor) or with doxycycline (which inhibits tTA-driven transcription) (Fig. S12A,B).

We selected three clones with minimal leakiness and high inducibility for downstream analysis (PSNBA-TRE1, PSNBB-TRE10 and PSNBB-TRE9). We renamed these cells STC (for SynNotch-TRE-mCherry) clones A1, B1 and B2, respectively. These receiver lines induced mCherry after co-culturing sender and receiver cells together for 24 h. mCherry was specifically induced in tagBFP-positive receiver cells that were in contact with EGFP-positive sender cells (Fig. 3D). We confirmed that mCherry is robustly induced in the majority of tagBFP-positive receiver cells following co-culture with a ninefold excess of CmGP1 sender cells at confluence (Fig. 3B,C,E,F).

These observations demonstrate that physical separation of the three transcriptional units in the genome of receiver cells, coupled to the use of internal ribosome entry sites and selectable markers within the units, can lead to the generation of receiver ESC lines that exhibit clear and specific induction of mCherry upon interaction with EGFP-expressing sender cells.

Extracellular membrane-tethered EGFP is required for contact-mediated transgene induction in receiver cells

It would be useful to make use of existing GFP fluorescent reporter ESCs (e.g. cell-state reporters or signalling reporters) to act as sender cells, in order to test how particular cell states may influence direct neighbours. However, many such cell lines make use of non-membrane-tethered GFP, which seems unlikely to interact with the anti-GFP nanobody on STC receiver cells. We therefore wished to test whether membrane tethering of EGFP to the extracellular space was absolutely necessary for effective neighbour labelling.

We cultured STC receiver cells alone (Fig. 3E), in the presence of CmGP1 sender cells (Fig. 3F), in the presence of a control cell line expressing untagged intracellular EGFP (E14GIP1) (Fig. 3G) or in the presence of CmGP1 sender cells containing an extra untagged intracellular EGFP transgene (CmGP1GH1) (Fig. 3H). E14GIP1

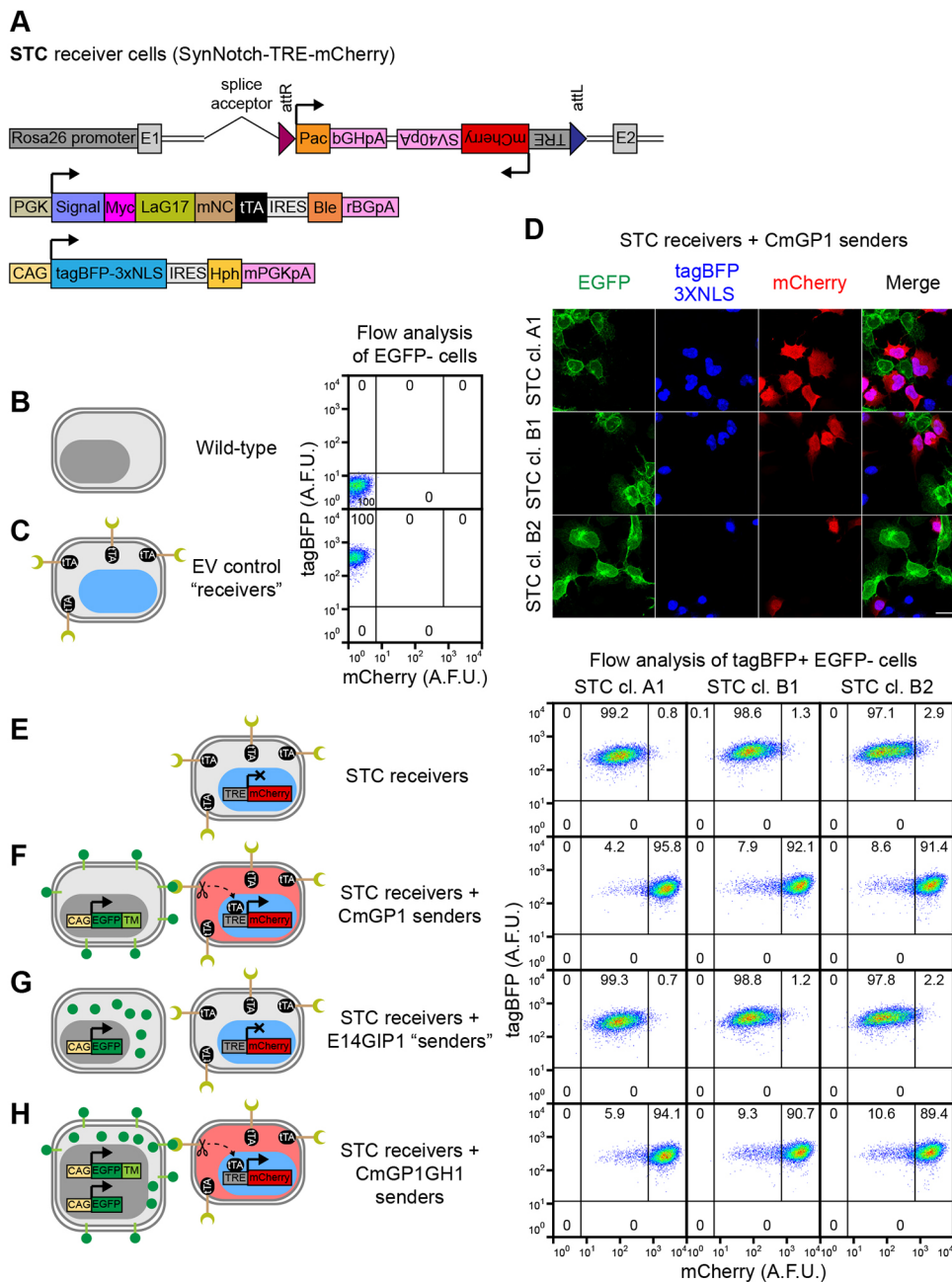


Fig. 3. Generation of clonal cell-cell interaction reporter STC receiver cells. (A) Summary of transgenes stably integrated into the genome of STC clonal ESC lines. (B,C) Flow cytometry analysis of mCherry and tagBFP-3xNLS expression in (B) wild-type and (C) control PSNBB-E cells containing all SynNPL receiver constructs, except for the TRE-mCherry cassette. These control cell lines were used to set gates for tagBFP and mCherry positivity. (D) Immunofluorescence of STC clones A1, B1 and B2 co-cultured with CmGP1 sender cells for 24 h (1:3 sender: receiver cell ratio). Scale bar: 30 μ m. (E-H) Flow cytometry analysis of mCherry and tagBFP-3xNLS expression in STC receiver cells cultured alone or in the presence of indicated EGFP-expressing cell lines (9:1 sender:receiver cell ratio). The mCherry-HI gate displayed in figure was set based on mCherry distribution in STC receiver cells cultured alone. Data in these panels were acquired simultaneously to data in B and C, and can be directly compared. In B,C,E-H, percentages of cells in each gate are indicated. Eleven-thousand cells were analysed for each sample. Data from a single experiment, representative of four biological replicates. Diagrams depicting the transgenes present in each cell type and expected mCherry and tagBFP-3xNLS expression patterns are displayed next to flow cytometry plots.

cells, which do not express membrane-tethered EGFP, did not induce mCherry above baseline levels in co-cultured STC receiver cells (Fig. 3E-G). mCherry is induced to similar levels following co-culture with either CmGP1 or CmGP1GH1 sender cells (Fig. 3F,H), suggesting that the additional untagged EGFP transgene in CmGP1GH1 cells does not interfere with mCherry induction. We conclude that cells containing intracellular GFP cannot function as sender cells unless supplemented with extracellular membrane-tethered EGFP.

tagBFP-3xNLS lineage label allows identification of EGFP cross-labelled receiver cells

In other cell types, a membrane-tethered anti-GFP nanobody can bind and internalise membrane-tethered GFP on neighbouring cells (Tang et al., 2020). This is also the case in ES cells (Fig. S12B): punctuate EGFP signal is visible in mCherry-expressing activated

receiver cells (Fig. S12C). It could therefore be difficult to unambiguously separate STC receiver cells from CmGP1 sender cells by flow cytometry based on EGFP expression alone (Fig. S12D). This problem is overcome by using the tagBFP-3xNLS lineage label in STC receiver cells (Fig. S12E). Furthermore, separation of sender and receiver cells based on EGFP alone can be achieved by using CmGP1GH1 sender cells, which contain a second EGFP transgene, leading to increased separation between sender cells and cross-labelled receiver cells (Fig. S12F,G).

Increasing sender:receiver cell ratios leads to increased transgene induction in receiver cells

We next asked how differing sender:receiver cell ratios affect the efficiency of neighbour labelling. We co-cultured STC receiver cells with different proportions of sender cells for 24 h (Fig. S13). We

observed that as few as 20% of sender cells were sufficient to induce mCherry in approximately half of the STC receiver cells, and that 90% sender cells could induce mCherry in over 90% of STC receiver cells (Fig. S13A,B). mCherry fluorescence follows a bimodal distribution in receiver cells exposed to ‘non-saturating’ numbers of sender cells, and a unimodal distribution in receiver cells exposed to ‘saturating’ numbers of sender cells (Fig. S13C-H). This suggests that STC receiver cells that have come into contact with sender cells can uniformly induce high levels of mCherry expression when co-culturing cells at a 9:1 sender:receiver cell ratio (Fig. S13I-K).

Kinetics of contact-dependent transgene induction in receiver cells

We next performed time-lapse microscopy. In order to capture a range of behaviours, we co-cultured CmGP1GH1 sender cells with STC receiver cells at a 1:1 sender:receiver ratio at moderate density, and filmed cells for 24 h (Fig. 4A, Movie 1). mCherry first became visible 5–6 h after initial sender-receiver contact (Fig. 4A, yellow arrowheads). We observed STC receiver cells that did not make contact with sender cells and remained mCherry negative (Fig. 4A, magenta arrowheads), and an STC receiver cell that made contact with a sender cell 2 h before the cells were fixed at the 24 h timepoint for immunofluorescence, and that remained mCherry negative (Fig. 4A, cyan arrowheads).

We then quantified the kinetics of mCherry induction. We co-cultured 10% STC receiver cells with 90% sender cells at high density in order to ensure interaction of almost every receiver cell with at least one sender cell (Fig. 4B, Movie 2). We analysed mCherry expression in receiver cells by flow cytometry over the course of 72 h (Fig. 4C-E, Fig. S14A,B), and by live imaging and tracking of individual cells over the course of 24 h (Fig. 4B,F,G, Fig. S14C-H). mCherry is first induced at low levels at around 5 h (Fig. 4D-G, Fig. S14A-H) and increases until around 48 h (Fig. 4D-G, Fig. S14A-B).

Minimum time of contact required for transgene induction

Relying on direct detection of mCherry (Fig. 4C-G) is likely to overestimate the minimum duration of cell contact required for mCherry induction because mCherry protein maturation will introduce a time-lag between initiation of mCherry transcription and the detection of mCherry fluorescence. Indeed, time-lapse analysis (Fig. 5A, Movie 3) provides an example of an STC receiver cell that remained in contact with a sender cell for 8 h, lost contact for 12 h after a cell division, but continued to increase mCherry expression after losing contact (Fig. 5A, white arrowheads).

We designed an experimental strategy to overcome this problem. We co-cultured 10% STC receiver cells with 90% CmGP1 sender cells for various time points between 0 and 24 h, then added doxycycline to the culture medium for a further 16 h (Fig. 5B). Doxycycline prevents tTA from binding to *TRE* sequences (Gossen and Bujard, 1992); hence, we expect doxycycline administration to halt *mCherry* transcription in receiver cells while still allowing time for mCherry protein to mature. This means that any mCherry signal observed after doxycycline administration should be ascribable to cell contact-dependent transcription that took place during the initial period of co-culture in doxycycline-free medium. In this experimental setting, we observed low but detectable induction of mCherry when cells had experienced only 2 h of doxycycline-free co-culture (Fig. 5C,D, Fig. S15).

These data collectively suggest that 2 h of sender-receiver contact may be sufficient for induction of low levels of mCherry, and that

mCherry levels will keep increasing in receiver cells for a period of time after the loss of sender-receiver contact. This neighbour-labelling system can therefore identify receiver cells that have had relatively brief interactions with sender cells or that have recently lost contact with sender cells.

Kinetics of contact-dependent mCherry perdurance in receiver cells

We next established how long mCherry signal persists following loss of tTA-mediated *mCherry* transcription. We co-cultured 10% STC receiver cells with 90% CmGP1GH1 cells for 24 h, then added doxycycline to the culture medium (to block the activity of tTA and halt *mCherry* transcription) and filmed the cells over 48 h (Fig. S16A,B, Movies 4,5). mCherry fluorescence barely changed for the initial 8–12 h, then gradually decreased until extinguishment around 38–40 h after doxycycline addition (Fig. S16A,B). To quantify this process, we co-cultured 10% STC receiver cells with 90% CmGP1 sender cells for 24 h, then added doxycycline to the culture medium and analysed mCherry fluorescence by flow cytometry at various timepoints (Fig. S16C). No reduction of mCherry signal was observed for the initial 8 h after doxycycline administration, then median mCherry expression decreased by approximately half at 16 h, and returned to background levels within 48 h (Fig. S16D-F). Quantification of live-imaging data at hourly timepoints broadly confirmed these observations, with mCherry levels halving after ~20–24 h and mCherry signal returning to background levels around 48 h (Fig. S16G). Taken together, these results suggest that induction of mCherry occurs more rapidly than loss of mCherry signal, presumably due to the high stability of this fluorescent protein, confirming the utility of this system for identifying both recent and current cell-cell interactions.

The SynNPL SynNotch cell-cell interaction reporter is functional in early mouse embryos

We asked whether the SynNPL system could function *in vivo* in early mouse embryos. We aggregated wild-type morulae with CmGP1GH1 sender cells and/or STC receiver cells, and cultured these to the blastocyst stage (Fig. 6). As expected, all chimaeric blastocysts (80/80) containing both sender and STC receiver cells induced expression of mCherry, whereas no wild-type blastocysts nor blastocysts containing only sender cells displayed mCherry expression (Fig. 6A,B). Eighteen out of 19 chimaeras containing STC receiver cells alone did not express readily detectable levels of mCherry (Fig. 6B), in line with the low proportion of mCherry-high cells observed *in vitro* in STC receiver cells cultured alone. Treatment of chimaeric embryos with the γ -secretase inhibitor DAPT suppressed mCherry induction, and withdrawal of DAPT allowed mCherry upregulation (Fig. S17), confirming that SynNotch receptor cleavage is required for mCherry induction.

All three STC clonal lines reliably induced mCherry within chimaeric embryos that also contained CmGP1GH1 sender cells (Fig. 5B, Fig. S18A), with mCherry generally appearing within 20 h of aggregation (Movie 6). As expected, some receiver cells remain unlabelled when given limited access to sender cells within chimeric blastocysts (aggregations performed with eight receiver cells and only one sender cell: Fig. S18B), in keeping with the contact-dependent nature of SynNotch activation. Post-implantation chimaeras containing both sender and receiver cells displayed mCherry induction throughout the body axis (Fig. S18C), in keeping with the observation that SynNotch labelling remained efficient after undirected differentiation in culture (5 days of LIF withdrawal), where we did, however, observe some clone-

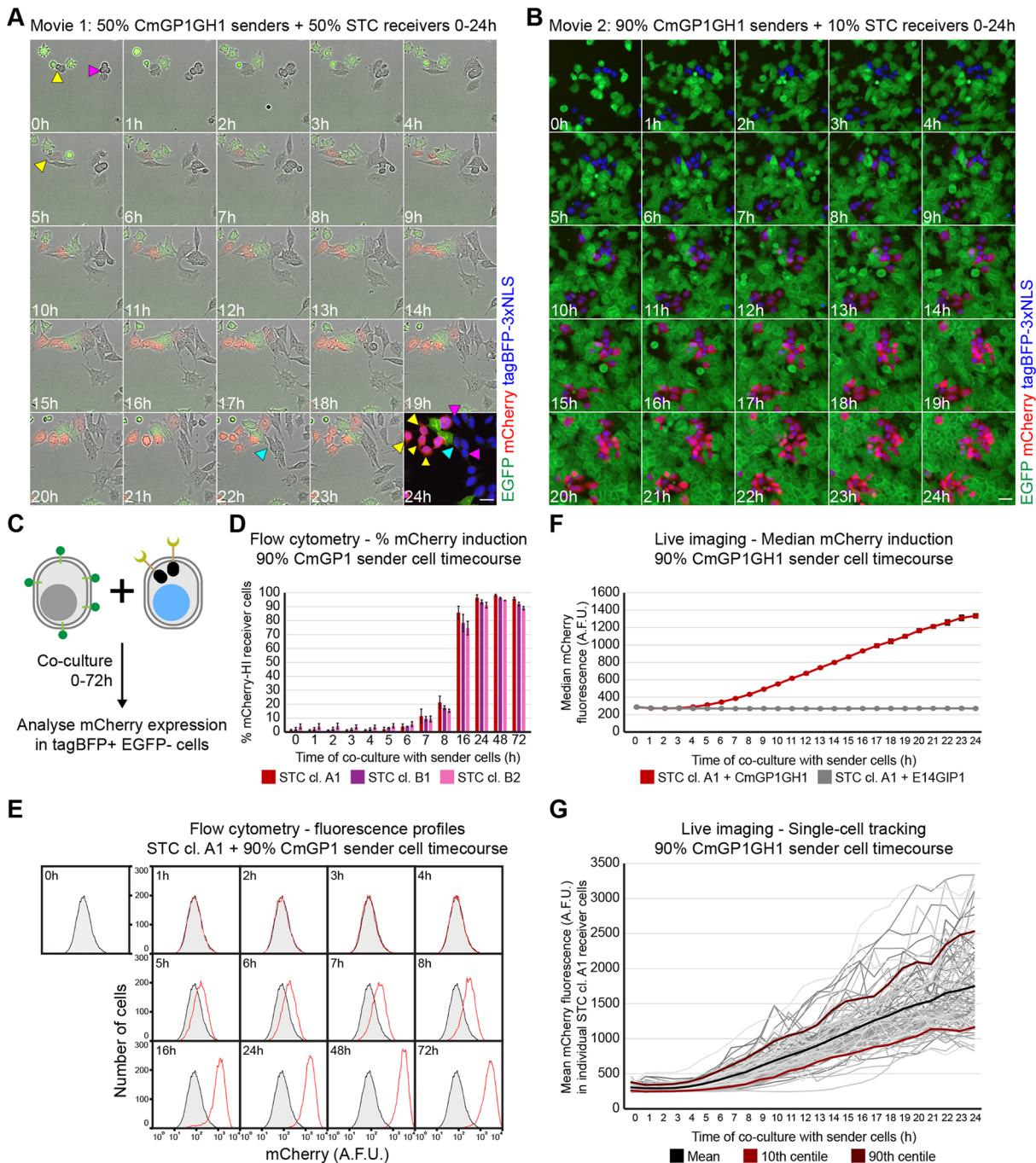


Fig. 4. Kinetics of mCherry induction in STC receiver cells. (A) Stills from Movie 1 displaying mCherry and EGFP expression in STC clone A1 receiver cells co-cultured with CmGP1GH1 sender cells (1:1 sender:receiver cell ratio). Immuofluorescence of cells after 24 h of filming is displayed as a 24 h timepoint, and includes tagBFP-3xNLS signal in place of a bright-field image. Scale bar: 30 μ m. Yellow arrowheads indicate initial STC receiver cell contact with sender cells, onset of mCherry expression, cell descendants at 24 h. Magenta arrowheads indicate STC receiver cell not making contact with sender cells, cell descendants at 24 h. Cyan arrowhead indicates initial STC receiver cell contact with sender cell, cell descendant at 24 h. (B) Stills from Movie 2 displaying tagBFP-3xNLS, mCherry and EGFP expression in STC clone A1 receiver cells co-cultured with CmGP1GH1 sender cells (9:1 sender:receiver cell ratio). Scale bar: 30 μ m. (C) Experimental setup to analyse the kinetics of mCherry upregulation in STC receiver cells by flow cytometry. (D) Percentage of mCherry-HI STC receiver cells following co-culture with CmGP1 sender cells for the indicated amount of time (9:1 sender:receiver cell ratio). Data are mean \pm s.d. of three independent experiments. A minimum of 8000 cells were analysed for each sample. The mCherry-HI gate was set based on mCherry distribution in STC receiver cells cultured alone. (E) Distribution of mCherry fluorescence in STC clone A1 receiver cells following co-culture with CmGP1 sender cells for the indicated amount of time (9:1 sender:receiver cell ratio). Data from a single experiment, representative of three biological replicates. STC clone A1 cells cultured alone (0 h) are displayed as a shaded black histogram in all panels. Ten-thousand cells were analysed for each sample. (F) Quantification of live imaging: median mCherry fluorescence intensity in STC clone A1 receiver cells following co-culture with CmGP1GH1 or E14GIP1 cells for the indicated amount of time (9:1 sender:receiver cell ratio). Average of three biological replicates, 10 random fields of view/replicate, minimum of 320 cells/replicate/timepoint. Data are mean \pm s.d. (G) Mean mCherry fluorescence intensity in individual STC clone A1 receiver cells tracked for 24 h while in co-culture with CmGP1GH1 sender cells (9:1 sender:receiver ratio). Tracks are displayed for 33 randomly selected cells for each of three biological replicates (99 cells total). Mean, 10th and 90th centile tracks are also displayed. A.F.U., arbitrary fluorescence units.

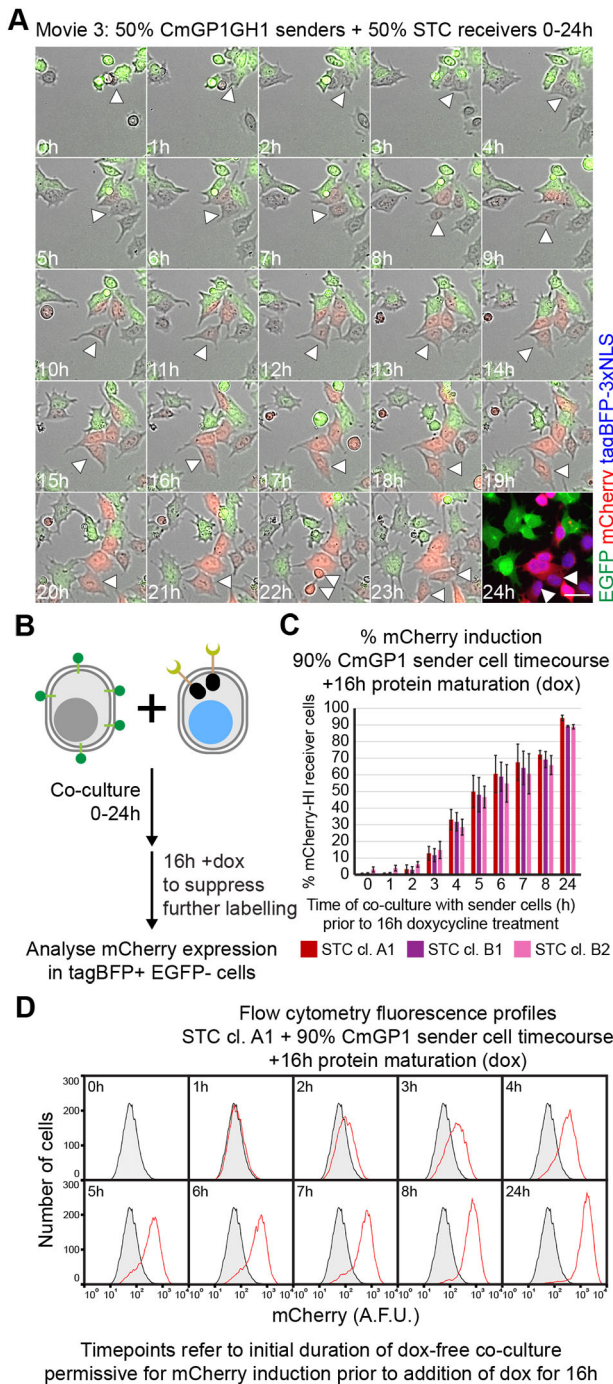


Fig. 5. Characterisation of minimal contact time required for mCherry induction in STC receiver cells. (A) Stills from Movie 3 displaying mCherry and EGFP expression in STC clone A1 receiver cells co-cultured with CmGP1GH1 sender cells (1:1 sender:receiver cell ratio). Immuofluorescence of cells after 24 h of filming is displayed as a 24 h timepoint, and includes tagBFP-3xNLS signal in place of a brightfield image. Scale bar: 30 μ m. White arrowheads label an STC receiver cell in contact with sender cells for 7 h, which then loses contact with sender cells between the 8 and 20 h timepoints while its levels of mCherry keep increasing. (B) Experimental setup to analyse kinetics of mCherry upregulation in STC receiver cells by flow cytometry, allowing time for protein maturation. Following sender:receiver cell co-culture for 0-24 h, 1 μ g/ml doxycycline (dox) was added to the culture medium for a further 16 h in order to inhibit tTA-mediated *mCherry* transcription, and allow translation and folding of previously transcribed *mCherry*. (C) Percentage of mCherry-HI STC receiver cells after co-culture with CmGP1 sender cells for the indicated amount of time and following a further 16 h of doxycycline treatment (9:1 sender:receiver cell ratio). Data are mean \pm s.d. of three independent experiments. A minimum of 8000 cells were analysed for each sample. The mCherry-HI gate was set based on mCherry distribution in STC receiver cells cultured alone in doxycycline for 16 h. (D) Distribution of mCherry fluorescence in STC clone A1 receiver cells following co-culture with CmGP1 sender cells for the indicated amount of time and 16 h doxycycline treatment (9:1 sender:receiver cell ratio). Data from a single experiment, representative of three biological replicates. STC clone A1 cells plated with CmGP1 sender cells in doxycycline-containing medium for 16 h ('0 h') are displayed as a shaded black histogram in all panels. Ten-thousand cells were analysed for each sample.

through the use of anchor proteins to capture diffusible receiver cell-activating signal (Toda et al., 2020).

We asked whether we could generate a synthetic stripe of transgene expression at the region of contact between sender and receiver cells. We plated CmGP1 sender and STC receiver cells in separate chambers of a removable multi-chamber cell culture insert and allowed them to reach confluence. We then removed the insert, allowing cells to grow in the space between chambers and make contact (Fig. 7A; a detailed description of stripe generation and characterisation can be found in the supplementary Materials and Methods, the Materials and Methods, and in Fig. S19). A distinct stripe of mCherry expression appeared at the sender:receiver border (Fig. 7B) 24 h after initial sender:receiver contact. This demonstrates that SynNotch technology can be successfully employed in mouse ESCs to generate synthetic patterns of gene expression.

Harnessing modularity of SynNPL SynNotch ESCs to synthetically alter cell fate

The modularity of our SynNPL SynNotch system design makes it straightforward to generate clonal receiver cell lines with inducible expression of any gene of interest. The transcription factor Neurog1 (neurogenin 1) drives neuronal differentiation of progenitor cells during mouse development (Cau et al., 2002; Ma et al., 1998; Yuan and Hassan, 2014). Ectopic expression of Neurog1 is sufficient to drive neuronal differentiation (Cai et al., 2000; Ma et al., 1996) even in mesodermal tissues (Perez et al., 1999) and in mouse ESCs cultured in pluripotent culture conditions (Velkey and O'Shea, 2013). We asked whether a TRE-inducible Neurog1 transgene in receiver cells would drive neuronal differentiation as a specific response to contact with sender cells.

We generated STN (SynNotch TRE-Neurog1) receiver cells by performing RMCE at the *Rosa26* landing pad in PSNB cell lines to replace the *mKate2-3xNLS* transgene with a *TRE-3xFlag-Neurog1* cassette (Fig. 7C, Fig. S20A). We co-cultured STN receiver cells with CmGP1 senders cells for 48 h, the timepoint at which we observed maximum mCherry induction in STC receiver cells (Fig. 4C,D, Fig. S14A,B). We confirmed this resulted in robust

dependent variability in the absence of antibiotic selection (Fig. S18D-F). These results suggest that the SynNPL neighbour-labelling system is functional, efficient and reliable *in vivo*.

Spatial confinement of sender and receiver cells leads to synthetic patterning

SynNotch technology has been successfully employed to generate synthetic patterns. Strategies to achieve this include co-culturing cells in a low sender:receiver cell ratio in order to create two-dimensional activated receiver cell rings surrounding a clone of sender cells (Morsut et al., 2016), creating self-organising cell aggregates through contact-mediated induction of adhesion molecules (Toda et al., 2018) and recreating morphogen gradients

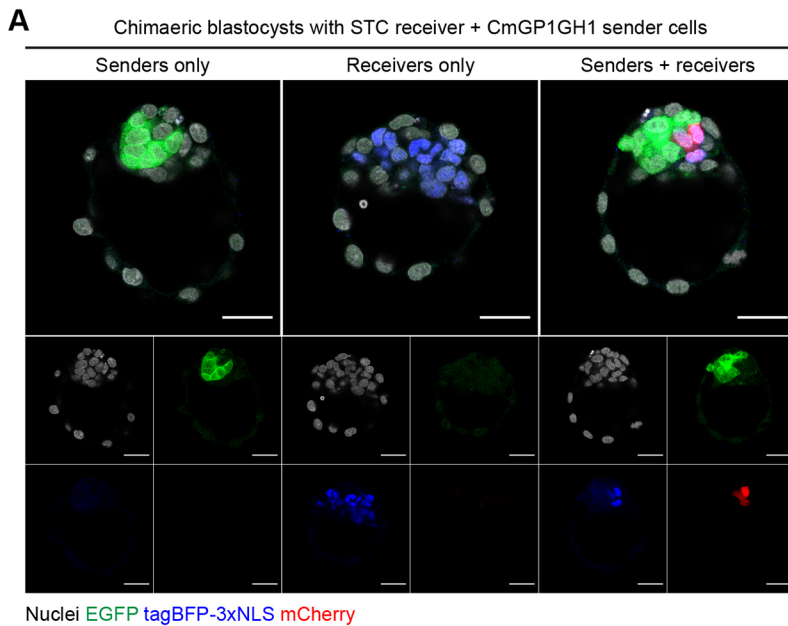


Fig. 6. Contact-mediated induction of mCherry in chimaeric blastocysts. (A) Chimaeric blastocysts containing STC clone B1 receiver cells and/or CmGP1GH1 sender cells. The images of the three embryos were taken from the same z-plane of a confocal stack and come from a single field of view. Nuclei were counterstained with DRAQ7. Scale bars: 30 μ m. (B) Quantification of embryos containing cells expressing readily detectable levels of mCherry ('mCherry-HI') across all experiments. Embryos containing both sender and receiver cells were used as a reference for scoring sender-only chimaeras, receiver-only chimaeras and wild-type embryos.

B

	mCherry-HI embryos / total embryos			
	All clones	STC cl. A1	STC cl. B1	STC cl. B2
Wild-type	0/11	-	-	-
Senders only	0/27	-	-	-
Receivers only	1/19	1/13	0/3	0/3
Receivers+senders	80/80	56/56	23/23	11/11

induction of 3xFlag-Neurog1 in STN receiver cells compared with STN receiver cells cultured alone (Fig. S20B).

We then sought to determine whether we could induce contact-mediated neuronal differentiation of receiver cells in pluripotent culture conditions, and whether we could engineer differentiation to occur in a synthetic pattern. We repeated the synthetic stripe patterning experiment described above (Fig. 7A,B), using STN receiver cells in place of STC receiver cells. We assessed the expression of the neuronal marker *Tubb3* 96 h after initial sender:receiver contact, and observed evident induction of *Tubb3* and acquisition of neuronal morphology by STN receiver cells at the sender:receiver border (Fig. 7D). We verified that E14GIP1 cytoplasmic EGFP control cells were unable to induce neuronal differentiation at the border with STN receiver cells (Fig. S21A). We observed that *Neurog1* is induced shortly after initial sender:receiver cell contact (Fig. S21B), and that *Tubb3* induction first occurs 48 h after initial interaction between sender and STN receiver cells (Fig. S21C).

We conclude that the interaction between EGFP-expressing sender cells and STN receiver cells can lead to contact-mediated *Neurog1* induction and neuronal differentiation of receiver cells in non-permissive culture conditions. This demonstrates that the SynNPL system can be readily used to generate clonal ESC lines for contact-mediated induction of transgenes of interest, and that these cell lines can in turn be used to manipulate cell-cell interactions in order to program synthetic cell fate decisions in response to contact with a particular cell population at desired locations in space.

DISCUSSION

Engineering SynNotch machinery (Morsut et al., 2016) into pluripotent cells opens up many opportunities for understanding how direct cell-cell interactions between neighbouring cells can control differentiation decisions, mediate cell competition (Sancho et al., 2013) and orchestrate morphogenesis (Gorfinkiel and

Martinez Arias, 2021) as cells differentiate in 2D or 3D culture. Mouse ES cells can contribute to chimaeric embryos, meaning that appropriately engineered cell lines can also be used to understand and control cell-cell interactions during early embryonic development. There are, however, particular challenges associated with engineering existing SynNotch technologies into pluripotent cells. Here, we describe how we overcame these challenges to generate the SynNPL system: a set of clonal SynNotch 'sender' and 'receiver' mouse ES cells engineered with optimised and modular SynNotch technology. We demonstrate the utility of the SynNPL system for monitoring cell-cell interactions both in culture and in early mouse embryos, and show that we can use this system to engineer contact-dependent cell fate decisions at the boundary between two populations of pluripotent cells.

Properties of sender cells

We generated sender cell lines expressing high and uniform levels of extracellular membrane-tethered EGFP. This transgenic construct was previously used for SynNotch sender cells (Morsut et al., 2016; Sgodda et al., 2020), and comprises EGFP fused to an N-terminal mouse IgGK signal sequence and a C-terminal human PDGFRB transmembrane domain. The addition of HA and Myc tags at the N- and C-termini of EGFP did not affect the ability of sender cells to induce mCherry expression in STC receiver cells (Fig. S13), so these epitope tags could be helpful for unequivocally identifying and isolating sender cells.

Furthermore, the LaG17 anti-GFP nanobody can also bind to *Aequorea victoria* YFP, CFP and BFP, and *Aequorea macrodactyla* CFP (Fridy et al., 2014), so membrane-tethered versions of these fluorophores could likely be used to induce transgene induction in our receiver cells.

It would be interesting to test whether other cell lines labelled with lipid anchor-tethered GFP (Kondoh et al., 1999; Nowotzschin

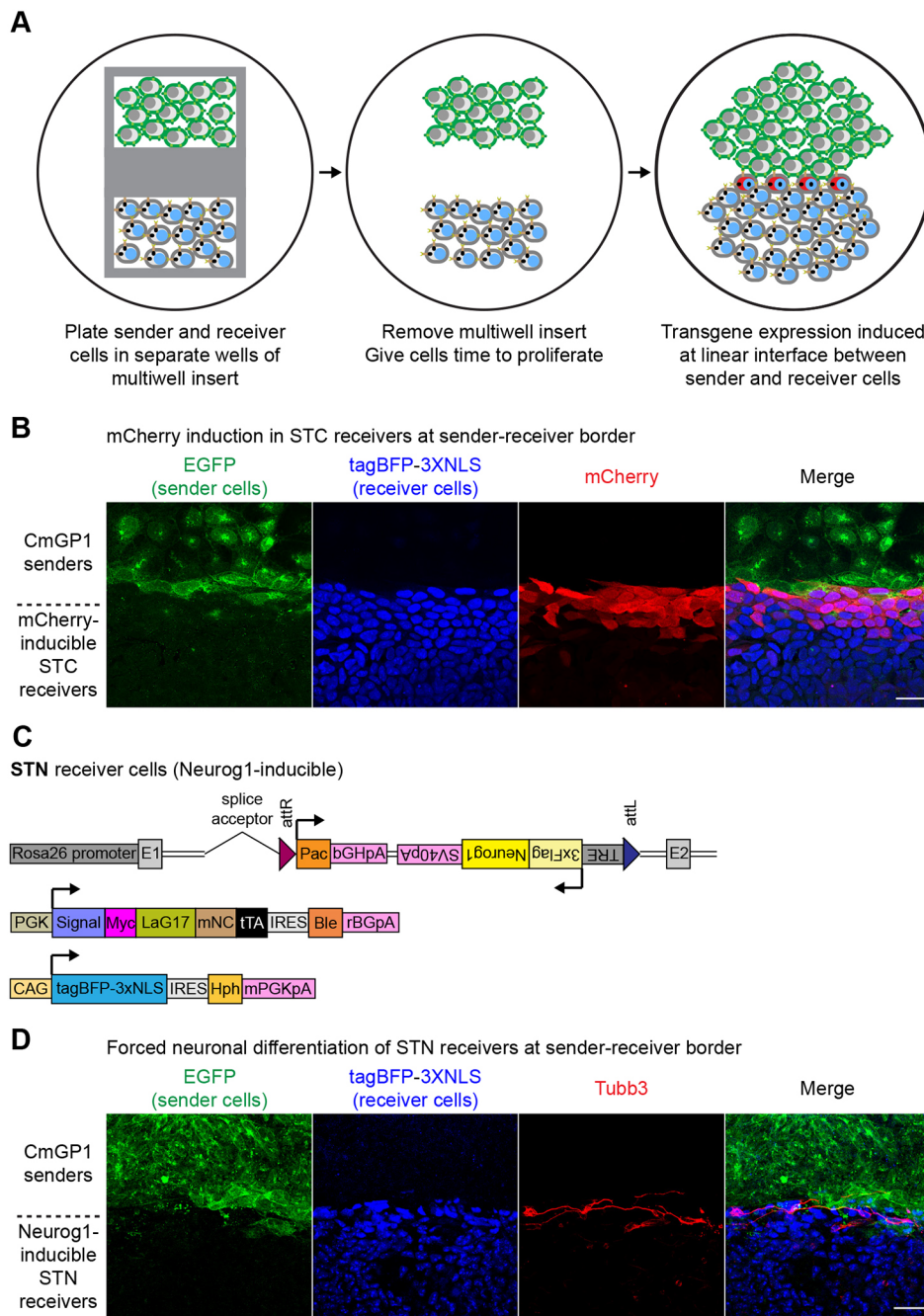


Fig. 7. Contact-mediated synthetic patterning of gene expression and fate programming. (A) Diagram illustrating synthetic patterning strategy: sender and receiver cells are grown to confluence in separate chambers of a multi-chamber culture insert. The insert is removed and cells are allowed to proliferate until they come into contact, which induces transgene expression in receiver cells in a stripe pattern. (B) Synthetic striped pattern of mCherry induction in STC clone B1 receiver ESCs in contact with CmGP1 sender ESCs. EGFP, tagBFP and mCherry immunofluorescence. (C) Summary of transgenes stably integrated into the genome of *Neurog1*-inducible STN clonal ESC lines. (D) Synthetic striped pattern of neuronal differentiation of STN receiver ES cells in contact with CmGP1 sender ESCs. EGFP, tagBFP and Tubb3 immunofluorescence. Scale bars: 30 μ m.

et al., 2009; Rhee et al., 2006; Shioi et al., 2011) could function as SynNotch sender cells; this would require extracellular GFP localisation and generation of sufficient tensile force upon receptor interaction (Morsut et al., 2016). GPI anchors GFP to the outer leaflet of the plasma membrane (Rhee et al., 2006; Sevcsik et al., 2015); GFP-GPI-labelled cells should therefore be capable of acting as sender cells. This does indeed appear to be the case in *Drosophila* (He et al., 2017).

'All-in-one' locus receiver cells display suboptimal functionality

Attempts at generating 'all-in-one' *Rosa26*-targeted receiver cells (termed SNCB⁺ and SNCB⁻ cells) were unsuccessful. The large variation in tagBFP expression and low proportion of mCherry-inducible ESCs in all clonal lines suggests that either

widespread transgene silencing or loss of DNA occurred at the *Rosa26* safe harbour locus in pluripotent cells. Furthermore, rederivation of clonal lines following fluorescence-activated cell sorting of single SNCB⁺ and SNCB⁻ cells led to re-establishment of the initial heterogeneous distributions of fluorophore expression (Figs S7, S8), suggesting that the all-in-one design is not optimal for use in pluripotent cells. We were able to overcome these problems by switching to a random-integration strategy, but it is possible that inclusion of IRES-antibiotic resistance cassettes and/or insulator sequences may provide an alternative route towards generating a reliable system without sacrificing the all-in-one-locus approach.

Landing pad ESCs provide system modularity

Targeting of a landing pad to the *Rosa26* safe harbour locus is an efficient strategy for rapid generation of multiple cell lines through

RMCE (Seibler et al., 2005; Tchorz et al., 2012; Tosti et al., 2018). Our cell lines, harbouring a *Rosa26-attP50-Neo-mKate2-attP50* landing pad, make it straightforward to target different transgenes to the same genomic locus in the same parental cell line. Our parental PSNB lines harbouring the *Rosa26* landing pad allowed us to initially test the functionality of SynNotch in ESCs with an inducible *mCherry* transgene in STC receiver cells, prior to generating genetically equivalent STN receiver cells with a *Neurogl1* transgene in place of *mCherry*. This modular design therefore makes it possible to readily switch between using SynNPL for monitoring and profiling the consequences of defined cell-cell interactions (based on contact-dependent mCherry expression) and using SynNPL for engineering contact-dependent cell behaviours (based on contact-dependent expression of any cell behaviour-determinant).

Describing the properties of the SynNPL system

We characterised various aspects of the SynNPL system that will help inform the experimental design for users of these cells. Previous studies have co-cultured senders and receiver cells at different ratios (ranging from 1:50 to 5:1), and for varying times (ranging from 10 min to several days) (Cho et al., 2018; Choe et al., 2021; He et al., 2017; Huang et al., 2020; Luo et al., 2019; Matsunaga et al., 2020; Morsut et al., 2016; Roybal et al., 2016; Sgodda et al., 2020; Srivastava et al., 2019; Toda et al., 2018, 2020; Wang et al., 2021; Yang et al., 2020). We analysed transgene induction in STC receiver cells at 11 different sender:receiver cell ratios (ranging from 1:19 to 9:1), and observed that higher proportions of sender cells in culture result in a higher proportion of receiver cells inducing mCherry. This is in line with the results obtained by Sgodda et al. (2020) when comparing three different sender:receiver cell ratios, and with the observations of (Morsut et al., 2016), who exposed receiver cells to varying concentrations of sender ligand. By finely varying the concentrations of sender ligand, Lim and colleagues described the transgene induction response as sigmoidal (Morsut et al., 2016), which was not evident in our data. It is, however, possible that by testing lower sender:receiver cell ratios this might also hold true in our SynNotch system.

When analysing transgene expression within single samples, we found that mCherry distribution follows a bimodal on/off response, indicative of the presence of receiver cells that do not interact with sender cells at low sender:receiver cell ratios. This bimodal pattern of transgene induction is also evident in data from Cantz and colleagues (Sgodda et al., 2020). The ability of individual sender cells to induce mCherry induction in STC receiver cells (as seen in Movies 1 and 3) implies that this system can be effectively employed to study the effect of interactions between receiver cells and individual and/or rare sender cells in relevant model systems.

We performed a high-resolution study of the kinetics of mCherry induction and downregulation in STC receiver cells. We observed low levels of mCherry induction in STC receiver cells after 2 h of co-culture with sender cells, provided we allowed time for subsequent protein maturation, and observed maximum mCherry induction following 48 h of co-culture. Previous studies making use of lentiviral-delivered transgenes suggest that 10 min may be sufficient for transgene activation in HEK293 receiver cells, and that 1 h may be sufficient for transgene induction in L929 receiver cells, as long as protein maturation time is allowed (Morsut et al., 2016; Sgodda et al., 2020). This is significantly faster than what we observed in this study, and may be ascribable to lentiviral transduction leading to higher levels of SynNotch receptor and/or

integration of multiple transgene copies compared with our clonal mouse ESC lines.

In our system, mCherry downregulation did not commence for at least 8 h after simulated loss of sender:receiver cell contact, with full loss of signal occurring after more than 40 h. This is in line with previous observations in L929 receiver cells, where inducible GFP transgene expression was lost between 24 and 50 h after sender cells were removed from culture (Morsut et al., 2016).

The kinetics of mCherry induction and downregulation suggest that this SynNotch system is suited for the study of cell-cell interactions with a temporal range of hours rather than minutes, and that ‘memory’ of such interactions will persist for a few days. mCherry signal intensity will be influenced not only by the duration of contact but also, where cells have moved apart, by the time elapsed since last contact: this may complicate interpretation of data from this system for some applications. Should this persistence of mCherry signal prove inconvenient for the study of particular processes, the PSNB landing pad parental cell lines can be used to readily generate cell interaction reporter receiver cells harbouring destabilised inducible transgenes with short half-lives.

Exploring the roles of cell-cell interactions *in vivo* and *in vitro*

We demonstrated that our clonal mouse ESC lines can be used *in vivo* in chimaeric embryos. The ability to conveniently switch between *in vitro* and *in vivo* experimentation was a key reason for us to establish SynNotch technology in mouse ESCs. Both the receiver lines we generated and the parental PSNB landing pad cell lines offer the power and flexibility to address questions we have so far been unable to answer in *in vitro* and *in vivo* settings. For example, the system could be employed in cell competition studies: STC receiver cells could be used to identify and isolate the direct neighbours of EGFP-tagged ‘loser’ cells, and profiled to study what changes are induced upon interaction with loser cells in order to bring about their elimination. Receiver cells could also be engineered to express candidate fitness-altering transgenes in response to interaction with EGFP-tagged wild-type sender cells, as successfully demonstrated in *Drosophila* by He et al. (2017).

The establishment of this system in mouse ESCs also allows the monitoring and manipulation of the effects of cell-cell interactions in specific cell types obtained through directed differentiation. We also demonstrated that our cell lines can be used to generate synthetic patterns of gene expression, resulting in spatially defined programming of cell fate. The combination of directed differentiation of ESCs, spatial confinement of sender and receiver cells, and contact-mediated cell fate engineering provides many possibilities for the study of cell-cell interactions in any developmental process of interest.

Concluding remarks

Cell-cell interactions are a shared feature of the development of all multicellular organisms. Although the particulars of these interactions vary greatly among eukaryotic supergroups, it is clear that they play an essential role in development (Armingol et al., 2021). The synthetic biology field has recently developed several applications to monitor cell communication, such as SynNotch (Morsut et al., 2016) and derivative systems (Zhu et al., 2022), direct transfer of fluorophores to neighbouring cells (Ombrato et al., 2019; Tang et al., 2020), and reconstitution of a fluorophore after interaction between different cell types carrying non-fluorescent fluorophore fragments (Kinoshita et al., 2020). We have here

demonstrated how SynNotch technology can be used to monitor and manipulate cell-cell interactions in mouse ESCs and in mouse embryos.

MATERIALS AND METHODS

Animal care and use

Animal experiments were performed under the UK Home Office project license PEEC9E359 and were approved by the Animal Welfare and Ethical Review Panel of the University of Edinburgh and within the conditions of the Animals (Scientific Procedures) Act 1986.

Chimaera generation

C57BL/6 female mice (Charles River) were superovulated (100 IU/ml PMSG and 100 IU/ml hCG intraperitoneal injections 48 h apart) and crossed with wild-type stud male mice. Pregnant mice were culled at embryonic day 2.5 (E2.5) by cervical dislocation, ovaries with oviducts were dissected and collected in pre-warmed M2 medium. Oviducts were flushed using PBS and a 20-gauge needle attached to a 1 ml syringe and filled with PB1 (Whittingham, 1974). E2.5 embryos were collected and washed in PB1, their zona pellucida removed using acidic Tyrode's solution and transferred to a plate with incisions where two clumps of approximately eight sender and eight receiver cells were added to each embryo. Embryos were then incubated at 37°C in 5% CO₂ for 48 h prior to fixation, or for 24 h prior to transfer to pseudopregnant females for the generation of post-implantation chimaeras. For DAPT treatment experiments, DAPT was equilibrated for several hours at 37°C before addition to embryos in order to avoid precipitation. Embryos subject to DAPT withdrawal were washed twice before being placed in DAPT-free medium. The sex of embryos used in this study was not determined. All reagents are listed in Table S1.

Mouse ESC culture

Mouse embryonic stem cells were routinely maintained on gelatinised culture vessels (Corning) at 37°C and 5% CO₂ in Glasgow Minimum Essential Medium (GMEM) supplemented with 10% foetal calf serum (FCS), 100 U/ml LIF (produced in-house), 100 nM 2-mercaptoethanol, 1× non-essential amino acids, 2 mM L-glutamine and 1 mM sodium pyruvate (medium referred to as 'ES cell culture medium' or 'LIF+FCS'). The medium was supplemented with 200 µg/ml G418, 2 µg/ml puromycin, 200 µg/ml hygromycin B and/or 100 µg/ml zeocin, as appropriate. For live imaging, GMEM was replaced with Phenol Red-free Dulbecco's Modified Eagle Medium (DMEM), with all other components of the culture medium used at identical concentrations. All reagents are listed in Table S1.

DNA constructs

pHR_SFFV_LaG17_synNotch_TetRVP64 (Addgene 79128) (Morsut et al., 2016) and pHR_EGFPligand (Addgene 79129) (Morsut et al., 2016) were kind gifts from Dr Wendell Lim (University of California San Francisco, CA, USA) and Dr Leonardo Morsut (University of Southern California, Los Angeles, CA, USA). pDisplay-GFP-TM (Han et al., 2004) was a kind gift from Dr Luis Ángel Fernández (CNB-CSIC, Madrid, Spain). CAG-φC31 integrase (Monetti et al., 2011) was a kind gift from Dr Andras Nagy (Lunenfeld-Tanenbaum Research Institute, Toronto, Canada). pHR_TRE-mCherry-PGK-tagBFP-WPRE was a kind gift from Dr Elise Cachat (University of Edinburgh, UK). pRosa26-DEST-1lox, pENTR-2xAttP50 and pENTR-2xAttB53 (Tosti et al., 2018) constructs were kind gifts from Dr Keisuke Kaji (University of Edinburgh, UK).

Untagged transmembrane EGFP constructs were generated by digesting pHR_EGFPligand with XhoI+NotI, and ligating the *IgGK signal-EGFP-PDGFRB TMD* cassette into XhoI+NotI-digested *pPyCAG-IRES-Pac* (Malaguti et al., 2019) or *pPyPGK-IRES-Pac* (Rao et al., 2020) vector backbones. HA- and Myc-tagged EGFP constructs were generated by PCR amplifying an *IgGK signal-HA-EGFP-Myc-PDGFRB TMD* cassette flanked by PspXI and NotI sites from pDisplay-GFP-TM, digesting the amplicon with PspXI+NotI and ligating the insert into XhoI+NotI-digested *pPyCAG-IRES-Pac* or *pPyPGK-IRES-Pac* vector backbones.

The *pPyPGK-CD8a signal-Myc-LaG17-Notch1 minimal transmembrane core-tTA-IRES-Ble* SynNotch receptor construct was generated by PCR amplifying a *CD8a signal-Myc-LaG17-Notch1 minimal transmembrane core-tTA* cassette flanked by XhoI and Bsu36I sites from pHR_SFFV_LaG17_synNotch_TetRVP64, digesting the amplicon with XhoI+Bsu36I and ligating the insert into a XhoI+Bsu36I-digested *pPyPGK-IRES-Ble* vector backbone. The mouse Notch1 minimal transmembrane core consists of residues 1427-1752 (Uniprot: Q01705).

The *pPyCAG-tagBFP-3xNLS-IRES-Hph* construct was generated by PCR amplifying a *tagBFP* cassette flanked by XhoI and KasI sites from pHR_TRE-mCherry-PGK-tagBFP-WPRE, digesting the amplicon with XhoI+KasI and ligating the insert into a XhoI+NotI-digested *pPyCAG-IRES-Hph* backbone (Malaguti et al., 2019) alongside oligonucleotides annealed to generate a 3xNLS fragment with KasI and NotI overhangs (Malaguti et al., 2013).

The *Rosa26* landing pad targeting vector was generated by Gateway Cloning (Invitrogen) of an *attL1-attP50-Neo-SV40pA-(CAG-mKate2-3xNLS-bGHpA)-attP50-attL2* cassette into the pRosa26-DEST-1lox targeting vector. Its final structure is as follows: *Rosa26 5'HA-splice acceptor-loxP-attP50-Neo-SV40pA-(CAG-mKate2-3xNLS-bGHpA)-attP50-Rosa26 3'HA-PGK-DTA-bGHpA*. Sequence in brackets is on the negative strand.

An *attB53-Pac-attB53* 'empty vector' construct for RMCE at the *Rosa26* locus was generated by adding a *Pac-bGHpA* cassette followed by an EcoRV restriction site to pENTR-2xAttB53 by Gibson assembly.

The *attB53-TRE-mCherry-attB53* RMCE construct used to generate STC receiver cells from PSNB landing pad lines was generated by PCR amplifying a *TRE-mCherry-SV40pA* cassette flanked by EcoRV-AscI and EcoRV-BamHI sites from pHR_TRE-mCherry-PGK-tagBFP-WPRE, digesting the amplicon with EcoRV, ligating the insert into EcoRV-digested *attB53-Pac-attB53* backbone and screening for insertion on the negative strand. The *attB53-tetO-mCherry-attB53* RMCE construct used to generate PSNB-tetO cells from PNSB landing pad lines was generated by PCR amplifying a *tetO-mCherry-rBGpA* cassette flanked by MluI and BamHI sites, digesting the amplicon with MluI+BamHI and ligating the insert into AscI+BamHI-digested *attB53-Pac-TRE-mCherry-attB53*.

The *attB53-TRE-3xFlag-Neurog1-attB53* RMCE construct used to generate STN receiver cells from PSNB landing pad lines was generated by PCR amplifying a *3xFlag-Neurog1* cassette flanked by NdeI and MfeI sites from wild-type mouse cDNA, digesting the amplicon with NdeI+MfeI and ligating the insert into NdeI+MfeI-digested *attB53-Pac-TRE-mCherry-attB53* backbone (in which *mCherry* is flanked by NfeI and MfeI sites).

attB53_SNCB+_attB53 and *attB53_SNCB-_attB53* constructs were generated in two steps. First, the base *attB53-Pac-bGHpA-attB53* RMCE construct was linearised with EcoRV, and ligated with a HincII-PGK-*CD8a signal-Myc-LaG17-Notch1 minimal transmembrane core-tTA*-HindIII fragment (digested from the SynNotch receptor construct described above) and a HindIII-*bGHpA*-EcoRV fragment, and clones were screened for insertion of the SynNotch receptor on the positive strand. Next, the resulting construct was linearised with EcoRV, and ligated with an EcoRV-*TRE-mCherry-SV40pA-PGK-tagBFP-PacI* fragment (digested from pHR_TRE-mCherry-PGK-tagBFP-WPRE) and a PacI-*bGHpA*-EcoRV fragment. Correct assembly on the positive and negative strands generated the *attB53_SNCB+_attB53* and *attB53_SNCB-_attB53* constructs, respectively. All reagents are listed in Table S1.

Transfections

For electroporations, 10⁷ ESCs were electroporated with 100 µg DNA using a BioRad GenePulser set to 800 V/3 µF. For nucleofections, 5×10⁵ ESCs were nucleofected with 5 µg DNA with the Lonza P3 Primary Cell Nucleofector Unit and kit, using program CG-104, and following manufacturer instructions. For lipofections, 10⁵ ESCs were lipofected with 3 µg DNA mixed with 3 µl Lipofectamine 3000 and 6 µl P3000 solution, following manufacturer instructions. For φC31-mediated RMCE, equal masses of RMCE constructs and CAG-φC31 vector were transfected.

Clonal ESC lines were generated by transfecting constructs of interest into ESCs, then plating cells at low density onto gelatinised 9 cm dishes in the

absence of selection. Selective medium was added 48 h post-transfection and replaced every other day. After 7–10 days, clones were manually picked, dissociated and replated into gelatinised 96-well culture plates. Clones were transferred to gelatinised vessels with larger culture areas when confluent, screened as appropriate, expanded and cryopreserved. All reagents are listed in Table S1.

Cell lines

E14Ju09 ESCs are a 129/Ola male wild-type clonal line derived from E14tg2a (Hamilton and Brickman, 2014; Hooper et al., 1987). Sender cells were generated by electroporating E14Ju09 ESCs with one of four constructs: *pPyCAG-IgGK signal-EGFP-PDGFRB TMD-IRES-Pac* (CmGP cells), *pPyPGK-IgGK signal-EGFP-PDGFRB TMD-IRES-Pac* (PmGP cells), *pPyCAG-IgGK signal-HA-EGFP-Myc-PDGFRB TMD-IRES-Pac* (CHmGMP cells) or *pPyPGK-IgGK signal-HA-EGFP-Myc-PDGFRB TMD-IRES-Pac* (PHmGMP cells). Simplified versions of the constructs are displayed in Fig. 2. HA and Myc tags were used in CHmGMP and PHmGMP cell lines as additional markers to identify sender cells, but are not essential given that sender cells can be identified by GFP fluorescence. CmGPIGH1 sender cells were generated by lipofecting CmGP1 sender cells with a *pPyCAG-EGFP-IRES-Hph* construct. E14GIP1 ‘cytoplasmic sender’ cells were generated by lipofecting E14Ju09 ESCs with a *pPyCAG-EGFP-IRES-Pac* construct.

EM35 landing pad cells were generated by electroporating E14Ju09 ESCs with the *Rosa26* landing pad targeting vector described above. Correct targeting was verified by genomic DNA PCR with the following primers: forward, GCGGACTGGCGGGACTA; reverse, GGGACAGGATAAG-TATGACATCATCAAG. Primer locations and expected band sizes are displayed in Fig. S3A. This PCR strategy was modified from that described by Mort et al. (2014) to suit the different sequence of our *Rosa26* targeting vector.

SNCB+ and SNCB– receiver cells were generated by electroporating EM35 ESCs with the constructs depicted in Figs S4A, S6A, and a *CAG-φC31 integrase* construct to mediate RMCE.

35SRZ landing pad cells were generated by electroporating EM35 landing pad cells with *pPyPGK-CD8a signal-Myc-LaG17-Notch1 minimal transmembrane core-tTA-IRES-Ble*.

PSNB landing pad cell lines were generated by nucleofecting 35SRZ ESCs with a *pPyCAG-tagBFP-3xNLS-IRES-Hph* construct. PSNB-A cells were derived from 35SRZ clone 9 (PSNB-A clone 10 renamed PSNB clone A). PSNB-B cells were derived from 35SRZ clone 86 (PSNB-B clone 3 renamed PSNB clone B).

STC receiver cells were generated by nucleofecting PSNB ESCs with *CAG-φC31 integrase* and the following RMCE construct: *attB53-Pac-bGHpA-(TRE-mCherry-SV40pA)-attB53*. Sequence in brackets is on the negative strand. STC clone A1 was derived from PSNB clone A; STC clones B1 and B2 were derived from PSNB clone B.

PSNB-tetO cells were generated by nucleofecting PSNB ESCs with *CAG-φC31 integrase* and the following RMCE construct: *attB53-Pac-bGHpA-(tetO-mCherry-SV40pA)-attB53*. Sequence in brackets is on the negative strand.

PNSB-E cells were generated by nucleofecting PSNB ESCs with *CAG-φC31 integrase* and the following RMCE construct: *attB53-Pac-bGHpA-attB53*.

STN receiver cells were generated by nucleofecting PSNB clone A ESCs with *CAG-φC31 integrase* and the following RMCE construct: *attB53-Pac-bGHpA-(TRE-3xFlag-Neurog1-SV40pA)-attB53*. Sequence in brackets is on the negative strand.

Cell lines generated in this study were routinely karyotyped by chromosome count and checked for absence of mycoplasma infection. All reagents are listed in Table S1.

Co-culture experiments

Sender and receiver cells were detached from culture vessels with accutase, quenched in ESC culture medium, pelleted by spinning at 300 g for 3 min, resuspended in ESC culture medium supplemented with 2 μg/ml puromycin and counted. Cells were plated at ratios described in figure legends, and at empirically determined optimal densities.

For flow cytometry experiments, cells were plated onto 12-well plates coated with 7.5 μg/ml fibronectin, at the following densities. For experiments carried out in the absence of doxycycline: 1 h–8 h, 4×10⁵ cells/well; 16 h, 2.4×10⁵ cells/well; 24 h, 1.6×10⁵ cells/well; 48 h, 8×10⁴ cells/well; 72 h, 4×10⁴ cells/well. For mCherry induction with 16 h doxycycline (Fig. 4F–H): 0–4 h, 2.4×10⁵ cells/well; 5–8 h, 1.6×10⁵ cells/well; 24 h, 8×10⁴ cells/well. For mCherry downregulation experiments (Fig. S14): 0 h–8 h, 1.6×10⁵ cells/well; 16 h, 1.2×10⁵ cells/well; 24 h, 8×10⁴ cells/well; 48 h, 4×10⁴ cells/well.

For immunofluorescence experiments, cells were plated on flamed 24 mm glass coverslips housed in a six-well plate coated with 7.5 μg/ml fibronectin.

For live-imaging experiments using a Nikon Ti-E microscope (Movies 1, 3–5), cells were plated onto an eight-well imaging slide coated with 7.5 μg/ml fibronectin, at the following densities. For mCherry induction experiments: 3×10⁴ cells/well. For mCherry downregulation experiments: 0–24 h, 2×10⁴ cells/well; 24–48 h, 10⁴ cells/well. For live-imaging experiments using a PerkinElmer Opera Phenix Plus microscope (Movie 2, Fig. S16G), cells were plated onto a 96-well imaging plate coated with 7.5 μg/ml fibronectin, at the following densities. For mCherry induction experiments: 9.6×10⁴ cells/well. For mCherry downregulation experiments: 0–24 h, 2×10⁴ cells/well; 24–48 h, 10⁴ cells/well. ESC culture medium was supplemented with 2 μg/ml puromycin, 200 μg/ml hygromycin B and 1× penicillin/streptomycin.

To test induction of 3xFlag-Neurog1 in STN receiver cells, CmGP1 sender cells and STN receiver cells were plated at a 9:1 ratio at a concentration of 2×10⁵ cells/well onto a 24 mm flamed glass coverslip housed in a six-well plate coated with 7.5 μg/ml fibronectin, then fixed and stained after 48 h. All reagents are listed in Table S1.

Synthetic patterning experiments

A 24 mm glass coverslip housed in a six-well plate was coated with 7.5 μg/ml fibronectin, then allowed to air dry. When fully dry, forceps were used to place a culture insert three-well silicon chamber on top of the coverslip; downward force was carefully exerted to secure it in place. 4×10⁴ cells were plated overnight in 70 μl culture medium in each of the three wells. Sender cells were plated in the central well, and receiver cells were plated in the outside wells. 2 ml culture medium were added outside of the three-well insert in order to prevent evaporation. The next day, the 2 ml culture medium outside the three-well insert were aspirated, and the 70 μl in each of the three wells were carefully removed in order not to dislodge the three-well insert. Each well was quickly washed with 70 μl PBS to remove any remaining cells in suspension. Forceps were used to detach the three-well insert from the glass coverslip, and 2.5 ml culture medium were added to the well. Culture medium was replaced daily. Growth of cells into the gaps between wells were monitored daily; following contact between sender and receiver cells, cells were kept in culture for a further 24 h (STC receivers+CmGP1 senders) or a further 96 h (STN receivers+CmGP1 senders) before fixation and immunofluorescence. For live imaging of mCherry stripe experiments, the three-well insert was placed in an Ibidi μ-Slide 4 Well instead of on a glass coverslip. All reagents are listed in Table S1.

Flow cytometry

Cells were washed in PBS, then detached from culture vessels with accutase. They were resuspended in ice-cold PBS+10% FCS, pelleted by spinning at 300 g for 3 min, resuspended in ice-cold PBS+10% FCS+300 nM DRAQ7 and placed on ice before analysing on a BD LSRFortessa flow cytometer. Forward and side-scatter width and amplitude were used to identify single cells in suspension; dead cells were excluded by gating on DRAQ7-negative cells; and tagBFP, GFP and mCherry/mKate2 expression was then analysed using V 450/50-A, B 530/30-A, Y/G 610/20-A laser/filters combinations, respectively. All reagents are listed in Table S1.

Immunofluorescence

Cells were plated on flamed glass coverslips coated with 7.5 μg/ml fibronectin and cultured as indicated in figure legends. Cells were washed with PBS, fixed in 4% formaldehyde in PBS for 20 min at room temperature

then washed three times in PBS for a total of 15 min. Cells were blocked overnight at 4°C in blocking solution (PBS+3% donkey serum+0.1% Triton X-100). Primary antibodies diluted in blocking solution were added for 3 h at room temperature and the coverslips were washed three times in PBS for a total of 30 min; secondary antibodies diluted in blocking solution were added for 1 h at room temperature and the coverslips were washed three times in PBS for a total of 30 min. The coverslips were then mounted onto glass slides in Prolong Gold mounting medium. For synthetic patterning experiments and chimaera staining, antibodies were incubated overnight at 4°C or 37°C, respectively, to improve penetration. Blastocysts were imaged in PBS in an imaging chamber, and scoring of mCherry-HI cells was performed manually using chimaeras containing both sender and receiver cells as a reference. Post-implantation chimaeras were dehydrated in methanol series in PBS/0.1% Triton X-100, clarified in 50% methanol/50% BABB (benzyl alcohol:benzyl benzoate 1:2 ratio) and transferred into 100% BABB before imaging. All imaging was performed on a Leica SP8 confocal microscope with a 40× immersion lens unless otherwise indicated. All reagents are listed in Table S1.

Live imaging

Cells to be imaged were allowed to adhere on culture vessels at room temperature for 15 min after plating, after which they were placed in a 37°C 5% CO₂ humidified chamber and imaged. For Movies 1, 3-5, imaging was performed with a widefield Nikon Ti-E microscope, 20× lens and Hamamatsu camera; images were taken at 10-min intervals for 24 h, and *xy* coordinates were saved. After live imaging, cells were fixed and stained for fluorophore expression, and imaged at the previously saved *xy* coordinates (Movies 1, 3). For Movie 2, Figs S16G and S19, imaging was performed with a PerkinElmer Opera PhenixPlus microscope, 20× lens. Images were taken at 1-h (Movie 2, Fig. S16G) or 90-min (Fig. S19) intervals for 24 h. Fully automated segmentation of tagBFP-positive nuclei, tracking and quantification of fluorescent signal intensity in live-imaging experiments was performed using the PerkinElmer Harmony software.

Filming of the morula to blastocyst transition was performed with a PerkinElmer Opera PhenixPlus confocal microscope. Sender and receiver cells were placed on opposite poles of morulae, and allowed to aggregate unperturbed for ~4 h prior to imaging, in order to ensure strong binding of ES cells to morulae. They were then transferred to wells of an uncoated Ibidi μ -Slide Angiogenesis imaging slide and imaged. Aside from an initial frame, it was not possible to capture tagBFP signal within the time-lapse movies as embryos were vulnerable to repeated stimulation with ultraviolet light. All reagents are listed in Table S1.

Acknowledgements

We thank Leonardo Morsut and Wendell Lim for developing the original SynNotch system, Elise Cachat and Keisuke Kaji for advice and reagents, Luis Ángel Fernández for the pDisplay-EGFP-TM plasmid, Andras Nagy for the CAG- ϕ C31 plasmid, Dónal O'Carroll and Pedro Moreira for assistance with generating chimaeric mice, Eve Moutaux for cloning initial versions of the RMCE constructs, and Alexandre Veiga and Matthew French for performing preliminary experiments with the original SynNotch constructs. We also thank Justyna Cholewa-Waclaw, Matthieu Vermeren and Charles Williams for assistance with time-lapse imaging, Fiona Rossi and Claire Cryer for flow cytometry support, and Theresa O'Connor, Helen Henderson and Marilyn Thomson for cell culture support. We are grateful to Leonardo Morsut and to members of the Lowell and Wilson labs for helpful discussions.

Competing interests

The authors declare no competing or financial interests.

Author contributions

Conceptualization: M.M., S.L.; Methodology: M.M., R.P.M., J.A., D.S., G.B.; Validation: M.M., J.A.; Formal analysis: M.M., R.P.M., J.A.; Investigation: M.M., R.P.M., J.A.; Resources: M.M., R.P.M., D.S., G.B.; Data curation: M.M., J.A.; Writing - original draft: M.M., S.L.; Writing - review & editing: M.M., J.A., S.L.; Visualization: M.M.; Supervision: M.M., G.B., S.L.; Project administration: S.L.; Funding acquisition: S.L.

Funding

This work was funded by a Wellcome Trust Senior Fellowship to S.L. (WT103789AIA) and by a Wellcome Trust Sir Henry Wellcome Fellowship to G.B. (WT100133). Open access funding provided by the University of Edinburgh. Deposited in PMC for immediate release.

Peer review history

The peer review history is available online at <https://journals.biologists.com/dev/article-lookup/doi/10.1242/dev.200226>

References

- Armingol, E., Officer, A., Harismendy, O. and Lewis, N. E. (2021). Deciphering cell-cell interactions and communication from gene expression. *Nat. Rev. Genet.* **22**, 71-88. doi:10.1038/s41576-020-00292-x
- Arnold, S. J. and Robertson, E. J. (2009). Making a commitment: cell lineage allocation and axis patterning in the early mouse embryo. *Nat. Rev. Mol. Cell Biol.* **10**, 91-103. doi:10.1038/nrm2618
- Blin, G., Wisniewski, D., Picart, C., Thery, M., Puecat, M. and Lowell, S. (2018). Geometrical confinement controls the asymmetric patterning of Brachyury in cultures of pluripotent cells. *Development* **145**, dev166025. doi:10.1242/dev.166025
- Blin, G., Sadurska, D., Portero Migueles, R., Chen, N., Watson, J. A. and Lowell, S. (2019). Nessys: a new set of tools for the automated detection of nuclei within intact tissues and dense 3D cultures. *PLoS Biol.* **17**, e3000388. doi:10.1371/journal.pbio.3000388
- Boggs, S. S., Gregg, R. G., Borenstein, N. and Smithies, O. (1986). Efficient transformation and frequent single-site, single-copy insertion of DNA can be obtained in mouse erythroleukemia cells transformed by electroporation. *Exp. Hematol.* **14**, 988-994.
- Bradley, A., Evans, M., Kaufman, M. H. and Robertson, E. (1984). Formation of germ-line chimaeras from embryo-derived teratocarcinoma cell lines. *Nature* **309**, 255-256. doi:10.1038/309255a0
- Cachat, E., Liu, W., Martin, K. C., Yuan, X., Yin, H., Hohenstein, P. and Davies, J. A. (2016). 2- and 3-dimensional synthetic large-scale de novo patterning by mammalian cells through phase separation. *Sci. Rep.* **6**, 20664. doi:10.1038/srep20664
- Cai, L., Morrow, E. M. and Cepko, C. L. (2000). Misexpression of basic helix-loop-helix genes in the murine cerebral cortex affects cell fate choices and neuronal survival. *Development* **127**, 3021-3030. doi:10.1242/dev.127.14.3021
- Cau, E., Casarosa, S. and Guillemot, F. (2002). Mash1 and Ngn1 control distinct steps of determination and differentiation in the olfactory sensory neuron lineage. *Development* **129**, 1871-1880. doi:10.1038/dev.129.8.1871
- Charrier, S., Ferrand, M., Zerbato, M., Précigout, G., Viornerly, A., Bucher-Laurent, S., Benkhelifa-Ziyyat, S., Merten, O. W., Perea, J. and Galy, A. (2011). Quantification of lentiviral vector copy numbers in individual hematopoietic colony-forming cells shows vector dose-dependent effects on the frequency and level of transduction. *Gene Ther.* **18**, 479-487. doi:10.1038/gt.2010.163
- Chen, C., Krohn, J., Bhattacharya, S. and Davies, B. (2011). A comparison of exogenous promoter activity at the ROSA26 locus using a PhiC31 integrase mediated cassette exchange approach in mouse ES cells. *PLoS One* **6**, e23376. doi:10.1371/journal.pone.0023376
- Cho, J. H., Okuma, A., Al-Rubaye, D., Intisar, E., Junghans, R. P. and Wong, W. W. (2018). Engineering Axl specific CAR and SynNotch receptor for cancer therapy. *Sci. Rep.* **8**, 3846. doi:10.1038/s41598-018-22525-6
- Choe, J. H., Watchmaker, P. B., Simic, M. S., Gilbert, R. D., Li, A. W., Krasnow, N. A., Downey, K. M., Yu, W., Carrera, D. A., Celli, A. et al. (2021). SynNotch-CAR T cells overcome challenges of specificity, heterogeneity, and persistence in treating glioblastoma. *Sci. Transl. Med.* **13**, eabe7378. doi:10.1126/scitranslmed.abe7378
- Davies, J. (2017). Using synthetic biology to explore principles of development. *Development* **144**, 1146-1158. doi:10.1242/dev.144196
- De Los Angeles, A., Ferrari, F., Xi, R., Fujiwara, Y., Benvenisty, N., Deng, H., Hochedlinger, K., Jaenisch, R., Lee, S., Leitch, H. G. et al. (2015). Hallmarks of pluripotency. *Nature* **525**, 469-478. doi:10.1038/nature15515
- Dias, A. S., de Almeida, I., Belmonte, J. M., Glazier, J. A. and Stern, C. D. (2014). Somites without a clock. *Science* **343**, 791-795. doi:10.1126/science.1247575
- Ebrahimkhani, M. R. and Ebisuya, M. (2019). Synthetic developmental biology: build and control multicellular systems. *Curr. Opin. Chem. Biol.* **52**, 9-15. doi:10.1016/j.cbpa.2019.04.006
- Evans, M. J. and Kaufman, M. H. (1981). Establishment in culture of pluripotential cells from mouse embryos. *Nature* **292**, 154-156. doi:10.1038/292154a0
- Fischer, S. C., Corujo-Simon, E., Lilao-Garzon, J., Stelzer, E. H. K. and Muñoz-Descalzo, S. (2020). The transition from local to global patterns governs the differentiation of mouse blastocysts. *PLoS One* **15**, e0233030. doi:10.1371/journal.pone.0233030
- Forsyth, J. E., Al-Anbaki, A. H., de la Fuente, R., Modare, N., Perez-Cortes, D., Rivera, I., Seaton Kelly, R., Cotter, S. and Plusa, B. (2021). IVEN: a quantitative tool to describe 3D cell position and neighbourhood reveals architectural changes

- in FGF4-treated preimplantation embryos. *PLoS Biol.* **19**, e3001345. doi:10.1371/journal.pbio.3001345
- Fridy, P. C., Li, Y., Keegan, S., Thompson, M. K., Nudelman, I., Scheid, J. F., Oeffinger, M., Nussenzweig, M. C., Fenyö, D., Chait, B. T. et al.** (2014). A robust pipeline for rapid production of versatile nanobody repertoires. *Nat. Methods* **11**, 1253-1260. doi:10.1038/nmeth.3170
- Friedrich, G. and Soriano, P.** (1991). Promoter traps in embryonic stem cells: a genetic screen to identify and mutate developmental genes in mice. *Genes Dev.* **5**, 1513-1523. doi:10.1101/gad.5.9.1513
- Gorfinkiel, N. and Martinez Arias, A.** (2021). The cell in the age of the genomic revolution: cell regulatory networks. *Cells Dev.* **168**, 203720. doi:10.1016/j.cdev.2021.203720
- Gossen, M. and Bujard, H.** (1992). Tight control of gene expression in mammalian cells by tetracycline-responsive promoters. *Proc. Natl. Acad. Sci. USA* **89**, 5547-5551. doi:10.1073/pnas.89.12.5547
- Gurdon, J. B.** (1987). Embryonic induction — molecular prospects. *Development* **99**, 285-306. doi:10.1242/dev.99.3.285
- Hamilton, W. B. and Brickman, J. M.** (2014). Erk signaling suppresses embryonic stem cell self-renewal to specify endoderm. *Cell Rep.* **9**, 2056-2070. doi:10.1016/j.celrep.2014.11.032
- Han, H.-J., Park, S.-G., Kim, S.-H., Hwang, S.-Y., Han, J., Traicoff, J., Kho, W.-G. and Chung, J.-Y.** (2004). Epidermal growth factor-like motifs 1 and 2 of Plasmodium vivax merozoite surface protein 1 are critical domains in erythrocyte invasion. *Biochem. Biophys. Res. Commun.* **320**, 563-570. doi:10.1016/j.bbrc.2004.06.008
- He, L., Huang, J. and Perrimon, N.** (2017). Development of an optimized synthetic Notch receptor as an in vivo cell-cell contact sensor. *Proc. Natl. Acad. Sci. USA* **114**, 5467-5472. doi:10.1073/pnas.1703205114
- Herbst, F., Ball, C. R., Tuorto, F., Nowrouzi, A., Wang, W., Zavidij, O., Dieter, S. M., Fessler, S., van der Hoeven, F., Kloz, U. et al.** (2012). Extensive methylation of promoter sequences silences lentiviral transgene expression during stem cell differentiation in vivo. *Mol. Ther.* **20**, 1014-1021. doi:10.1038/mt.2012.46
- Ho, C. and Morsut, L.** (2021). Novel synthetic biology approaches for developmental systems. *Stem Cell Rep.* **16**, 1051-1064. doi:10.1016/j.stemcr.2021.04.007
- Hong, S., Hwang, D.-Y., Yoon, S., Isacson, O., Ramezani, A., Hawley, R. G. and Kim, K.-S.** (2007). Functional analysis of various promoters in lentiviral vectors at different stages of in vitro differentiation of mouse embryonic stem cells. *Mol. Ther.* **15**, 1630-1639. doi:10.1038/sj.mt.6300251
- Hooper, M., Hardy, K., Handyside, A., Hunter, S. and Monk, M.** (1987). HPRT-deficient (Lesch-Nyhan) mouse embryos derived from germline colonization by cultured cells. *Nature* **326**, 292-295. doi:10.1038/326292a0
- Huang, J., Zhou, W., Dong, W., Watson, A. M. and Hong, Y.** (2009). Directed, efficient, and versatile modifications of the Drosophila genome by genomic engineering. *Proc. Natl. Acad. Sci. USA* **106**, 8284-8289. doi:10.1073/pnas.0900641106
- Huang, H., Zhang, X., Lv, J., Yang, H., Wang, X., Ma, S., Shao, R., Peng, X., Lin, Y. and Rong, Z.** (2020). Cell-cell contact-induced gene editing/activation in mammalian cells using a SynNotch-CRISPR/Cas9 system. *Protein Cell* **11**, 299-303. doi:10.1007/s13238-020-00690-1
- Johnson, M. H. and Ziomek, C. A.** (1983). Cell interactions influence the fate of mouse blastomeres undergoing the transition from the 16- to the 32-cell stage. *Dev. Biol.* **95**, 211-218. doi:10.1016/0012-1606(83)90019-2
- Kinoshita, M. and Smith, A.** (2018). Pluripotency deconstructed. *Dev. Growth Differ.* **60**, 44-52. doi:10.1111/dgd.12419
- Kinoshita, N., Huang, A. J. Y., McHugh, T. J., Miyawaki, A. and Shimogori, T.** (2020). Diffusible GRAPHIC to visualize morphology of cells after specific cell-cell contact. *Sci. Rep.* **10**, 14437. doi:10.1038/s41598-020-71474-0
- Kondoh, G., Gao, X.-H., Nakano, Y., Koike, H., Yamada, S., Okabe, M. and Takeda, J.** (1999). Tissue-inherent fate of GPI revealed by GPI-anchored GFP transgenesis. *FEBS Lett.* **458**, 299-303. doi:10.1016/S0014-5793(99)01172-2
- Liew, C.-G., Draper, J. S., Walsh, J., Moore, H. and Andrews, P. W.** (2007). Transient and stable transgene expression in human embryonic stem cells. *Stem Cells* **25**, 1521-1528. doi:10.1634/stemcells.2006-0634
- Luo, H., Wu, X., Sun, R., Su, J., Wang, Y., Dong, Y., Shi, B., Sun, Y., Jiang, H. and Li, Z.** (2019). Target-dependent expression of IL12 by SynNotch receptor-engineered NK92 cells increases the antitumor activities of CAR-T cells. *Front. Oncol.* **9**, 1448. doi:10.3389/fonc.2019.01448
- Ma, Q., Kintner, C. and Anderson, D. J.** (1996). Identification of neurogenin, a vertebrate neuronal determination gene. *Cell* **87**, 43-52. doi:10.1016/S0092-8674(00)81321-5
- Ma, Q., Chen, Z., del Barco Barrantes, I., de la Pompa, J. L. and Anderson, D. J.** (1998). neurogenin1 is essential for the determination of neuronal precursors for proximal cranial sensory ganglia. *Neuron* **20**, 469-482. doi:10.1016/S0896-6273(00)80988-5
- Malaguti, M., Nistor, P. A., Blin, G., Pegg, A., Zhou, X. and Lowell, S.** (2013). Bone morphogenic protein signalling suppresses differentiation of pluripotent cells by maintaining expression of E-Cadherin. *Elife* **2**, e01197. doi:10.7554/eLife.01197
- Malaguti, M., Migueles, R. P., Blin, G., Lin, C.-Y. and Lowell, S.** (2019). Id1 stabilizes epiblast identity by sensing delays in nodal activation and adjusting the timing of differentiation. *Dev. Cell* **50**, 462-477.e5. doi:10.1016/j.devcel.2019.05.032
- Martin, G. R.** (1981). Isolation of a pluripotent cell line from early mouse embryos cultured in medium conditioned by teratocarcinoma stem cells. *Proc. Natl. Acad. Sci. USA* **78**, 7634-7638. doi:10.1073/pnas.78.12.7634
- Matsuda, M., Koga, M., Woltjen, K., Nishida, E. and Ebisuya, M.** (2015). Synthetic lateral inhibition governs cell-type bifurcation with robust ratios. *Nat. Commun.* **6**, 6195. doi:10.1038/ncomms7195
- Matsunaga, S., Jeremiah, S. S., Miyakawa, K., Kurotaki, D., Shizukuishi, S., Watashi, K., Nishitsuji, H., Kimura, H., Tamura, T., Yamamoto, N. et al.** (2020). Engineering cellular biosensors with customizable antiviral responses targeting Hepatitis B virus. *iScience* **23**, 100867. doi:10.1016/j.isci.2020.100867
- McBurney, M. W., Sutherland, L. C., Adra, C. N., Leclair, B., Rudnicki, M. A. and Jardine, K.** (1991). The mouse Pdgk-1 gene promoter contains an upstream activator sequence. *Nucleic Acids Res.* **19**, 5755-5761. doi:10.1093/nar/19.20.5755
- Monetti, C., Nishino, K., Biechele, S., Zhang, P., Baba, T., Woltjen, K. and Nagy, A.** (2011). PhiC31 integrase facilitates genetic approaches combining multiple recombinases. *Methods* **53**, 380-385. doi:10.1016/j.ymeth.2010.12.023
- Morsut, L., Roybal, K. T., Xiong, X., Gordley, R. M., Coyle, S. M., Thomson, M. and Lim, W. A.** (2016). Engineering customized cell sensing and response behaviors using synthetic Notch receptors. *Cell* **164**, 780-791. doi:10.1016/j.cell.2016.01.012
- Mort, R. L., Ford, M. J., Sakaue-Sawano, A., Lindstrom, N. O., Casadio, A., Douglas, A. T., Keighren, M. A., Hohenstein, P., Miyawaki, A. and Jackson, I. J.** (2014). Fucci2a: a bicistronic cell cycle reporter that allows Cre mediated tissue specific expression in mice. *Cell Cycle* **13**, 2681-2696. doi:10.4161/15384101.2015.945381
- Nishida-Aoki, N. and Gujral, T. S.** (2019). Emerging approaches to study cell-cell interactions in tumor microenvironment. *Oncotarget* **10**, 785-797. doi:10.18632/oncotarget.26585
- Niwa, H., Yamamura, K. and Miyazaki, J.** (1991). Efficient selection for high-expression transfectants with a novel eukaryotic vector. *Gene* **108**, 193-199. doi:10.1016/0378-1119(91)90434-D
- Nowotschin, S. and Hadjantonakis, A.-K.** (2010). Cellular dynamics in the early mouse embryo: from axis formation to gastrulation. *Curr. Opin. Genet. Dev.* **20**, 420-427. doi:10.1016/j.gde.2010.05.008
- Nowotschin, S., Eakin, G. S. and Hadjantonakis, A.-K.** (2009). Dual transgene strategy for live visualization of chromatin and plasma membrane dynamics in murine embryonic stem cells and embryonic tissues. *Genesis* **47**, 330-336. doi:10.1002/dvg.20500
- Ombrato, L., Nolan, E., Kurelac, I., Mavousian, A., Bridgeman, V. L., Heinze, I., Chakravarty, P., Horswell, S., Gonzalez-Gualda, E., Maccacchione, G. et al.** (2019). Metastatic-niche labelling reveals parenchymal cells with stem features. *Nature* **572**, 603-608. doi:10.1038/s41586-019-1487-6
- Pera, M. F. and Tam, P. P. L.** (2010). Extrinsic regulation of pluripotent stem cells. *Nature* **465**, 713-720. doi:10.1038/nature09228
- Perez, S. E., Rebelo, S. and Anderson, D. J.** (1999). Early specification of sensory neuron fate revealed by expression and function of neurogenins in the chick embryo. *Development* **126**, 1715-1728. doi:10.1242/dev.126.8.1715
- Pfaff, N., Lachmann, N., Ackermann, M., Kohlscheen, S., Brendel, C., Maetzig, T., Niemann, H., Antoniou, M. N., Grez, M., Schambach, A. et al.** (2013). A ubiquitous chromatin opening element prevents transgene silencing in pluripotent stem cells and their differentiated progeny. *Stem Cells* **31**, 488-499. doi:10.1002/stem.1316
- Pfeifer, A., Ikawa, M., Dayn, Y. and Verma, I. M.** (2002). Transgenesis by lentiviral vectors: lack of gene silencing in mammalian embryonic stem cells and preimplantation embryos. *Proc. Natl. Acad. Sci. USA* **99**, 2140-2145. doi:10.1073/pnas.251682798
- Posfai, E., Lanner, F., Mulas, C. and Leitch, H. G.** (2021). All models are wrong, but some are useful: establishing standards for stem cell-based embryo models. *Stem Cell Rep.* **16**, 1117-1141. doi:10.1016/j.stemcr.2021.03.019
- Rao, C., Malaguti, M., Mason, J. O. and Lowell, S.** (2020). The transcription factor E2A drives neural differentiation in pluripotent cells. *Development* **147**, dev184093. doi:10.1242/dev.184093
- Rhee, J. M., Pirity, M. K., Lackan, C. S., Long, J. Z., Kondoh, G., Takeda, J. and Hadjantonakis, A.-K.** (2006). In vivo imaging and differential localization of lipid-modified GFP-variant fusions in embryonic stem cells and mice. *Genesis* **44**, 202-218. doi:10.1002/dvg.20203
- Rossant, J. and Tam, P. P. L.** (2009). Blastocyst lineage formation, early embryonic asymmetries and axis patterning in the mouse. *Development* **136**, 701-713. doi:10.1242/dev.017178
- Roybal, K. T., Williams, J. Z., Morsut, L., Rupp, L. J., Kolinko, I., Choe, J. H., Walker, W. J., McNally, K. A. and Lim, W. A.** (2016). Engineering T cells with customized therapeutic response programs using synthetic notch receptors. *Cell* **167**, 419-432.e16. doi:10.1016/j.cell.2016.09.011
- Sancho, M., Di-Gregorio, A., George, N., Pozzi, S., Sánchez, J. M., Pernaute, B. and Rodríguez, T. A.** (2013). Competitive interactions eliminate unfit embryonic

- stem cells at the onset of differentiation. *Dev. Cell* **26**, 19-30. doi:10.1016/j.devcel.2013.06.012
- Santorelli, M., Lam, C. and Morsut, L.** (2019). Synthetic development: building mammalian multicellular structures with artificial genetic programs. *Curr. Opin. Biotechnol.* **59**, 130-140. doi:10.1016/j.copbio.2019.03.016
- Schlissel, G. and Li, P.** (2020). Synthetic developmental biology: understanding through reconstitution. *Annu. Rev. Cell Dev. Biol.* **36**, 339-357. doi:10.1146/annurev-cellbio-020620-090650
- Schultz, R. M.** (1985). Roles of cell-to-cell communication in development. *Biol. Reprod.* **32**, 27-42. doi:10.1095/biolreprod32.1.27
- Seibler, J., Küter-Luks, B., Kern, H., Streu, S., Plum, L., Mauer, J., Kühn, R., Brüning, J. C. and Schwenk, F.** (2005). Single copy shRNA configuration for ubiquitous gene knockdown in mice. *Nucleic Acids Res.* **33**, e67-e67. doi:10.1093/nar/gni065
- Sekine, R., Shibata, T. and Ebisuya, M.** (2018). Synthetic mammalian pattern formation driven by differential diffusivity of Nodal and Lefty. *Nat. Commun.* **9**, 5456. doi:10.1038/s41467-018-07847-x
- Sevcsik, E., Brameshuber, M., Fölser, M., Weghuber, J., Honigmann, A. and Schütz, G. J.** (2015). GPI-anchored proteins do not reside in ordered domains in the live cell plasma membrane. *Nat. Commun.* **6**, 6969. doi:10.1038/ncomms7969
- Sgodda, M., Alfken, S., Schambach, A., Eggenschwiler, R., Fidzinski, P., Hummel, M. and Cantz, T.** (2020). Synthetic notch-receptor-mediated transmission of a transient signal into permanent information via CRISPR/Cas9-based genome editing. *Cells* **9**, 1929. doi:10.3390/cells9091929
- Shcherbo, D., Murphy, C. S., Ermakova, G. V., Solovieva, E. A., Chepurnykh, T. V., Shcheglov, A. S., Verkhusha, V. V., Pletnev, V. Z., Hazelwood, K. L., Roche, P. M. et al.** (2009). Far-red fluorescent tags for protein imaging in living tissues. *Biochem. J.* **418**, 567-574. doi:10.1042/BJ20081949
- Shioi, G., Kiyonari, H., Abe, T., Nakao, K., Fujimori, T., Jang, C.-W., Huang, C.-C., Akiyama, H., Behringer, R. R. and Aizawa, S.** (2011). A mouse reporter line to conditionally mark nuclei and cell membranes for in vivo live-imaging. *Genesis* **49**, 570-578. doi:10.1002/dvg.20758
- Smithies, O., Gregg, R. G., Boggs, S. S., Koralewski, M. A. and Kucherlapati, R. S.** (1985). Insertion of DNA sequences into the human chromosomal β -globin locus by homologous recombination. *Nature* **317**, 230-234. doi:10.1038/317230a0
- Srivastava, S., Salter, A. I., Liggitt, D., Yechan-Gunja, S., Sarvothama, M., Cooper, K., Smythe, K. S., Dudakov, J. A., Pierce, R. H., Rader, C. et al.** (2019). Logic-gated ROR1 chimeric antigen receptor expression rescues T cell-mediated toxicity to normal tissues and enables selective tumor targeting. *Cancer Cell* **35**, 489-503.e8. doi:10.1016/j.ccell.2019.02.003
- Stern, C.** (1936). Somatic crossing over and segregation in drosophila melanogaster. *Genetics* **21**, 625-730. doi:10.1093/genetics/21.6.625
- Tam, P. P. L. and Loebel, D. A. F.** (2007). Gene function in mouse embryogenesis: get set for gastrulation. *Nat. Rev. Genet.* **8**, 368-381. doi:10.1038/nrg2084
- Tang, R., Murray, C. W., Linde, I. L., Kramer, N. J., Lyu, Z., Tsai, M. K., Chen, L. C., Cai, H., Gitler, A. D., Engleman, E. et al.** (2020). A versatile system to record cell-cell interactions. *Elife* **9**, e61080. doi:10.7554/eLife.61080
- Tchorz, J. S., Suply, T., Ksiazek, I., Giachino, C., Cloëtta, D., Danzer, C.-P., Doll, T., Isken, A., Lemaistre, M., Taylor, V. et al.** (2012). A Modified RMCE-compatible Rosa26 locus for the expression of transgenes from exogenous promoters. *PLoS One* **7**, e30011. doi:10.1371/journal.pone.0030011
- Toda, S., Blanch, L. R., Tang, S. K. Y., Morsut, L. and Lim, W. A.** (2018). Programming self-organizing multicellular structures with synthetic cell-cell signaling. *Science* **361**, 156-162. doi:10.1126/science.aat0271
- Toda, S., McKeithan, W. L., Hakkinen, T. J., Lopez, P., Klein, O. D. and Lim, W. A.** (2020). Engineering synthetic morphogen systems that can program multicellular patterning. *Science* **370**, 327-331. doi:10.1126/science.abc0033
- Tosti, L., Ashmore, J., Tan, B. S. N., Carbone, B., Mistri, T. K., Wilson, V., Tomlinson, S. R. and Kaji, K.** (2018). Mapping transcription factor occupancy using minimal numbers of cells in vitro and in vivo. *Genome Res.* **28**, 592-605. doi:10.1101/gr.227124.117
- Toth, T., Balassa, T., Bara, N., Kovacs, F., Kriston, A., Molnar, C., Haracska, L., Sukosd, F. and Horvath, P.** (2018). Environmental properties of cells improve machine learning-based phenotype recognition accuracy. *Sci. Rep.* **8**, 10085. doi:10.1038/s41598-018-28482-y
- Velkey, J. M. and O'Shea, K. S.** (2013). Expression of neurogenin 1 in mouse embryonic stem cells directs the differentiation of neuronal precursors and identifies unique patterns of down-stream gene expression. *Dev. Dyn.* **242**, 230-253. doi:10.1002/dvdy.23920
- Wang, L., Long, J., Chen, H., Sun, S., Lv, K., Li, Q. and Wang, X.** (2021). Manipulation of focal Wnt activity via synthetic cells in a double-humanized zebrafish model of tumorigenesis. *Int. J. Cancer* **148**, 2815-2824. doi:10.1002/ijc.33458
- Whittingham, D. G.** (1974). Embryo banks in the future of developmental genetics. *Genetics* **78**, 395-402. doi:10.1093/genetics/78.1.395
- Wu, G., Liu, N., Rittelmeyer, I., Sharma, A. D., Sgodda, M., Zaehres, H., Bleidiš, M., Greber, B., Gentile, L., Han, D. W. et al.** (2011). Generation of healthy mice from gene-corrected disease-specific induced pluripotent stem cells. *PLoS Biol.* **9**, e1001099. doi:10.1371/journal.pbio.1001099
- Yang, Z.-J., Yu, Z.-Y., Cai, Y.-M., Du, R.-R. and Cai, L.** (2020). Engineering of an enhanced synthetic Notch receptor by reducing ligand-independent activation. *Commun. Biol.* **3**, 116. doi:10.1038/s42003-020-0848-xdoi:10.1038/s42003-019-0734-6
- Yang, B. A., Westerhof, T. M., Sabin, K., Merajver, S. D. and Aguilar, C. A.** (2021). Engineered tools to study intercellular communication. *Adv. Sci.* **8**, 2002825. doi:10.1002/advs.202002825
- Yuan, L. and Hassan, B. A.** (2014). Neurogenins in brain development and disease: an overview. *Arch. Biochem. Biophys.* **558**, 10-13. doi:10.1016/j.abb.2014.05.028
- Zhu, I., Liu, R., Garcia, J. M., Hyrenius-Wittsten, A., Piraner, D. I., Alavi, J., Israni D. V., Liu, B., Khalil A. S. and Roybal K. T.** (2022). Modular design of synthetic receptors for programmed gene regulation in cell therapies. *Cell* **185**, 1431-1443.e16. doi:10.1016/j.cell.2022.03.023

Supplementary Materials and Methods

Design and characterisation of an “all-in-one” design for mCherry inducible receiver cells

We generated a donor plasmid for recombination-mediated cassette exchange (RMCE) into EM35 cells, with a Pac (puromycin resistance) gene for positive selection of recombinant clones, and convenient restriction sites for the inclusion of several transcriptional units. We made use of this tool to generate ESC clonal lines containing the SynNotch receptor, the constitutive tagBFP transgene and the TRE-mCherry all within the *Rosa26* locus (Figs. S4-S6). We named these cells SNCB, for SynNotch-mCherry-tagBFP. The tagBFP and TRE-mCherry cassettes were either placed on the + strand (SNCB+, Fig. S4A) or on the - strand (SNCB-, Fig. S6A).

We screened 30 SNCB+ clones by analysing the levels of mCherry and tagBFP fluorescence in the absence of sender cells (Fig. S4B-E). Although all clones should be genetically identical, we observed variation between them: 2 clones expressed no mCherry nor tagBFP, suggesting they may have integrated only part of the construct, whereas the remaining 28 clones had broad variations in tagBFP expression, with a subset of tagBFP-high cells displaying low levels of mCherry expression (Fig. S4E). We selected two clones with low levels of mCherry leakiness (SNCB+4, SNCB+16) and co-cultured these with 4 different sender clones for 24 hours, a period of time shown to be sufficient for mCherry induction by SynNotch in L929 fibroblasts (Morsut et al., 2016) (Fig. S5A-L). The small subset of mCherry-leaky cells induced mCherry to higher levels, suggesting that the system was functional in this subset of cells, but the majority (>90%) of cells remained mCherry-negative (Figs. S5E,F,K,L). In order to exclude the unlikely possibility that lack of mCherry induction in receiver ESCs was due to lack of interaction with sender cells, we imaged SNCB+4 cells cultured alone or in the presence of CHmGMP19 sender cells for 24 hours. We did not observe mCherry expression in the absence of sender cells, but, as seen in the flow cytometry data, a proportion of cells did not express tagBFP either (Fig. S5M). We observed mCherry induction in a small number of cells following co-culture with sender cells, but most EGFP-negative cells in contact with EGFP-positive sender cells did not induce mCherry expression (Fig. S5M).

We then screened 7 SNCB- clones as above (Fig. S6B-E). The fluorescence distribution looked radically different from the SNCB+ clones, with only one clone (SNCB-6) displaying a clear tagBFP-positive subpopulation of cells (Fig. S6E). Co-culture with sender cells for 24h resulted in higher levels of mCherry expression in this subpopulation, which suggests the system is functional in these cells, but approximately half of the cells in this clone remained mCherry-negative (Fig. S6E).

Taken together, these results suggest that subsets of cells within SNCB+ and SNCB- clonal lines have the capability of functioning as SynNotch receiver cells. We therefore asked whether isolation and re-cloning of these cells may lead to the generation of functional SynNotch receiver lines.

We attempted to subclone cells from the SNCB+4 and SNCB-6 lines by sorting single cells based on their tagBFP and mCherry levels and generating new clonal lines. We selected cells which were tagBFP-high and mCherry-low in the absence of sender cells (+4BHCL, -6BHCL), tagBFP-high and mCherry-high in the presence of sender cells (+4BHCH, -6BHCH), and rare SNCB+4 cells which were tagBFP-medium and mCherry-positive in the presence of sender cells (+4BMC+) (Figs. S7A-C, S8A-C). After clonal expansion, a subset of cells in all clones lost tagBFP and mCherry expression, with overall tagBFP and mCherry expression patterns looking remarkably similar to those of the two parental lines. +4BHCH and -6BHCH cells had slightly better inducibility than the parental lines, but a significant proportion of cells lost tagBFP and mCherry expression (Figs. S7D-F, S8D,E). This suggests that sorting and subcloning of SNCB+4 and SNCB-6 cells did not result in the generation of functional receiver ESCs.

We next asked whether lack of mCherry induction in receiver cells could be ascribable to the SynNotch receptor construct not being expressed by all cells. We stained wild-type, SNCB+4 and CHmGMP19 cells for Myc expression (Fig. S9); a Myc tag is present on both the SynNotch receptor construct and the extracellular EGFP in CHmGMP19 cells (Figs. 2B,J, S4A). We found that although all SNCB+4 cells expressed Myc above background level, its pattern of expression only appeared to be consistent with cell membrane localisation in a subset of cells. Furthermore, the levels of expression were significantly lower than those of Myc-EGFP in CHmGMP19 sender cells (Fig. S9).

In summary, receiver cell lines harbouring all three transcriptional units required for SynNotch receiver function within the *Rosa26* landing pad do not exhibit uniform behaviour, displaying variable levels of tagBFP, variable inducibility of mCherry, and low levels of the SynNotch receptor. Despite this, mCherry is induced by subpopulations of tagBFP-positive receiver cells in response to interaction with EGFP-positive sender cells. These results suggest that the SynNotch receptor construct and TRE-mCherry cassette can function as expected in ESCs, but that further optimisation is required to obtain a reliable contact-reporting system. We have included this suboptimal strategy in this report in order to inform researchers who wish to establish SynNotch technology in other experimental models of interest.

Generation and characterisation of synthetic stripe pattern of mCherry expression

In order to generate a stripe pattern of mCherry expression, 4×10^4 sender and STC receiver cells were plated in adjacent wells of a 3-well cell culture insert and left to attach and spread overnight. The next morning, wells were washed with PBS to remove any floating cells, and the insert was carefully removed to avoid detaching clumps of cells. The smaller the culture vessel the insert was housed in, the harder this became, with clumps of cells visibly detaching in small multiwell plates. Examples are displayed in Fig. S19A. Additional wash steps were used in these circumstances to reduce the risk of clumps settling down onto different cells and inducing mCherry expression before a linear border was formed (e.g. sender cells landing in the middle of the receiver “domain” or vice versa). This phenomenon could not always be prevented, and where possible we would recommend housing the insert onto a 24cm glass coverslip in a 6-well plate to reduce the risk of this process occurring.

Following insert removal, the expansion of sender and receiver cells was monitored in order to identify the time of initial contact. This varied between experiments, potentially as a result of leftover glue from the insert in the gap between sender and receiver cells affecting cell proliferation and migration. Initial contact was made approximately 48 hours after insert removal (Fig. S19A). Formation of a stripe along the entire length of the border was evident by 24 hours after initial contact (Fig. S19A), in line with the kinetics of mCherry upregulation in non-patterned culture (Fig. 4).

Timelapse imaging of stripe formation is complicated by the thickness and size of the structure to be imaged, which in our setup led to sample bleaching (Fig. S19B), making it inappropriate to draw fluorescence intensity-based conclusions.

Over time, the mCherry signal changes from a narrow signal at the point of contact to a diffuse gradient into the receiver cell domain (Fig. S19A,B). This is caused by several factors:

1. Sender cells can infiltrate into the receiver cell domain at the bottom of the dish, activating mCherry expression in patches of cells beyond the linear border (Fig. S19B).
2. Sender cells can migrate on top of receiver cells, activating mCherry induction beyond the linear border (Fig. S19C).
3. Activated receiver cells can divide perpendicularly to the linear border, contributing to diffusion of mCherry signal (Fig. S19B, yellow arrowheads).

Table S1. Reagents

REAGENT	SOURCE	IDENTIFIER	CONCENTRATION
Antibodies and nuclear counterstain			
Mouse monoclonal anti-Flag	Sigma-Aldrich	Cat# F3165; RRID: AB_259529	1:1000
Chicken polyclonal anti-GFP	Abcam	Cat# ab13970; RRID: AB_300798	1:1000
Goat polyclonal anti-Myc	Abcam	Cat# ab9132; RRID: AB_307033	1:1000
Mouse monoclonal anti-Myc AlexaFluor 488 conjugate	Santa Cruz	Cat# sc-40 AF488; RRID: AB_2892598	1:200
Rabbit polyclonal anti-LaminB1	Abcam	Cat#ab16048; RRID: AB_443298	1:1000
Rat monoclonal anti-mCherry	Invitrogen	Cat# M11217; RRID: AB_2536611	1:1000
Mouse monoclonal anti-Nup107 (NPC)	Abcam	Cat# ab24609; RRID: AB_448181	1:1000
Rabbit polyclonal anti-tRFP (tagBFP)	Evrogen	Cat# AB233; RRID: AB_2571743	1:1000
Mouse monoclonal anti-Tubb3	Biologend	Cat# 801201; RRID: AB_2313773	1:1000
DRAQ7	Abcam	Cat# ab109202	1 μ M (IF); 300 nM (flow cytometry)
DAPI	Biotium	Cat# 40043	1 μ M
Chemicals and solutions			
2-Mercaptoethanol	Gibco	Cat# 31350010	100 nM
Accutase	Sigma-Aldrich	A6964	
Benzyl alcohol	Alfa Aesar	Cat# 100-51-6	
Benzyl benzoate	Sigma	Cat# B9550	
Chorulon (hCG)	Intervet	Cat# CH-475-1	100 IU/ml
DAPT	Abcam	Cat# ab120633	100 μ M
DMEM, high glucose, no glutamine, no phenol red	Gibco	Cat# 31053028	
Donkey serum	Sigma-Aldrich	Cat# D9663	3% v/v
Doxycycline hyclate	Sigma-Aldrich	Cat# D9891	1 μ g/ml
Dulbecco's phosphate buffered saline (PBS)	Sigma-Aldrich	Cat# D8537	
Fibronectin from bovine plasma solution	Sigma-Aldrich	Cat# F1141	
Foetal calf serum	Life Technologies	Cat# 10270106	10% v/v
Formaldehyde 37-41%	Fisher Scientific	Cat# F/1501/PB08	4% w/v
Gelatin	Sigma-Aldrich	Cat# G1890	0.1% w/v
Geneticin (G418)	Gibco	Cat# 11811031	200 μ g/ml
Glasgow Minimum Essential Medium	Sigma-Aldrich	Cat# G5154	
Hygromycin B	Gibco	Cat# 10687010	200 μ g/ml

REAGENT	SOURCE	IDENTIFIER	CONCENTRATION
L-Glutamine	Thermo Scientific	Cat# 25030024	2 mM
Lipofectamine 3000 transfection reagent	Life Technologies	Cat# L3000008	
M2 medium	Sigma-Aldrich	Cat# M7167	
MEM Non-essential amino acids solution (100×)	Gibco	Cat# 11140050	1×
Penicillin/streptomycin	Gibco	Cat# 15140122	100 U/ml
PMSG	ProSpec	Cat# HOR-272	100 IU/ml
Prolong Gold Antifade Mountant	Thermo Fisher	Cat# P36930	
Puromycin dihydrochloride	Sigma-Aldrich	Cat# P8833	2 µg/ml
Sodium pyruvate	Gibco	Cat# 11360039	1 mM
Triton X-100	Sigma-Aldrich	Cat# X100	0.1% v/v
Trypsin EDTA 0.25%	Gibco	Cat# 25200072	0.05% w/v
Tyrode's solution, acidic	Sigma-Aldrich	Cat# T1788	
Zeocin	Gibco	Cat# R25001	100 µg/ml
Cell culture substrates and inserts			
3 well silicone culture insert	Ibidi	Cat# 80369	
µ-Slide 8 Well	Ibidi	Cat# 80826	
µ-Slide 4 Well	Ibidi	Cat# 80426	
µ-Plate 96 Well Black	Ibidi	Cat# 89626	
µ-Slide Angiogenesis, uncoated	Ibidi	Cat# 81501	
Glass coverslip, 24 mm diameter	VWR	Cat# 631-1583	
Plastic flasks and plates for routine cell culture	Corning	Various	
DNA constructs			
pHR_EGFpligand	Morsut et al. (2016)	Addgene 79129	
pHR_SFFV_LaG17_synNotch_TetRVP64	Morsut et al. (2016)	Addgene 79128	
pDisplay-EGFP-TM	Han et al. (2004)		
pHR_TRE-mCherry-PGK-tagBFP-WPRE	Elise Cachat, University of Edinburgh		
CAG-φC31 integrase	Monetti et al. (2011)	Similar plasmid available: Addgene 62658	
pRosa26-DEST-1lox	Tosti et al. (2018)		
pENTR-2xAttP50	Tosti et al. (2018)		
pENTR-2xAttB53	Tosti et al. (2018)		
pPyCAG-EGFP-TM-IRES-Pac	This study	Addgene 183603	
pPyPGK-EGFP-TM-IRES-Pac	This study	Addgene 183604	
pPyCAG-HA-EGFP-Myc-TM-IRES-Pac	This study	Addgene 183605	
pPyPGK-HA-EGFP-Myc-TM-IRES-Pac	This study	Addgene 183606	
pPyPGK-Myc-LaG17-Notch1TM-tTA-IRES-Ble	This study	Addgene 183607	
p PyCAG-tagBFP-3xNLS-IRES-Hph	This study	Addgene 183608	
pmROSA26-attP50-Neo-mKate2-3xNLS-attP50	This study	Addgene 183609	
attB53-Pac-attB53	This study	Addgene 183610	
attB53-Pac-TRE-mCherry-attB53	This study	Addgene 183611	
attB53-Pac-tetO-mCherry-attB53	This study	Addgene 183612	
attB53-Pac-TRE-3xFlag-Neurog1-attB53	This study	Addgene 183613	
attB53_SNCB+_attB53	This study	Addgene 183614	
attB53_SNCB-_attB53	This study	Addgene 183615	
Cell lines			
E14Ju09 mouse ESCs (129/Ola, male)	Hamilton and		

REAGENT	SOURCE	IDENTIFIER	CONCENTRATION
	Brickman (2014)		
CmGP1 sender mouse ESCs (129/Ola, male)	This study		
CHmGMP19 sender mouse ESCs (129/Ola, male)	This study		
CmGP1GH1 sender mouse ESCs (129/Ola, male)	This study		
E14GIP1 mouse ESCs (129/Ola, male)	This study		
EM35 mouse ESCs (129/Ola, male)	This study		
SNCB+ receiver mouse ESCs (129/Ola, male)	This study		
SNCB- receiver mouse ESCs (129/Ola, male)	This study		
35SRZ mouse ESCs (129/Ola, male)	This study		
PSNB mouse ESCs (129/Ola, male)			
PSNB-E mouse ESCs (129/Ola, male)	This study		
PSNB-tetO receiver mouse ESCs (129/Ola, male)	This study		
STC receiver mouse ESCs (129/Ola, male)	This study		
STN receiver mouse ESCs (129/Ola, male)	This study		

FIGURE S1

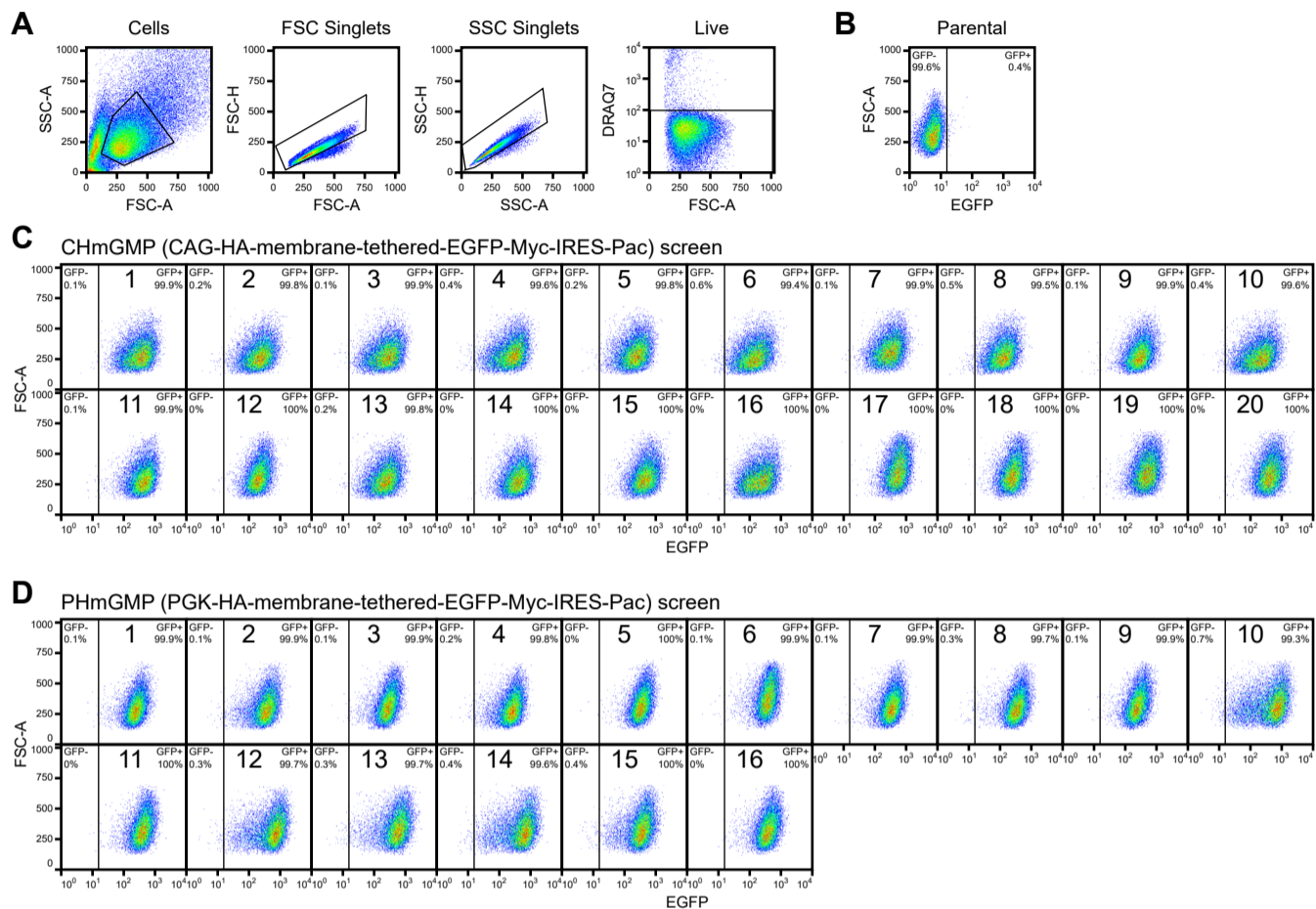


Fig. S1. Screening of HA- and Myc-tagged EGFP clonal sender ESC lines.

(A) Flow cytometry gating strategy to analyse single live cells, making use of forward scatter (FSC) and side scatter (SSC) height (H) and amplitude (A), and of the cell-impermeable DRAQ7 nuclear counterstain. (B) EGFP fluorescence distribution in parental wild-type cells. (C-D) EGFP fluorescence distribution in (C) CHmGMP and (D) PHmGMP clones. Percentages of EGFP-positive and -negative cells are indicated in figure. 15000 cells were analysed for each sample in (B-D). All units of measurement are arbitrary fluorescence units (A.F.U.). n=1.

FIGURE S2

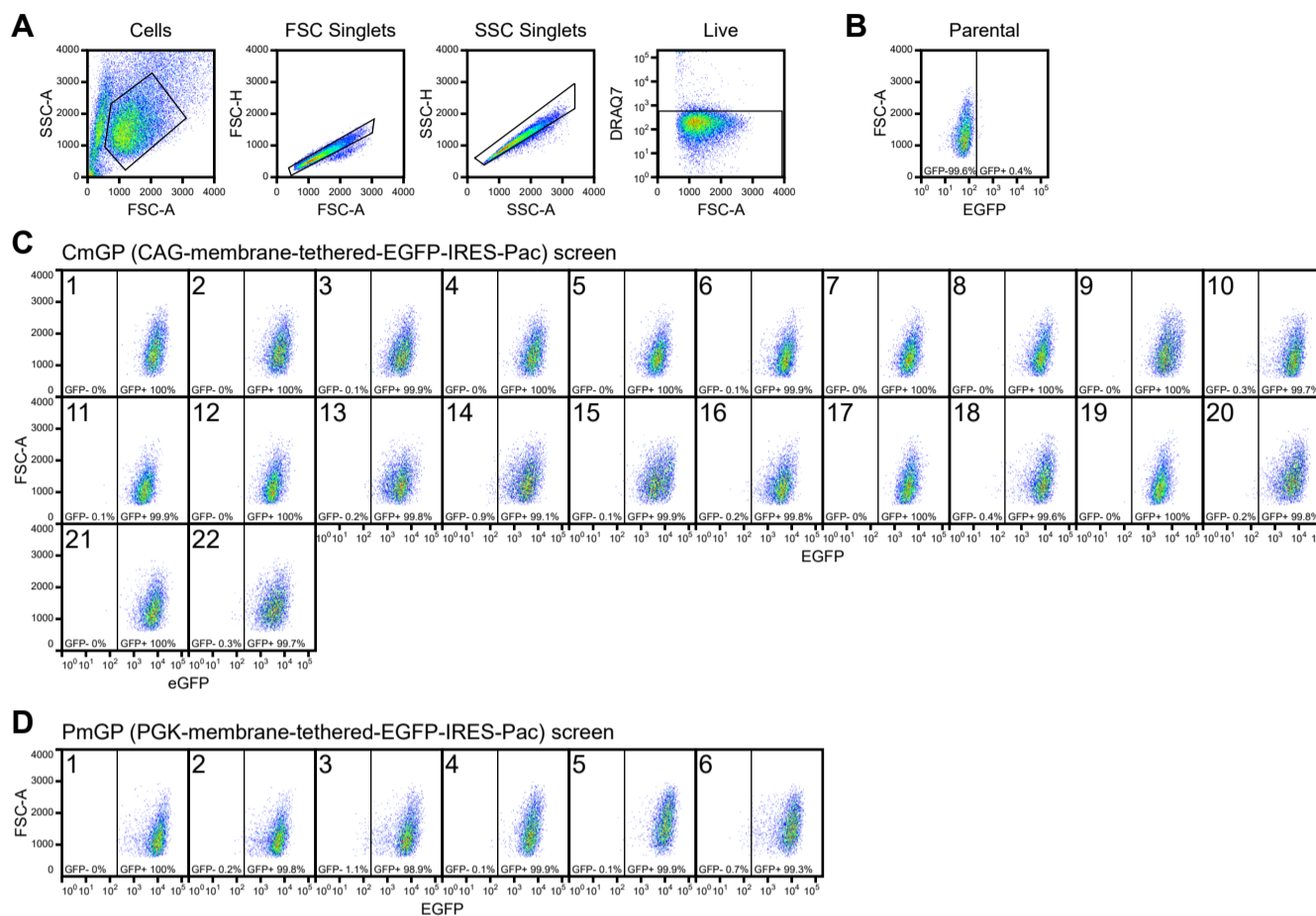


Fig. S2. Screening of untagged EGFP clonal sender ESC lines.

(A) Flow cytometry gating strategy to analyse single live cells. (B) EGFP fluorescence distribution in parental wild-type cells. (C-D) EGFP fluorescence distribution in (C) CmGP and (D) PmGP clones. Percentages of EGFP-positive and -negative cells are indicated in figure. 5000 cells were analysed for each sample in (B-D). All units of measurement are arbitrary fluorescence units (A.F.U.), and values are not directly comparable to those in Fig. S1. n=1.

FIGURE S3

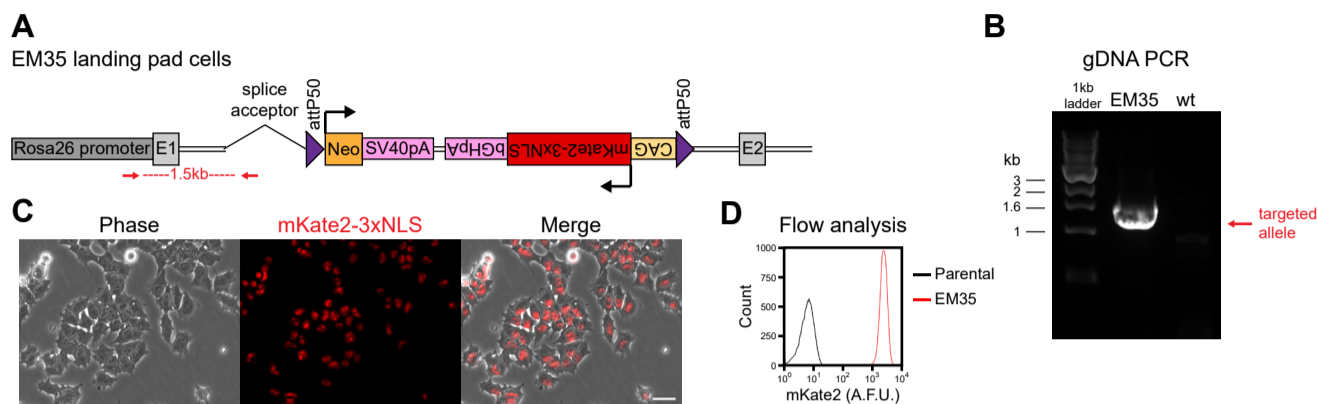
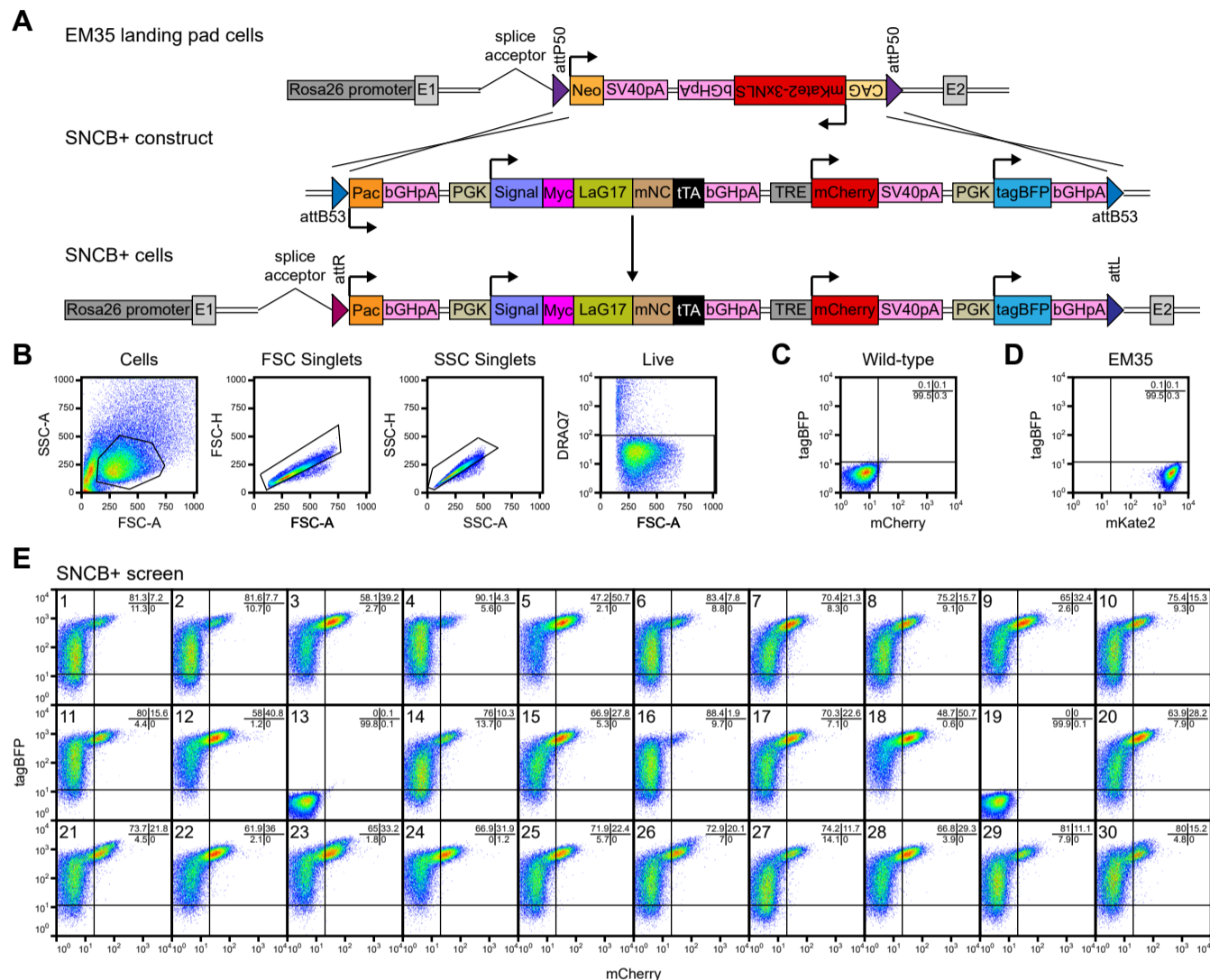


Fig. S3. Generation of a safe harbour site landing pad master ESC line.

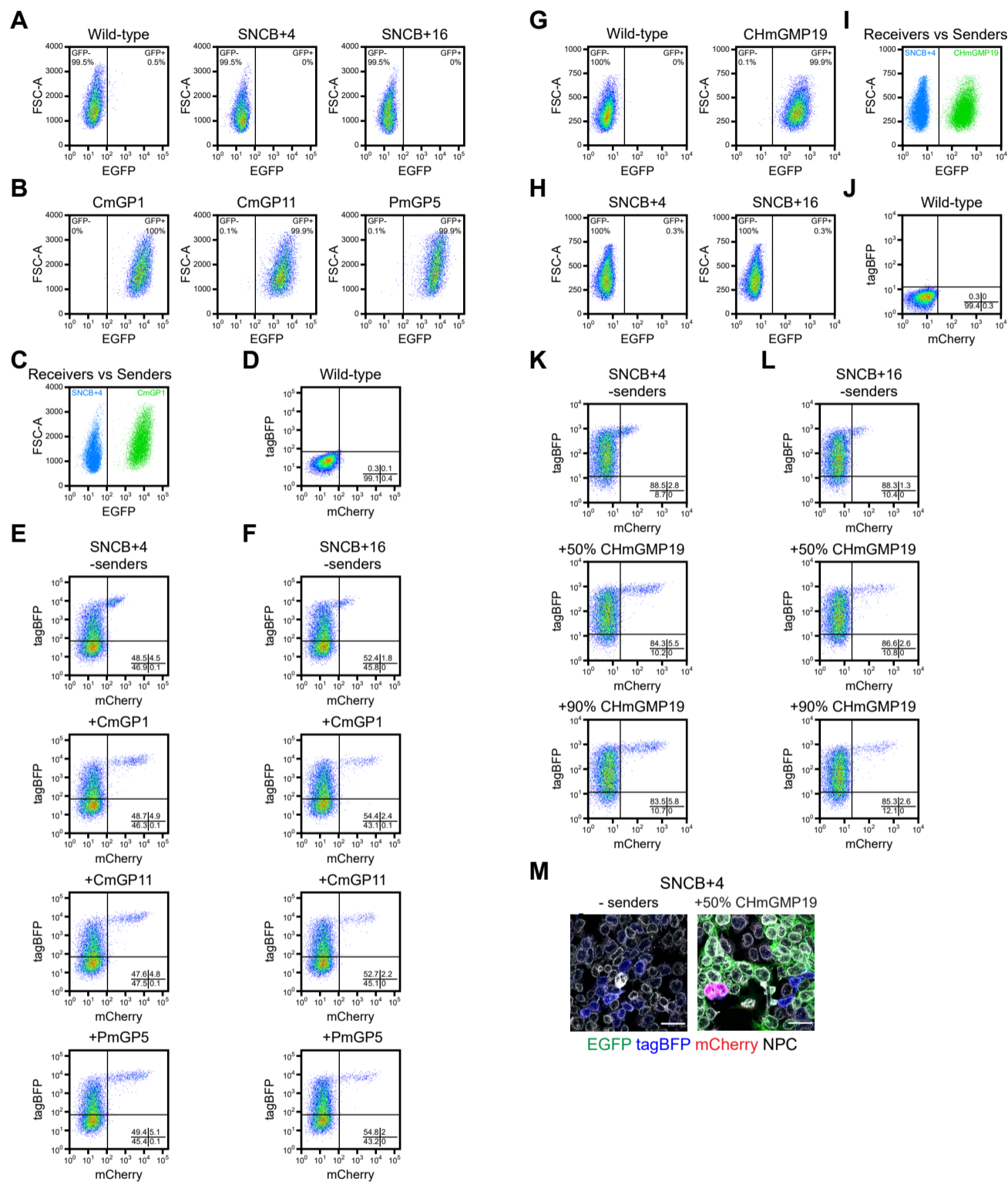
(A) Diagram of targeted *Rosa26* allele in EM35 landing pad RMCE clonal ESC line. Locations of primers for testing of correct targeting event are shown as red arrows. Abbreviations: E1: exon 1; E2: exon 2. (B) Genomic DNA PCR validation of correct landing pad insertion at the *Rosa26* locus, using the primers shown in (A). Expected band sizes: correct targeting event: 1534bp; wild-type: no amplification. Abbreviations: gDNA: genomic DNA; wt: parental wild-type. (C) Phase-contrast and mKate2-3xNLS images of live EM35 ESCs, showing nuclear mKate2 signal in all cells. Scale bar: 30µm. (D) Flow cytometry analysis of mKate2-3xNLS expression in parental wild-type and EM35 cells. 20000 cells are displayed for each sample. Data from a single experiment, representative of five biological replicates.

FIGURE S4

**Fig. S4. Generation and screening of SNCB+ clonal receiver ESC lines.**

(A) Strategy to replace Neo-mKate2 cassette with SNCB+ cassette in EM35 landing pad ESCs through ϕ C31 integrase-mediated RMCE. (B) Flow cytometry gating strategy to analyse single live cells. (C) tagBFP and mCherry fluorescence distribution in wild-type ESCs. (D) tagBFP and mKate2 fluorescence distribution in parental EM35 landing pad ESCs. The same laser/filter combinations were used to detect both mKate2 and mCherry fluorescence. (E) tagBFP and mCherry fluorescence distribution in SNCB+ clonal ESC lines cultured in the absence of sender cells. Percentages of cells in each quadrant are indicated in figure. 35000 cells were analysed for each sample in (C-E). All units of measurement are arbitrary fluorescence units (A.F.U.). $n=1$.

FIGURE S5

**Fig. S5. Screening of SNCB+ clones 4 and 16.**

(A-B) EGFP fluorescence distribution in (A) wild-type, SNCB+4, SNCB+16 receiver cells and (B) CmGP1, CmGP11, PmGP5 sender cells. (C) Comparison of EGFP fluorescence distribution in SNCB+4 receiver cells and CmGP1 sender cells. The two cell populations can be separated in co-culture experiments on the basis of EGFP expression. (D) tagBFP and mCherry fluorescence distributions in wild-type cells. (E-F) tagBFP and mCherry fluorescence distributions in (E) SNCB+4 and (F) SNCB+16 receiver ESCs cultured alone or in the presence of CmGP1, CmGP11, PmGP5 sender ESCs for 24 hours. All units of measurement are arbitrary fluorescence units (A.F.U.). (G-H) EGFP fluorescence distribution in (G) wild-type, CHmGMP19 sender cells and (H) SNCB+ clones 4 and 16 receiver cells. (I) Comparison of EGFP fluorescence distribution in SNCB+4 receiver cells and CHmGMP19 sender cells. The two cell populations can be separated in co-culture experiments on the basis of EGFP expression. (J) tagBFP and mCherry fluorescence distributions in wild-type cells. (K-L) tagBFP and mCherry fluorescence distributions in (K) SNCB+4 and (L) SNCB+16 receiver ESCs cultured alone or in the presence of CHmGMP19 sender ESCs at 1:1 and 9:1 sender:receiver cell ratios for 24 hours. Experiments in panels (A-F) were carried out separately from those in panels (G-L) and fluorescence intensity values are not directly comparable. 15000 cells are displayed in plots in (D-F, G,H, J-L), 15000 cells/sample are displayed in plot in (I), 10000 cells are displayed in plots in (A,B), 10000 cells/sample are displayed in plot in (C). (M) Immunofluorescence of SNCB+4 cells cultured alone or in the presence of CHmGMP19 sender cells for 24 hours (1:1 sender:receiver cell ratio). Scale bar: 30µm. n=1.

FIGURE S6

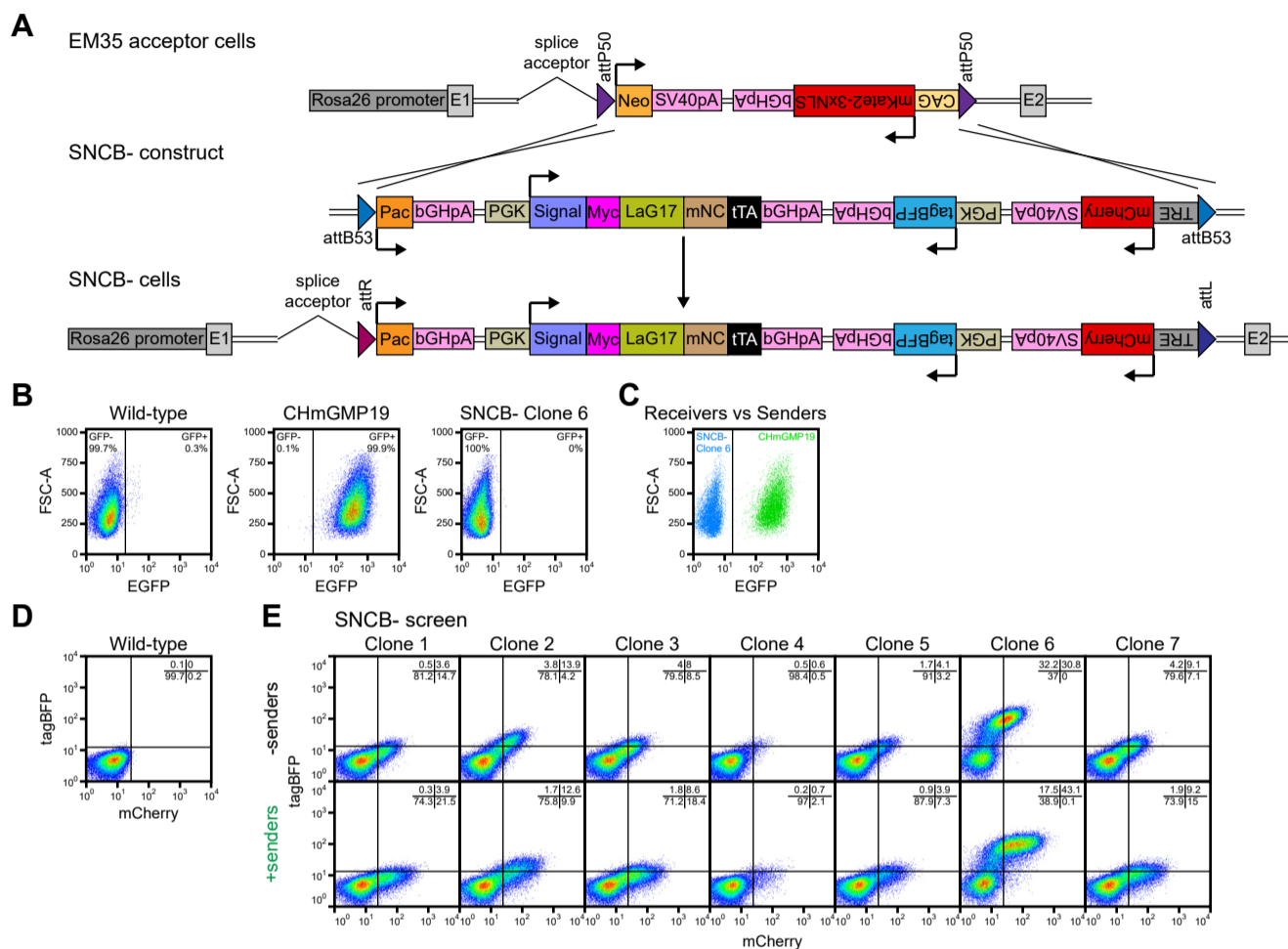


Fig. S6. Generation and screening of SNCB- clonal receiver ESC lines.

(A) Strategy to replace Neo-mKate2 cassette with SNCB- cassette in EM35 landing pad ESCs through ϕ C31 integrase-mediated RMCE. (B) EGFP fluorescence distribution in wild-type, CHmGMP19 sender cells and SNCB- clone 6 receiver cells. (C) Comparison of EGFP fluorescence distribution in SNCB- clone 6 receiver cells and CHmGMP19 sender cells. The two cell populations can be separated in co-culture experiments on the basis of EGFP expression. (D) tagBFP and mCherry fluorescence distribution in wild-type ESCs. (E) tagBFP and mCherry fluorescence distribution in SNCB- clonal ESC lines cultured alone or in the presence of CHmGMP19 sender cells for 24 hours. Percentages of cells in each quadrant are indicated in figure. 35000 cells are displayed in plots in (B), 35000 cells/sample are displayed in plot in (C), 50000 cells are displayed in plots in (D-E). All units of measurement are arbitrary fluorescence units (A.F.U.). n=1.

FIGURE S7

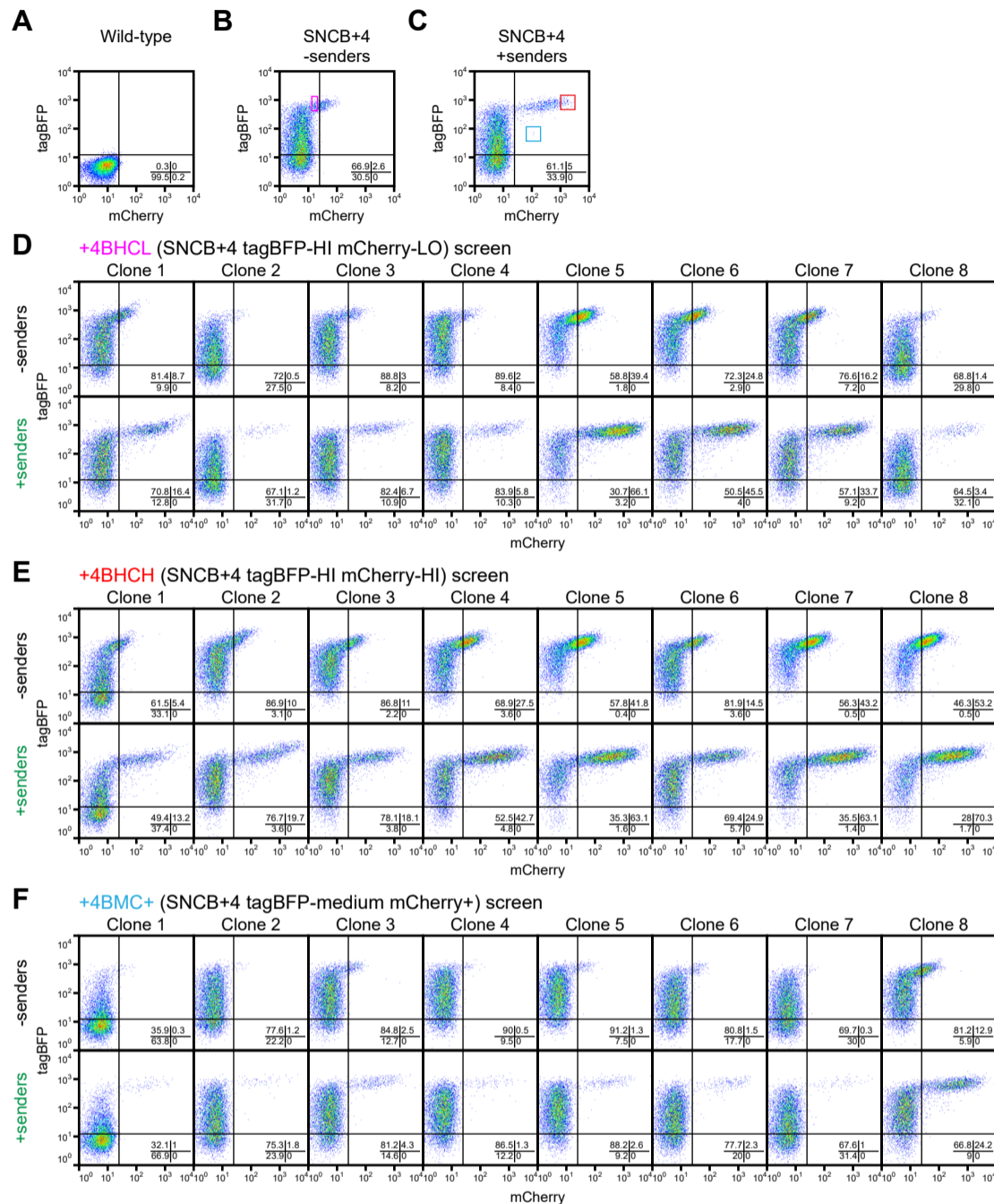
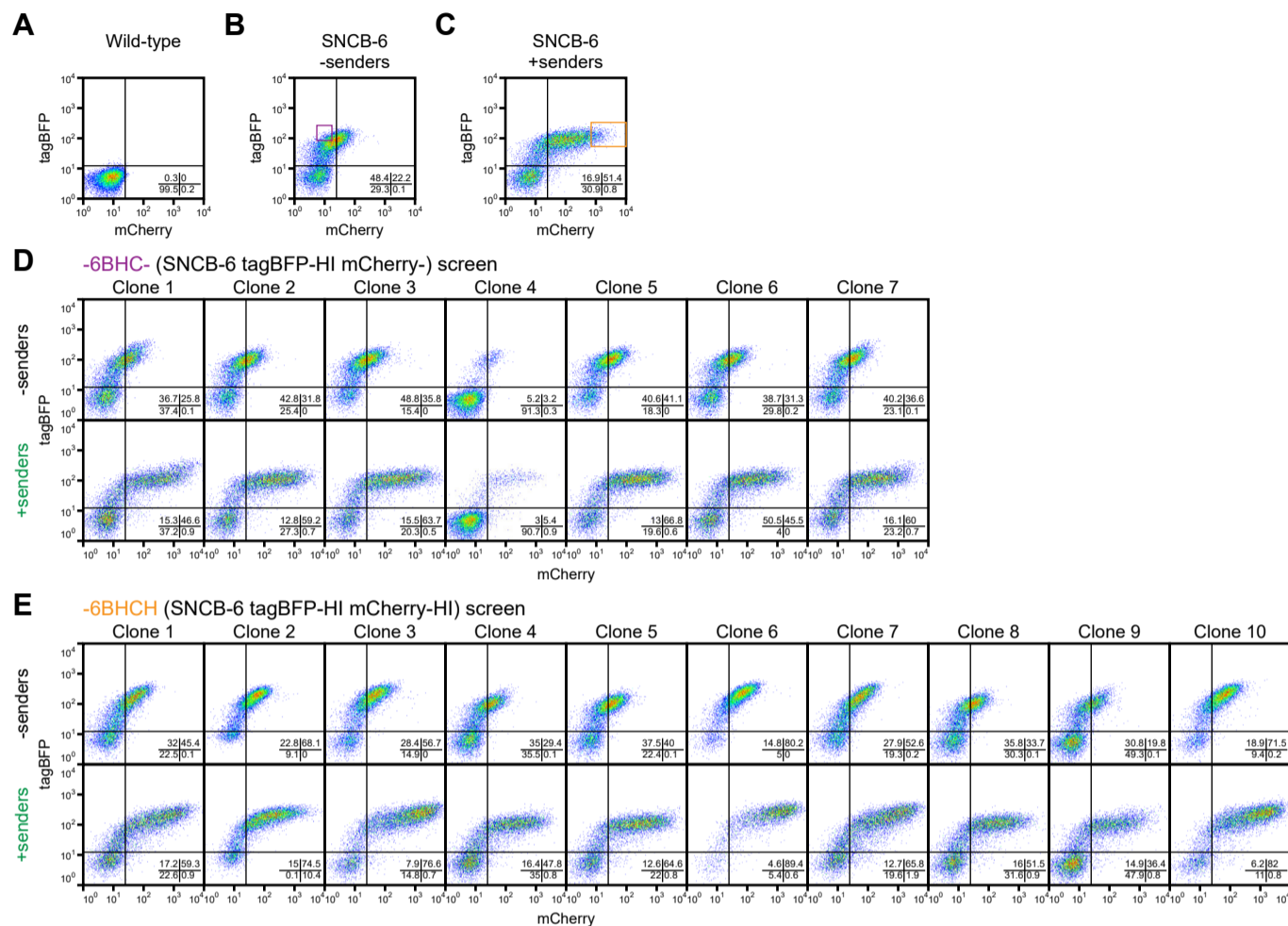


Fig. S7. Derivation of clonal ESC lines through sorting of SNCB+4 ESCs.

(A) tagBFP and mCherry fluorescence distribution in wild-type ESCs. (B) tagBFP and mCherry fluorescence distribution in SNCB+4 ESCs cultured in the absence of sender cells. Sorting gate for derivation of SNCB+4 tagBFP-HI mCherry-LO (+4BHCL) clonal sorted lines is shown in magenta. (C) tagBFP and mCherry fluorescence distribution in SNCB+4 ESCs co-cultured with CHmGMP19 sender cells for 24 hours. Sorting gate for derivation of SNCB+4 tagBFP-HI mCherry-HI (+4BHCH) clonal sorted lines is shown in red, sorting gate for derivation of SNCB+4 tagBFP-Medium mCherry+ (+4BMC+) clonal sorted lines is shown in blue. (D-F) tagBFP and mCherry fluorescence distribution in (D) +4BHCL, (E) +4BHCH and (F) +4BMC+ receiver ESCs cultured alone or in the presence of CHmGMP19 sender cells for 24 hours. Percentages of cells in each quadrant are indicated in figure. 15000 cells are displayed in plots in (A-C), 10000 cells are displayed in plots in (D-F). All units of measurement are arbitrary fluorescence units (A.F.U.). n=1.

FIGURE S8

**Fig. S8. Derivation of clonal ESC lines through sorting of SNCB-6 ESCs.**

(A) tagBFP and mCherry fluorescence distribution in wild-type ESCs. (B) tagBFP and mCherry fluorescence distribution in SNCB-6 ESCs cultured in the absence of sender cells. Sorting gate for derivation of SNCB-6 tagBFP-HI mCherry- (-6BHC-) clonal sorted lines is shown in purple. (C) tagBFP and mCherry fluorescence distribution in SNCB-6 ESCs co-cultured with CHmGMP19 sender cells for 24 hours. Sorting gate for derivation of SNCB-6 tagBFP-HI mCherry-HI (-6BHCH) clonal sorted lines is shown in orange. (D-E) tagBFP and mCherry fluorescence distribution in (D) -6BHC- and (E) -6BHCH receiver ESCs cultured alone or in the presence of CHmGMP19 sender cells for 24 hours. Percentages of cells in each quadrant are indicated in figure. 15000 cells are displayed in plots in (A-C), 10000 cells are displayed in plots in (D-E). All units of measurement are arbitrary fluorescence units (A.F.U.). n=1.

FIGURE S9

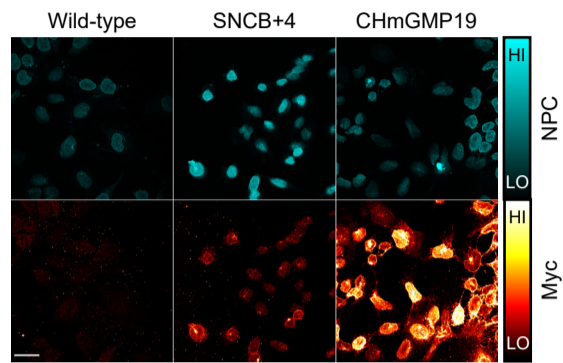
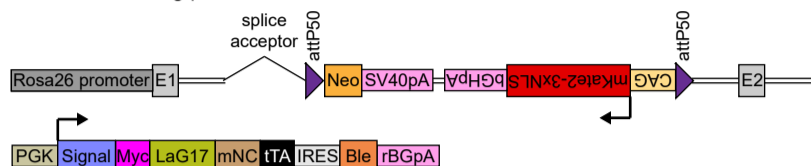


Fig. S9. The SynNotch receptor is expressed at low levels in SNCB+4 ESCs.

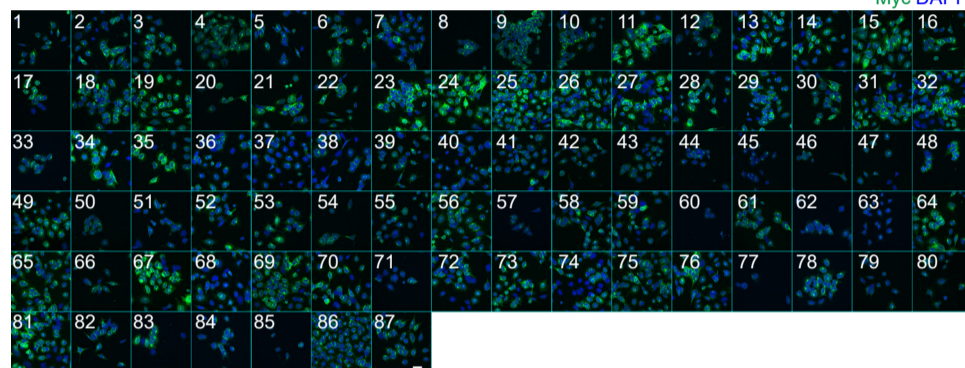
Immunofluorescence of wild-type, SNCB+4 and CHmGMP19 cells. Colour lookup tables for NPC and Myc are displayed on the right of the images. Scale bar: 30 μ m.

FIGURE S10

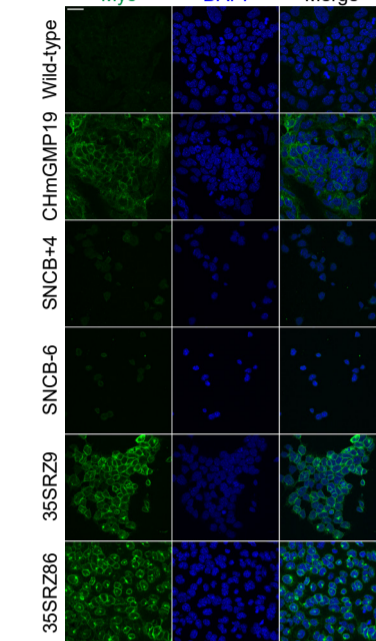
A 35SRZ landing pad cells



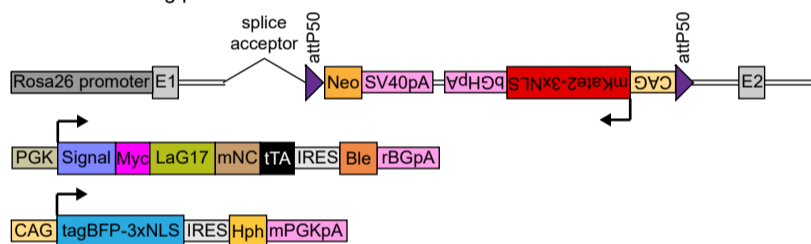
B 35SRZ screen



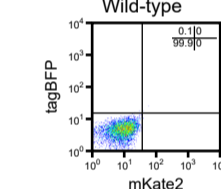
C



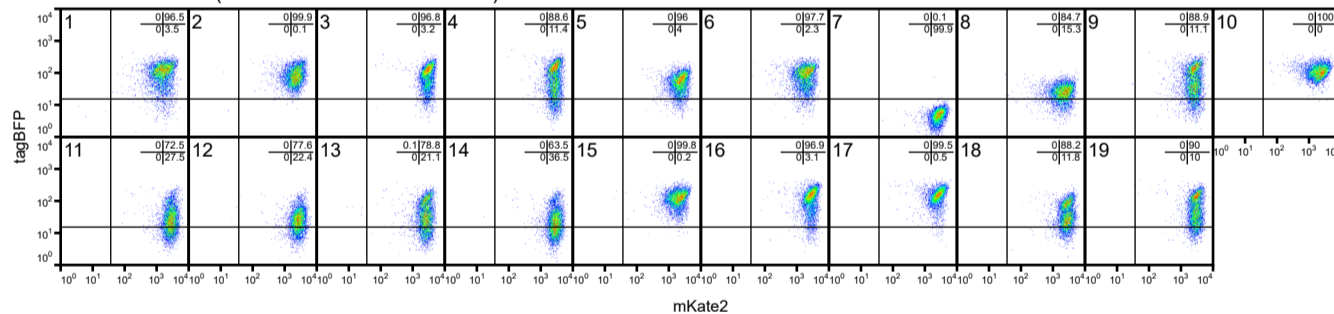
D PSNB landing pad cells



E



F PSNB-A screen (clones derived from 35SRZ9)



G PSNB-B screen (clones derived from 35SRZ86)

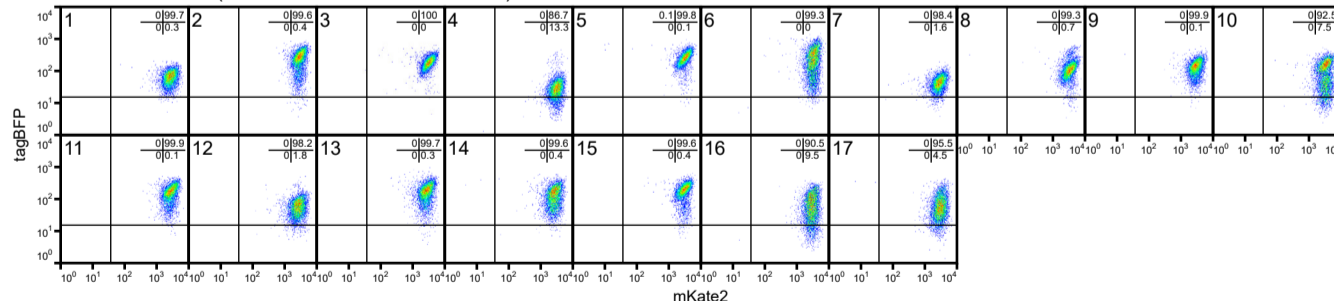


Fig. S10. Generation of 35SRZ and PSNB clonal landing pad ESC lines.

(A) Summary of transgenes stably integrated into the genome of 35SRZ clonal ESC lines. (B) Myc immunofluorescence in 87 35SRZ clonal ESC lines. Nuclei are counterstained with DAPI. Scale bar: 30µm. (C) Myc immunofluorescence in wild-type, CHmGMP19 sender cells, SNCB+4, SNCB-6 receiver cells, 35SRZ clones 9 and 86 landing pad cells. The images for 35SRZ clones 9 and 86 are magnified versions of those in panel (B). (D) Summary of transgenes stably integrated into the genome of PSNB clonal ESC lines. (E) tagBFP and mKate2 fluorescence distribution in wild-type ESCs. (F) tagBFP and mKate2 fluorescence distribution in 19 PSNB-A clonal ESC lines. These lines were derived from 35SRZ clone 9 ESCs. (G) tagBFP and mKate2 fluorescence distribution in 17 PSNB-B clonal ESC lines. These lines were derived from 35SRZ clone 86 ESCs. Percentages of cells in each quadrant are indicated in figure. 6500 cells are displayed in flow cytometry plots. All units of measurement are arbitrary fluorescence units (A.F.U.). n=1.

FIGURE S11

A SynNotch reporter transgenes

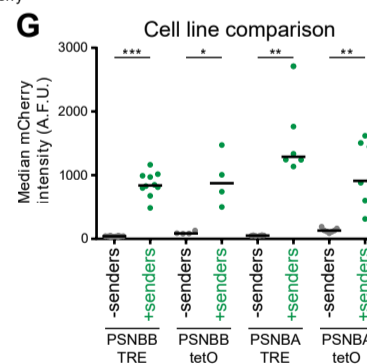
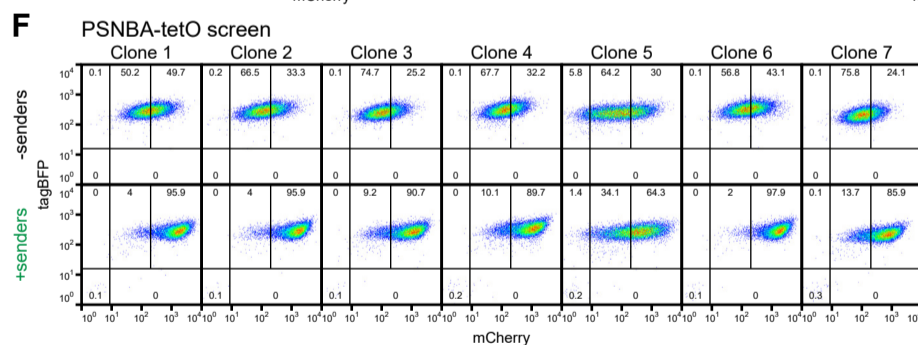
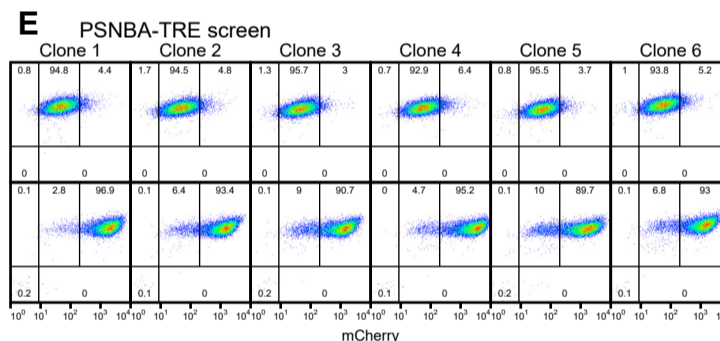
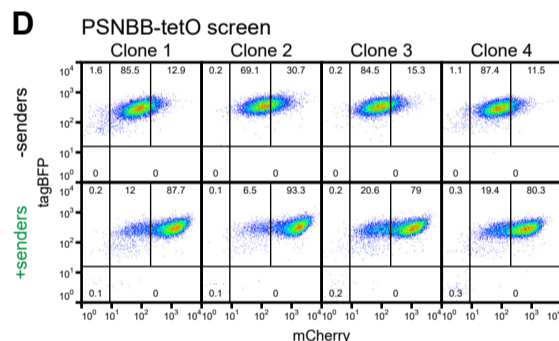
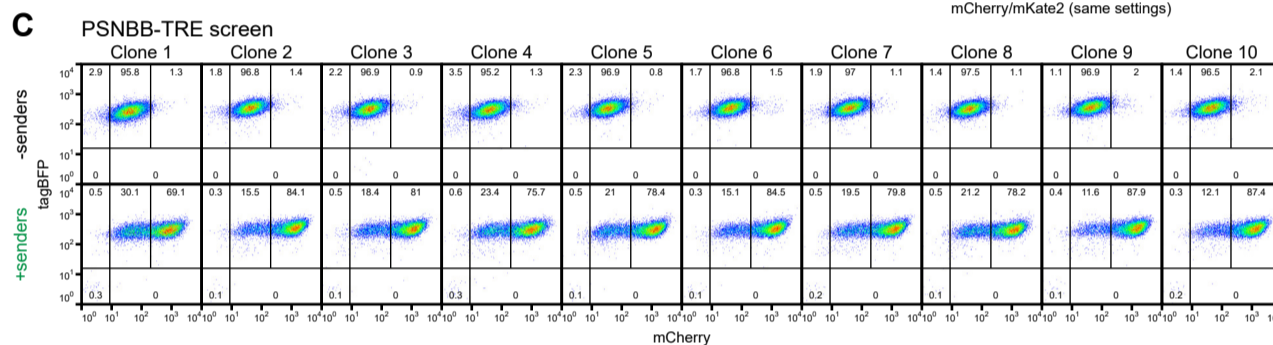
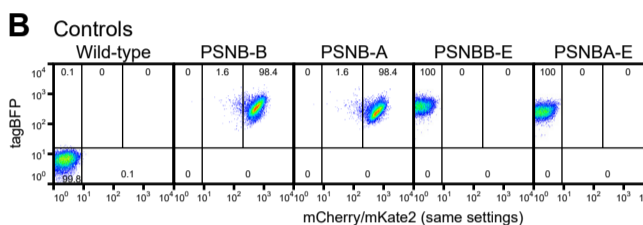
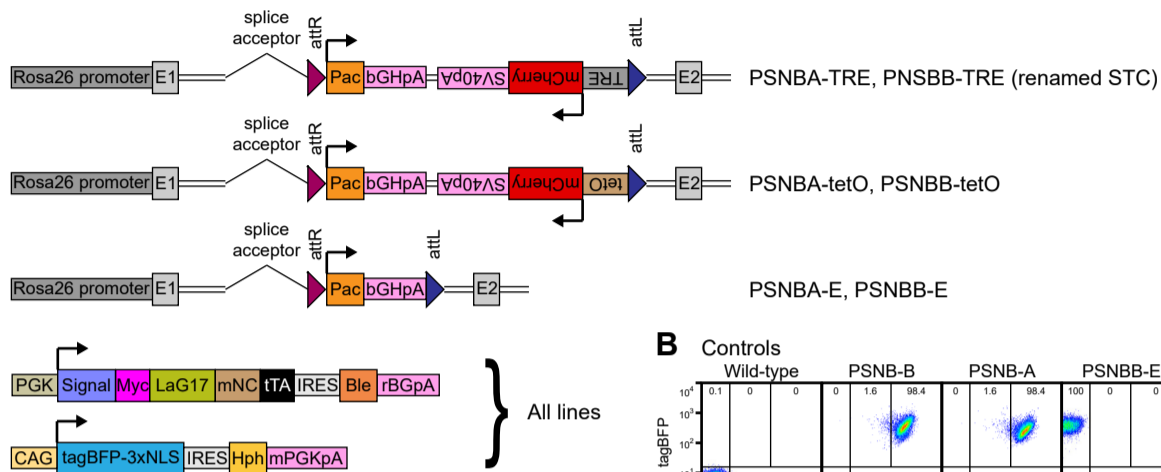
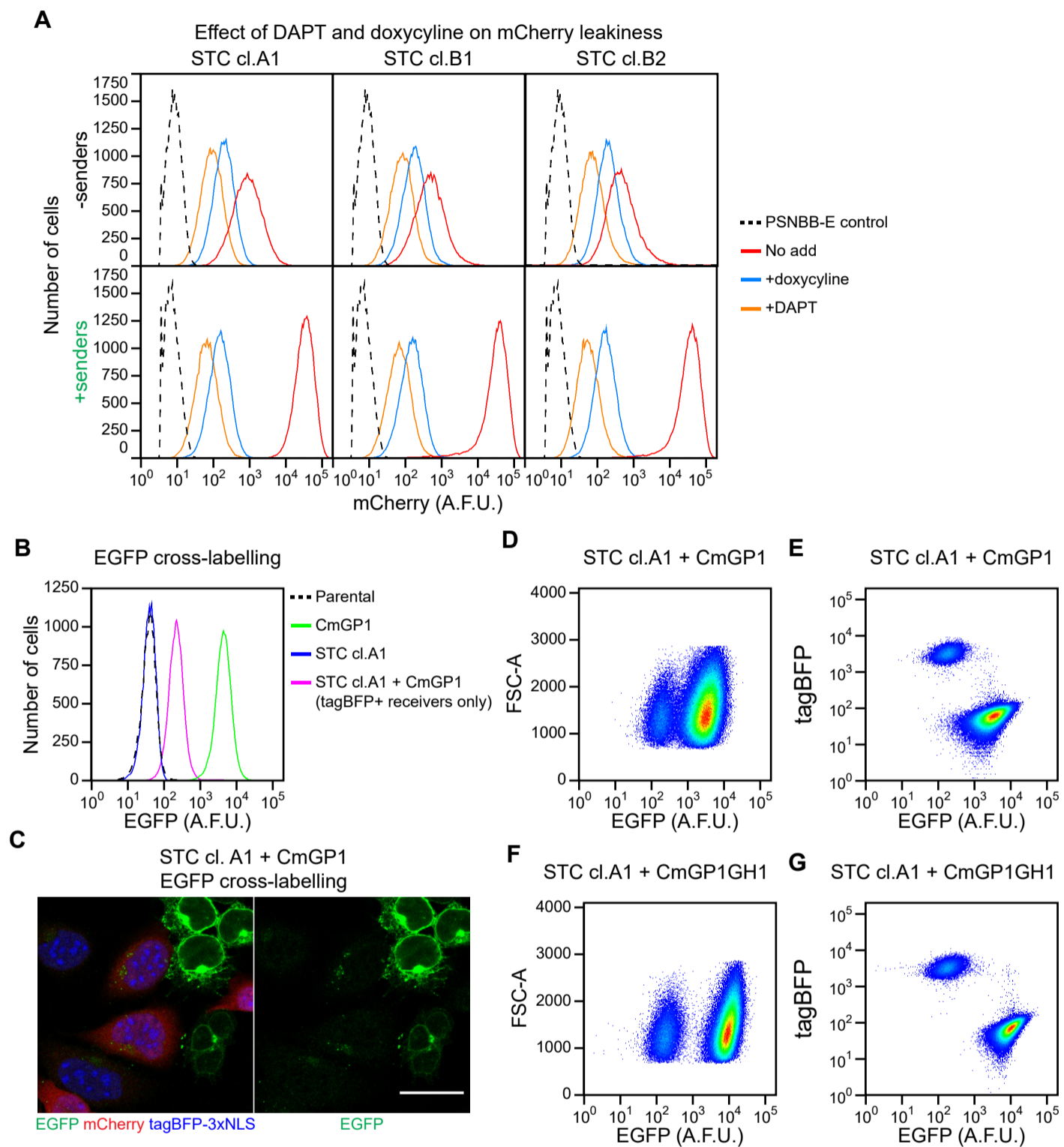


Fig. S11. Generation and screening of PSNB-TRE (STC), PSNB-tetO and PSNB-E clonal receiver ESC lines.

(A) Summary of transgenes stably integrated into the genome of PSNB-TRE (STC), PSNB-tetO and PSNB-E clonal ESC lines. (B) tagBFP and mCherry/mKate2 fluorescence distribution in wild-type, PSNB and PSNB-E ESCs. (C-F) tagBFP and mCherry fluorescence distribution in (C) PSNBB-TRE, (D) PSNBB-tetO, (E) PSNBA-TRE and (F) PSNBA-tetO clonal ESC lines cultured alone or in the presence of CHmGMP19 sender cells for 24 hours. Percentages of cells in each quadrant are indicated in figure. 15000 cells are displayed in flow cytometry plots. All units of measurement are arbitrary fluorescence units (A.F.U.). n=1. (G) Comparison of median mCherry levels in PSNBB-TRE, PSNBB-tetO, PSNBA-TRE and PSNB-tetO cell lines. Each dot represents a different clone. Horizontal bar: median. Paired t-test p-values: *<0.05, **<0.01, ***<0.001.

FIGURE S12

**Fig. S12. Characterisation of STC receiver cells.**

(A) Flow cytometry analysis of mCherry expression in tagBFP+ EGFP- STC receiver clones A1, B1 and B2 cultured alone or in the presence of CmGP1 sender cells at a 9:1 sender:receiver ratio for 48 hours. Cells were cultured in the presence of 100 μ M DAPT, 1 μ g/ml doxycycline, or in the absence of both as indicated. PSNBB-E cells are included as a negative control. 40000 cells were analysed for each sample. (B) Flow cytometry analysis of EGFP expression in wild-type cells, CmGP1 sender cells, STC cl.A1 receiver cells cultured alone, and tagBFP+ STC cl.A1 receiver cells co-cultured with CmGP1 sender cells for 48 hours. 25000 cells were analysed for each sample. (C) Immunofluorescence analysis showing punctuate EGFP staining within STC cl.A1 receiver cells co-cultured with CmGP1 sender cells for 24h hours. Scale bar 20 μ m. (D-G) Flow cytometry analysis of STC clone A1 receiver cells co-cultured with (D,E) CmGP1 or (F,G) CmGP1GH1 sender cells at a 9:1 sender:receiver ratio for 48 hours. 20000 cells were analysed for each sample. A.F.U. = arbitrary fluorescence units. All flow data comes from single experiments, representative of three biological replicates.

FIGURE S13

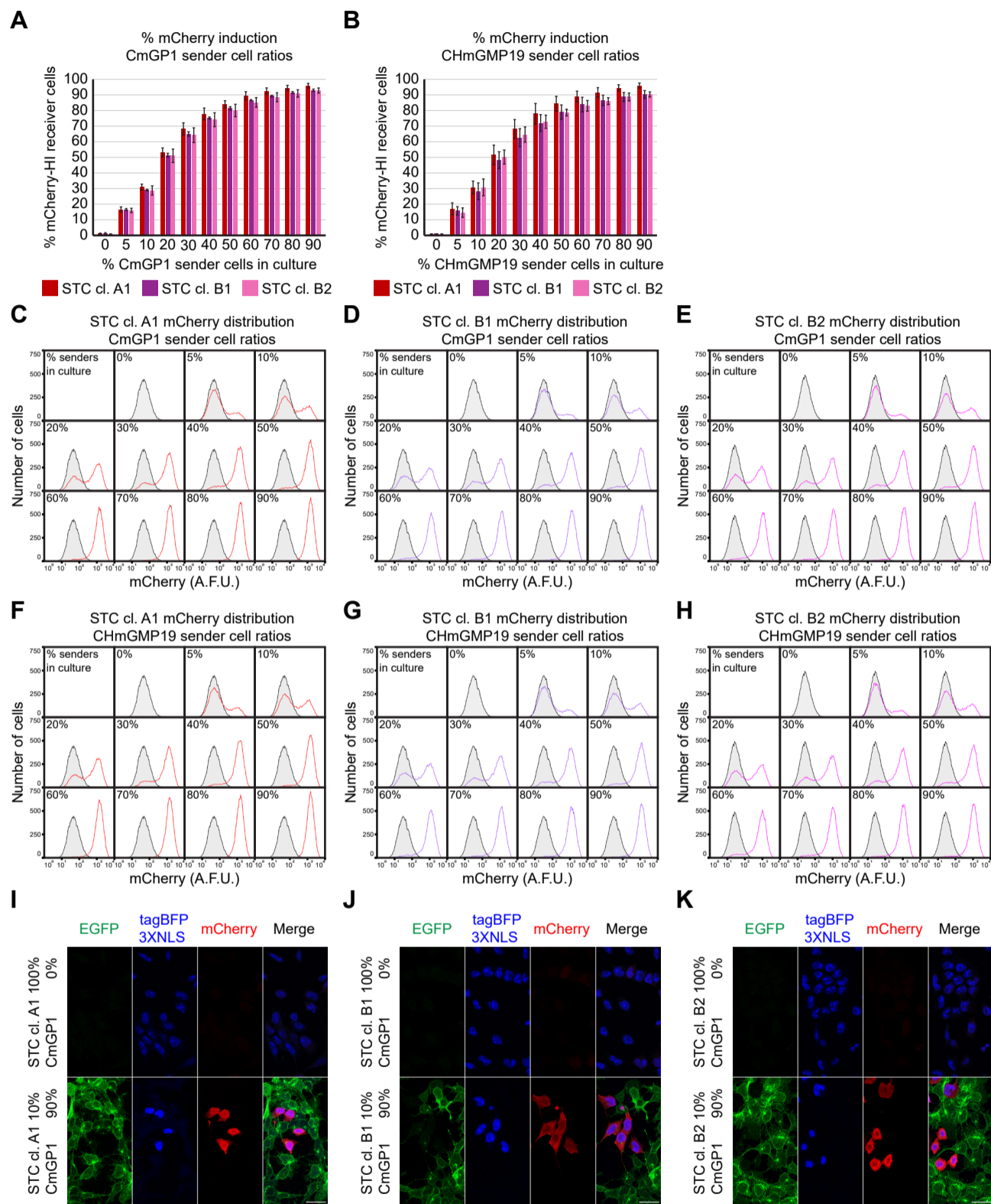


Fig. S13. Effect of varying sender:receiver cell ratios on mCherry induction in STC receiver cells.

(A-B) Percentage of mCherry-HI STC receiver cells following 24 hours of co-culture with (A) CmGP1 or (B) CHmGMP19 sender cells at varying sender:receiver cell ratios. Data presented as mean \pm standard deviation of three independent experiments. A minimum of 16000 cells were analysed for each sample. (C-H) Distribution of mCherry fluorescence in (C,F) STC clone A1, (D,G) STC clone B1 and (E,H) STC clone B2 receiver cells following 24 hours of co-culture with (C-E) CmGP1 or (F-H) CHmGMP19 sender cells at varying sender:receiver cell ratios. Data from a single experiment, representative of three biological replicates. STC clone A1, B1 and B2 cells cultured alone ("0%") are displayed as a shaded black histogram in all panels in (C-H). 23000 cells were analysed for each sample. A.F.U.: arbitrary fluorescence units. (I-K) Immunofluorescence of (I) STC clone A1, (J) STC clone B1 and (K) STC clone B2 receiver cells cultured alone or in the presence of CmGP1 sender cells (9:1 sender:receiver cell ratio). Scale bar: 30 μ m.

FIGURE S14

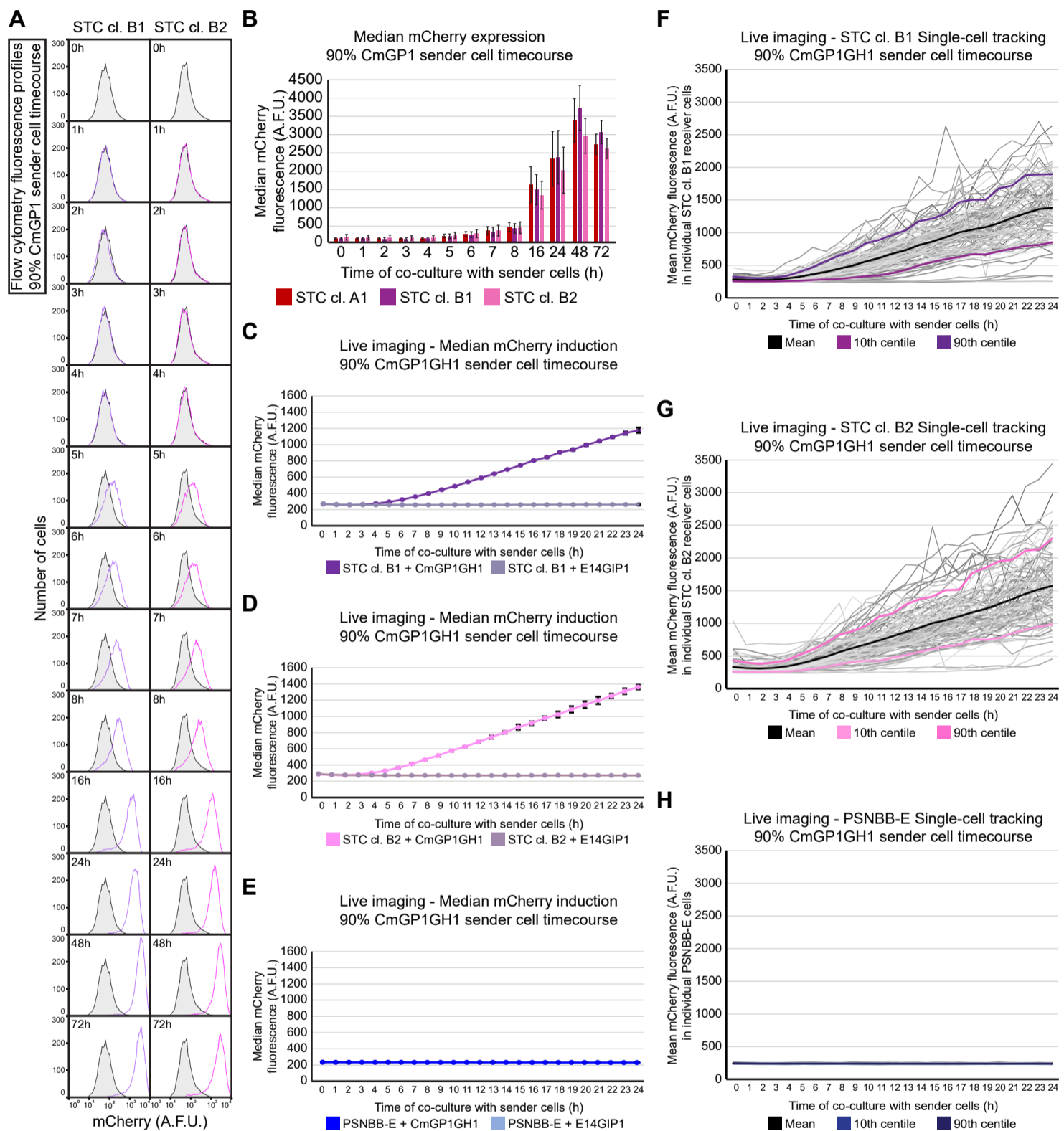
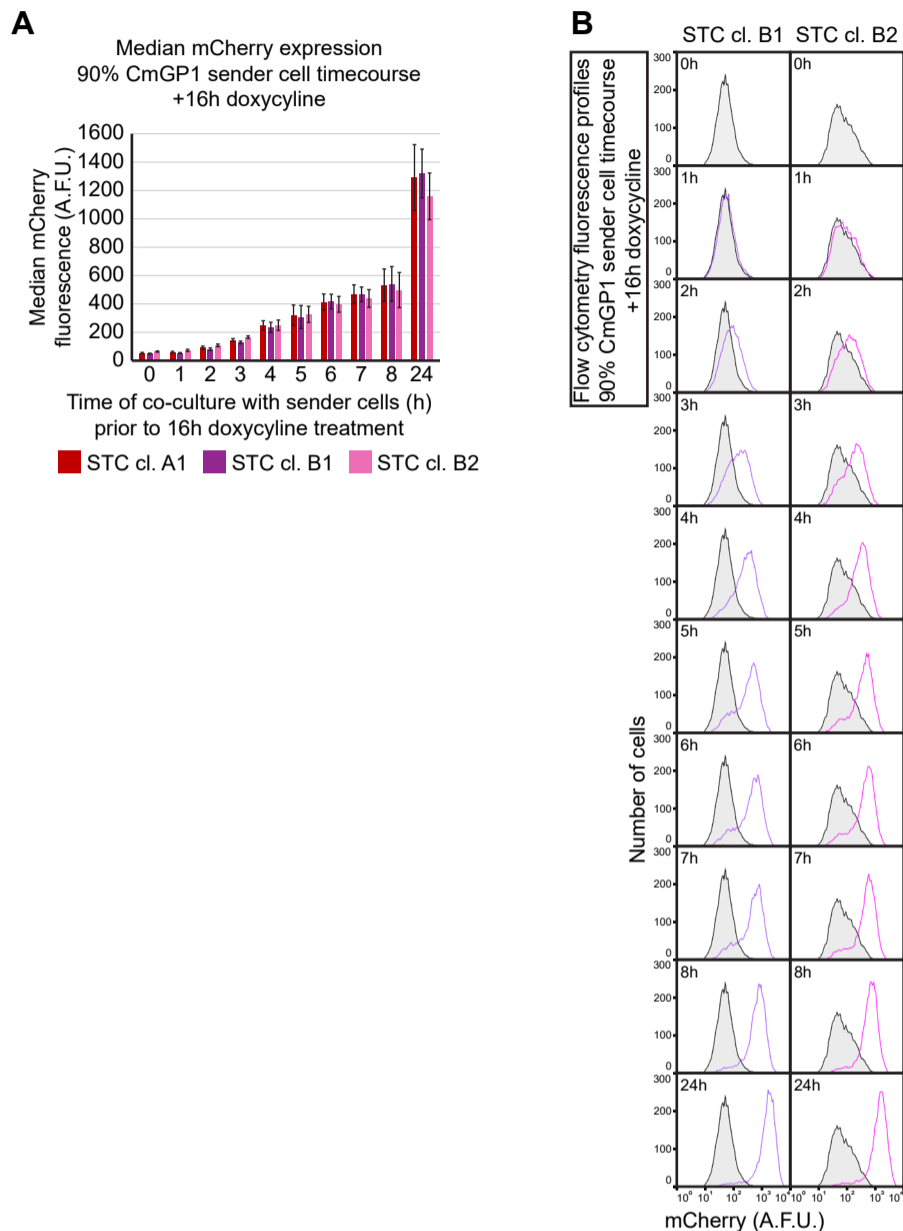


Fig. S14. Kinetics of mCherry induction in STC clones B1 and B2.

(A) Flow cytometry analysis of distribution of mCherry fluorescence in STC clones B1 and B2 following co-culture with CmGP1 sender cells for the indicated amount of time (9:1 sender:receiver cell ratio). Data from a single experiment, representative of three biological replicates. Receiver cells cultured alone ("0h") are displayed as a shaded black histogram in all panels. 10000 cells were analysed for each sample. (B) Flow cytometry analysis of median mCherry expression in STC receiver cells following co-culture with CmGP1 sender cells for the indicated amount of time (9:1 sender:receiver cell ratio). Data presented as mean \pm standard deviation of three independent experiments. A minimum of 8000 cells were analysed for each sample. (C-E) Quantification of live imaging: median mCherry fluorescence intensity in (C) STC clone B1 receiver cells, (D) STC clone B2 receiver cells, (E) PSNBB-E control cells following co-culture with CmGP1GH1 or E14GIP1 cells for the indicated amount of time (9:1 sender:receiver cell ratio). Average of 3 biological replicates, 10 fields of view/replicate, minimum of 446 cells/replicate/timepoint. Error bars: standard deviation. (F-H) Mean mCherry fluorescence intensity in individual (F) STC clone B1, (G) STC clone B2, (H) PSNBB-E cells tracked for 24 hours whilst in co-culture with CmGP1GH1 sender cells (9:1 sender:receiver ratio). Tracks are displayed for 33 cells for each of 3 biological replicates (99 cells total). Mean, 10th, and 90th centile tracks are also displayed. A.F.U.: arbitrary fluorescence units. All data in this figure were acquired at the same time as those in Figure 4, and are therefore directly comparable.

FIGURE S15**Fig. S15. Characterisation of minimal contact time required for mCherry induction in STC clones B1 and B2.**

(A) Median mCherry expression in STC receiver cells following co-culture with CmGP1 sender cells for the indicated amount of time and 16 hours doxycycline treatment (9:1 sender:receiver cell ratio). Data presented as mean \pm standard deviation of three independent experiments. A minimum of 8000 cells were analysed for each sample. (B) Distribution of mCherry fluorescence in STC clones B1 and B2 following co-culture with CmGP1 sender cells for the indicated amount of time and 16 hours doxycycline treatment (9:1 sender:receiver cell ratio). Data from a single experiment, representative of three biological replicates. STC clone B1 and B2 cells plated with CmGP1 sender cells in doxycycline-containing medium for 16 hours (“0h”) are displayed as shaded black histograms in all panels. 10000 cells were analysed for each sample. A.F.U.: arbitrary fluorescence units. All data in this figure were acquired at the same time as those in Figure 5, and are therefore directly comparable.

FIGURE S16

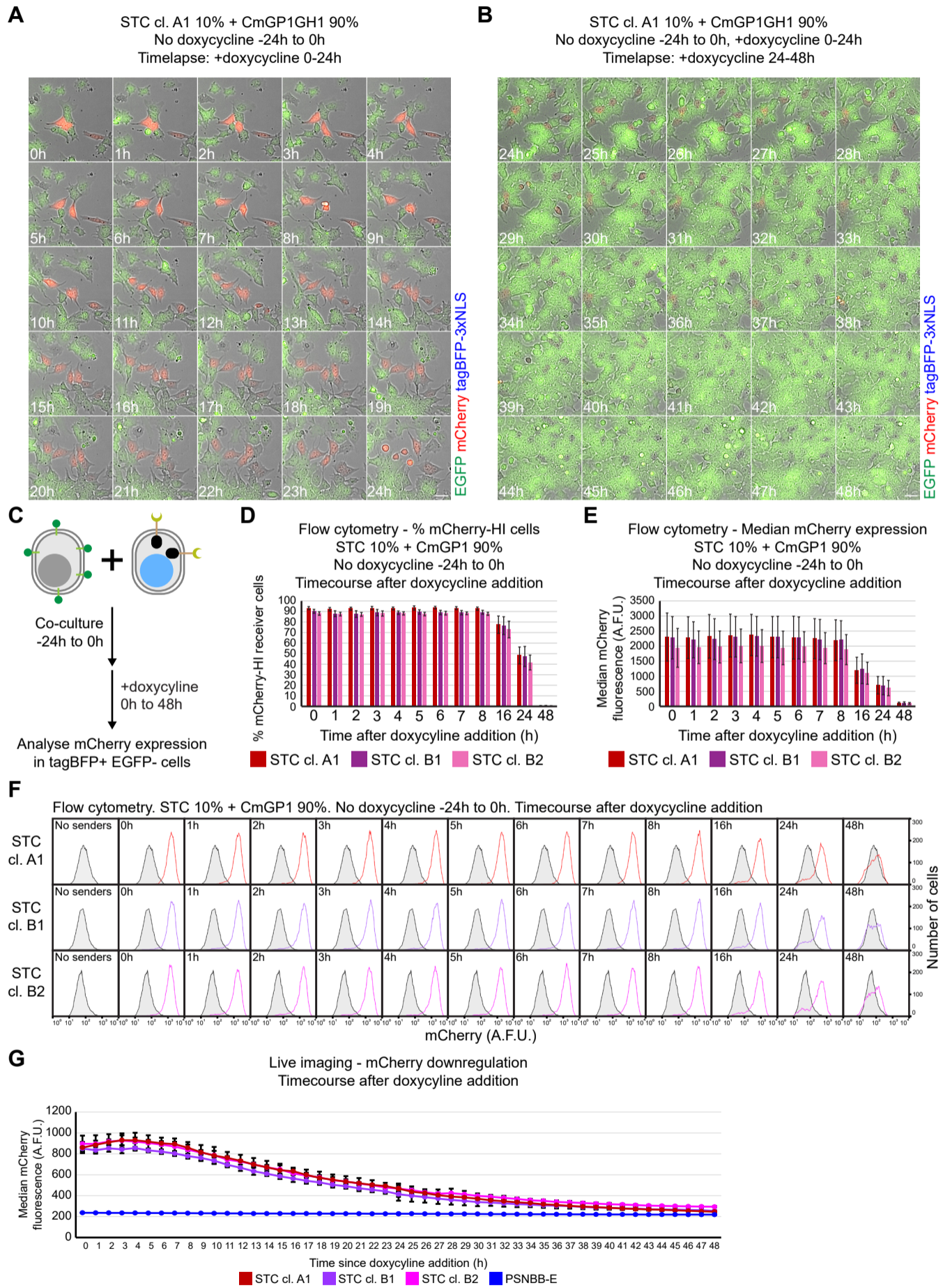
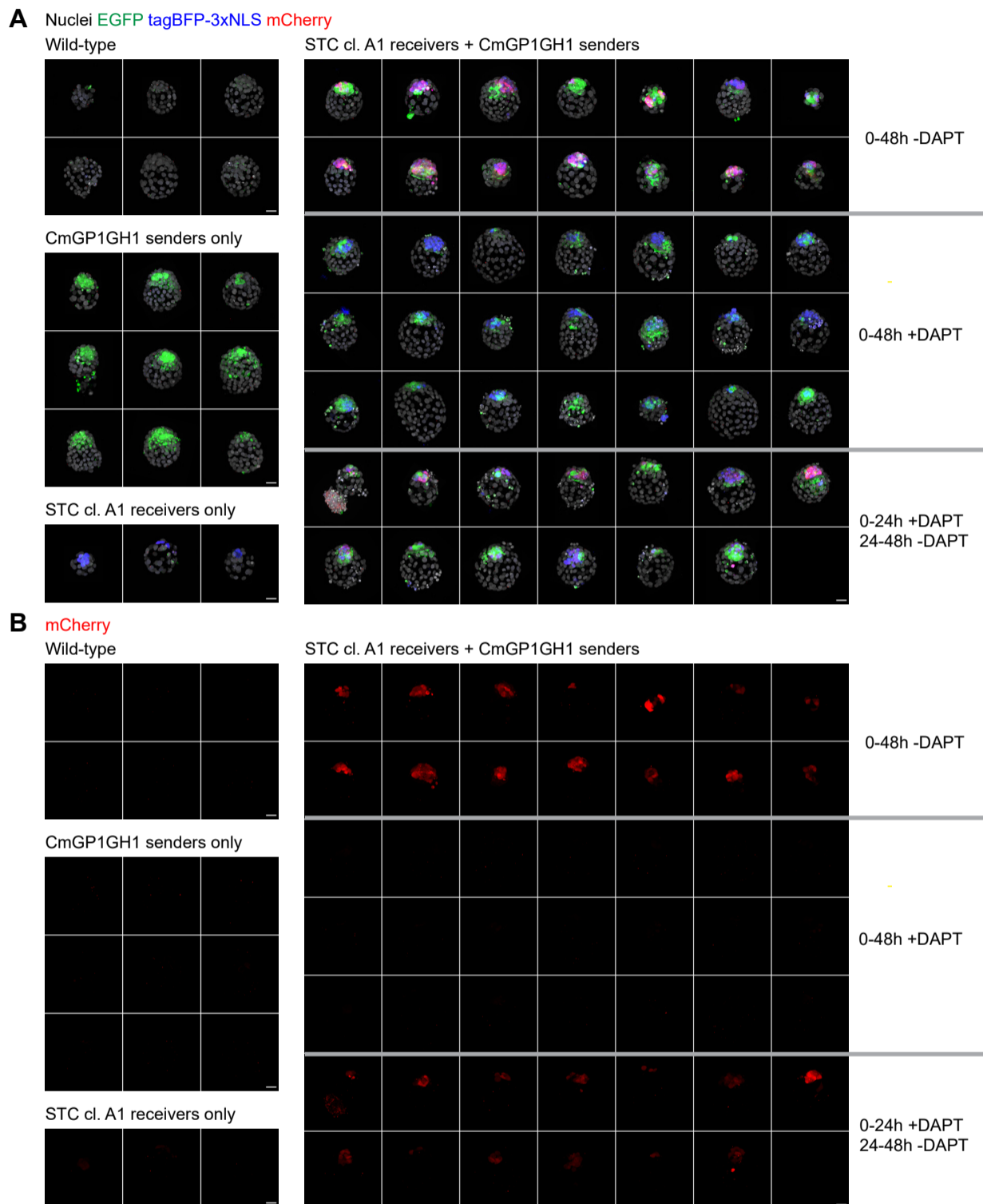


Fig. S16. Kinetics of mCherry downregulation in STC receiver cells.

(A-B) Stills from Movies 4 and 5 displaying mCherry and EGFP expression in STC clone A1 receiver cells co-cultured with CmGP1GH1 sender cells for 24 hours (9:1 sender:receiver cell ratio), prior to treatment with 1µg/ml doxycycline. Filming was carried out between (A) 0 and 24 hours after doxycycline addition or (B) 24 and 48 hours after doxycycline addition. Scale bar: 30µm. (C) Experimental setup to analyse kinetics of mCherry downregulation in STC receiver cells by flow cytometry. Following sender:receiver cell co-culture for 24 hours, 1µg/ml doxycycline was added to the culture medium for 0-48 hours in order to inhibit tTA-mediated *mCherry* transcription, after which cells were analysed by flow cytometry. (D) Percentage of mCherry-HI STC receiver cells and (E) median mCherry expression in STC receiver cells following 24 hours co-culture with CmGP1 sender cells (9:1 sender:receiver cell ratio), and doxycycline treatment for the indicated amount of time. Data presented as mean ± standard deviation of three independent experiments. A minimum of 7500 cells were analysed for each sample. (F) Distribution of mCherry fluorescence in STC receiver cells following co-culture with CmGP1 sender cells for 24 hours (9:1 sender:receiver cell ratio) and doxycycline treatment for the indicated amount of time. Data from a single experiment, representative of three biological replicates. STC clone A1, B1 and B2 cells cultured alone (“No senders”) are displayed as shaded black histograms in all panels. 9000 cells were analysed for each sample. (G) Quantification of live imaging: median mCherry fluorescence intensity in STC clone A1, B1, B2 receiver cells and PSNBB-E control cells following 24 hours of co-culture with CmGP1GH1 (9:1 sender:receiver ratio) prior to treatment with 1µg/ml doxycycline. mCherry intensity was calculated at hourly timepoints. Movies for 0-24h and 24-48h periods were acquired separately; in order to display data on the same graph, the 24-48h data were scaled linearly, so that the 24 hour timepoint would match the 24 hour timepoint in the 0-24h movie. Scaling was performed independently for each of the four cell lines presented. Average of 3 biological replicates, 10 fields of view/replicate, minimum of 173 cells/replicate/timepoint. Error bars: standard deviation. A.F.U.: arbitrary fluorescence units.

FIGURE S17**Fig. S17. DAPT treatment of chimaeric blastocysts.**

(A) Comparison of expression levels of EGFP, tagBFP-3xNLS and mCherry in wild-type and chimaeric blastocysts containing STC clone A1 and/or CmGP1GH1 sender cells. Following morula aggregation, embryos were either left untreated for 48 hours, treated with 100µM DAPT for 48 hours, or treated with 100µM DAPT for 24 hours, then washed and transferred to DAPT-free culture medium. Nuclei were counterstained with DRAQ7. Scale bar: 30µm. (B) Same embryos as shown in panel (A), displaying the mCherry channel only. Scale bar: 30µm. All images were acquired on a PerkinElmer Opera Phenix Plus.

FIGURE S18

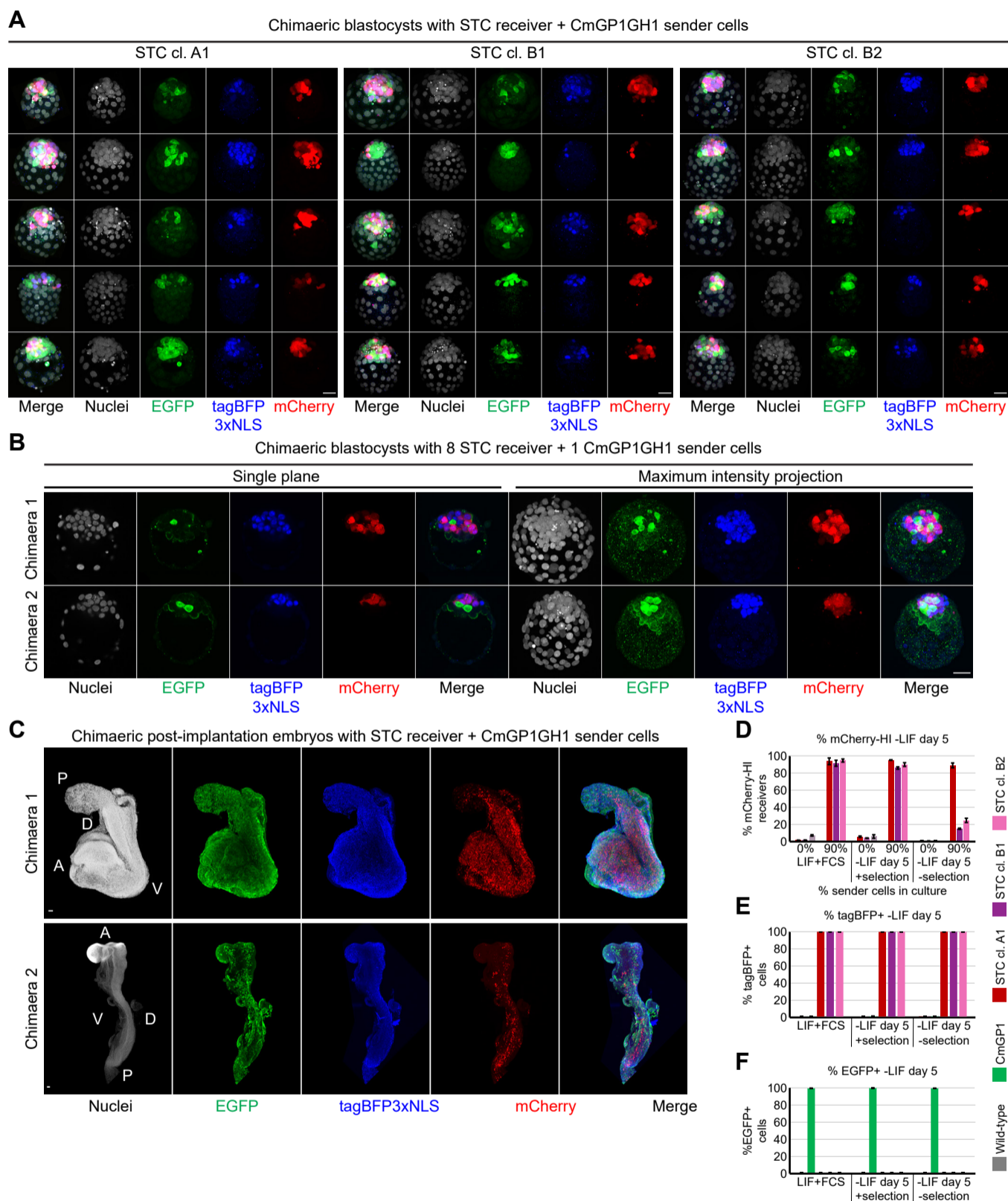
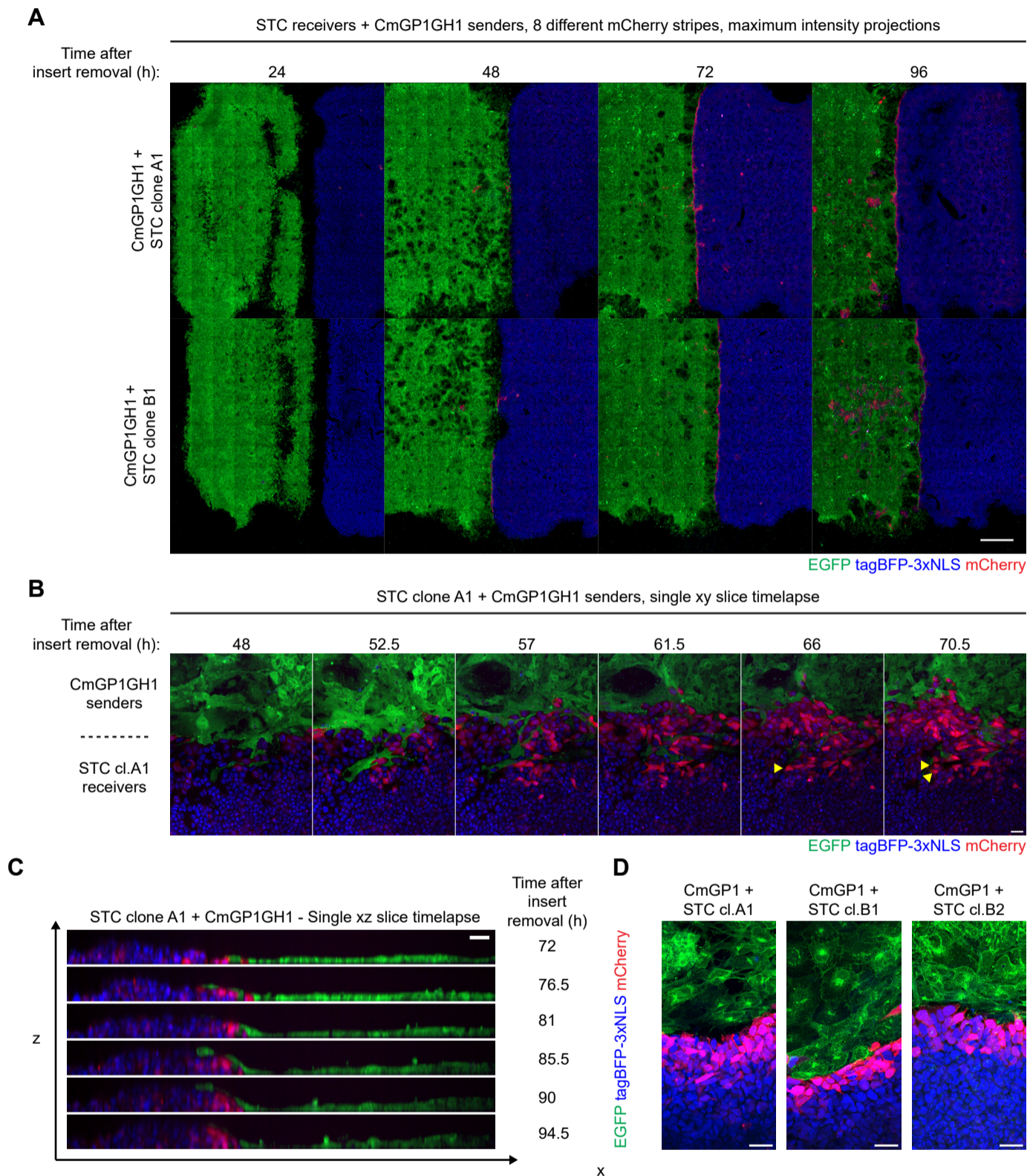


Fig. S18. SyNPL cells contribute to pre-implantation and post-implantation chimaeras.(A) Maximum intensity projections of chimaeric blastocysts containing STC clone A1, B1 or B2 receiver cells and CmGP1GH1 sender cells. Images were taken separately, and fluorescence intensities are not directly comparable. Nuclei were counterstained with DRAQ7. Scale bars: 30 μ m.

(B) Chimaeric blastocysts generated by morula aggregation of 1 CmGP1GH1 and 8 STC clone A1 receiver cells. Nuclei were counterstained with DRAQ7. Scale bars: 30 μ m. (C) Maximum intensity projections of post-implantation chimaeric embryos containing STC clone A1 and CmGP1GH1 sender cells. Images were taken separately, and fluorescence intensities are not directly comparable. Nuclei were counterstained with DAPI (top) or DRAQ7 (bottom). Scale bars: 30 μ m. A: Anterior, P: Posterior, D: Dorsal; V: Ventral. Images in (A) and (C) were acquired on a Leica SP8, images in (B) were acquired on a PerkinElmer Opera Phenix Plus.

(D) Flow cytometry analysis of mCherry expression in STC clone A1, B1 or B2 receiver cells cultured in pluripotency conditions (LIF +FCS) or subject to LIF withdrawal either in the presence or in the absence of selective antibiotics for 4 days. Cells were passaged on day 2 and day 4. On day 4, cells were replated either alone or with CmGP1 sender cells (cultured in the same conditions) for a further 24 hours, before being assayed by flow cytometry. (E-F) Flow cytometry analysis of (E) tagBFP and (F) EGFP expression in wild-type cells, CmGP1 sender cells, and STC clone A1, B1 and B2 receiver cells cultured alone in pluripotency conditions (LIF+FCS) or in LIF withdrawal medium either in the presence or in the absence of selective antibiotics for 5 days. Cells were passaged on day 2 and day 4.

FIGURE S19**Fig. S19. Characterisation of synthetic stripe pattern of mCherry expression.**

(A) Low magnification view of synthetic stripe patterns of mCherry expression, generated by co-culture of STC clones A1 or B1 receiver cells with CmGP1GH1 sender cells. Each image represents a separate stripe. Scale bar: 1mm. (B) Timelapse imaging of border between STC clone A1 receiver and CmGP1GH1 sender cells. Photobleaching led to reduction in signal intensity over time. Single confocal slice at the bottom of the dish. Yellow arrowheads indicate activated receiver cell division in plane perpendicular to sender:receiver border, contributing to stripe diffusion. (C) Timelapse imaging of border between STC clone A1 receiver and CmGP1GH1 sender cells. Photobleaching led to reduction in signal intensity over time. Single xz slice, showing thickness of border region. Sender cells can be seen migrating on top of receiver cells. Scale bar: 30 μ m. All images were acquired on a PerkinElmer Opera Phenix Plus microscope. (D) Immunofluorescence analysis of EGFP, tagBFP-3xNLS and mCherry expression in synthetic stripe patterns generated by co-culture of STC clones A1, B1 or B2 receiver cells with CmGP1 sender cells. Scale bar: 30 μ m. Images represent maximum intensity projections of single confocal slices acquired on a Leica SP8 microscope. Samples were stained and imaged independently, expression levels are therefore not directly comparable.

FIGURE S20

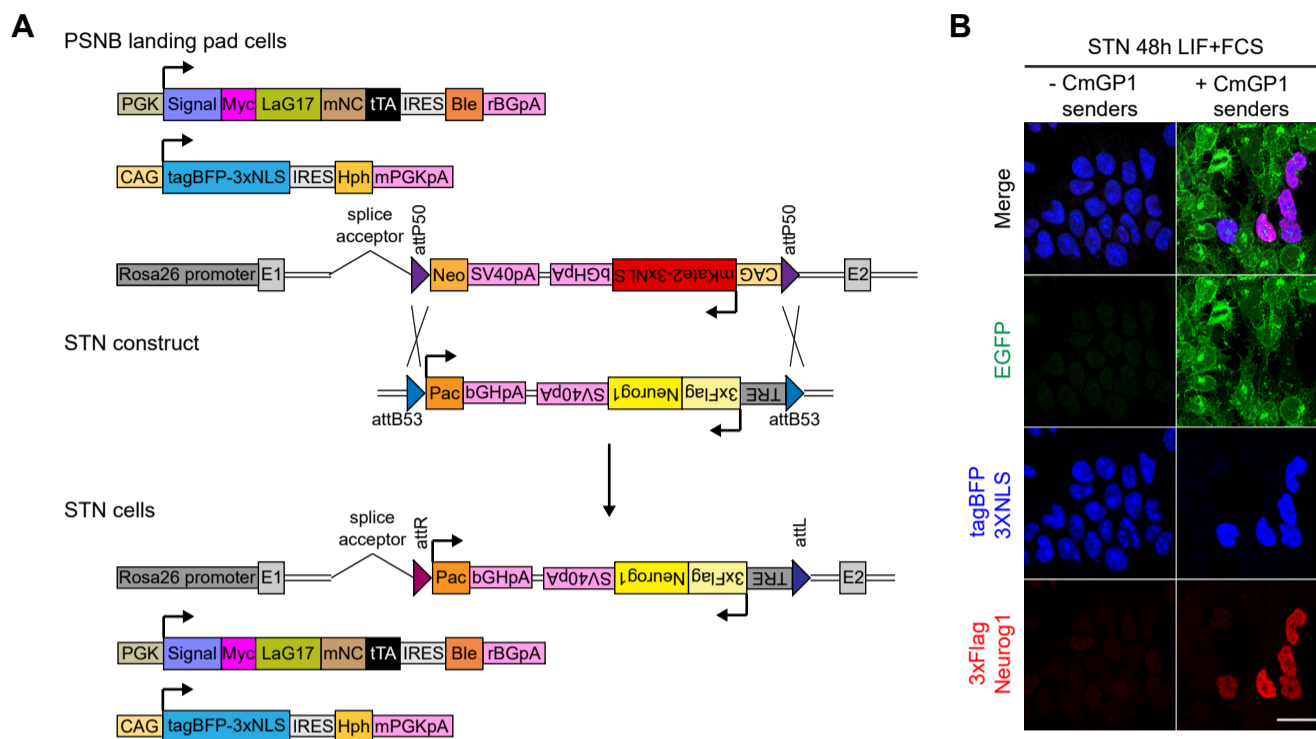


Fig. S20. Generation of Neurogenin1-inducible STN receiver cells.

(A) Strategy to replace Neo-mKate2 cassette with STN cassette in PSNB landing pad ESCs through ϕ C31 integrase-mediated RMCE. (B) EGFP, tagBFP and Flag immunofluorescence of STN receiver ESCs co-cultured for 48 hours with CmGP1 sender ESCs (9:1 sender:receiver cell ratio) in ESC culture medium (“LIF+FCS”). Scale bar: 30 μ m.

FIGURE S21

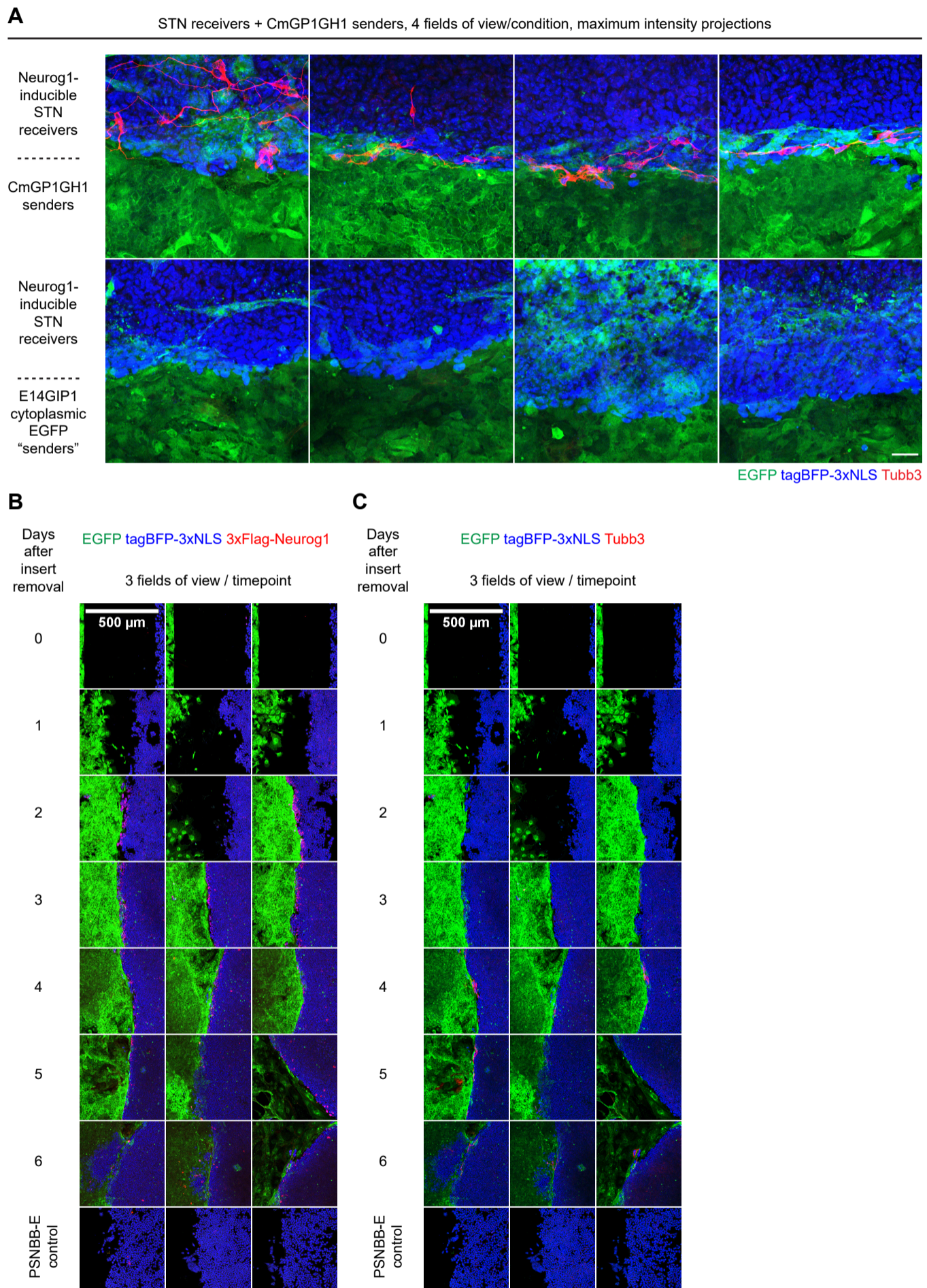
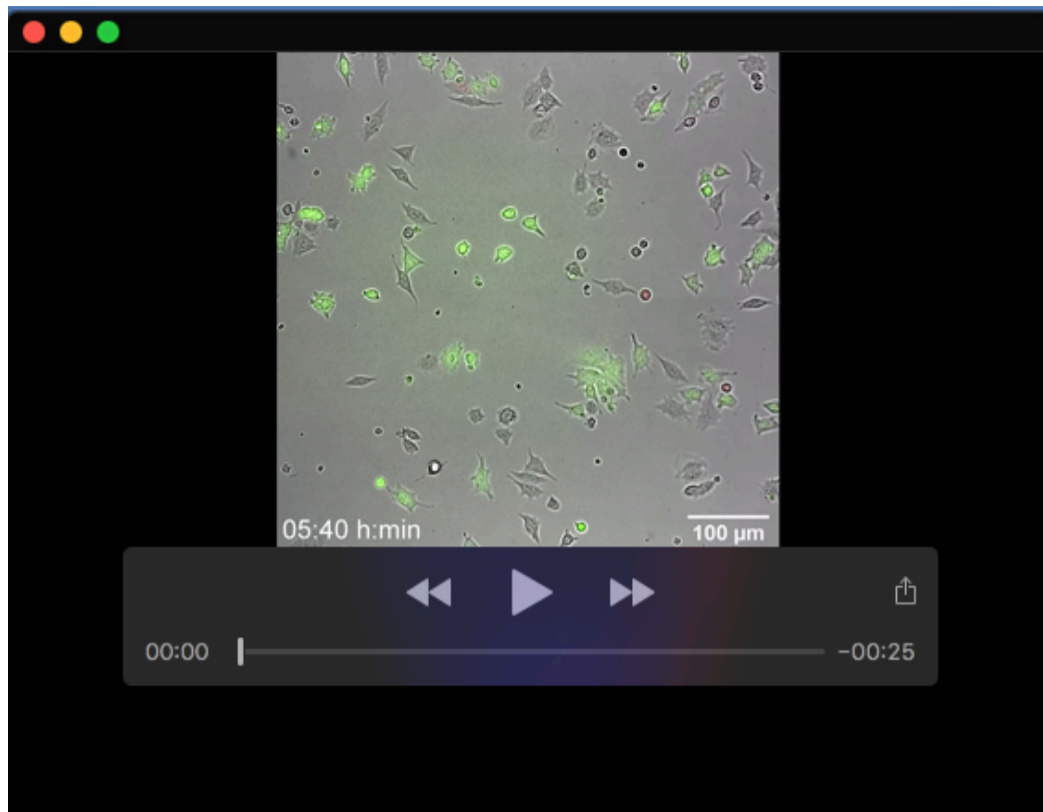
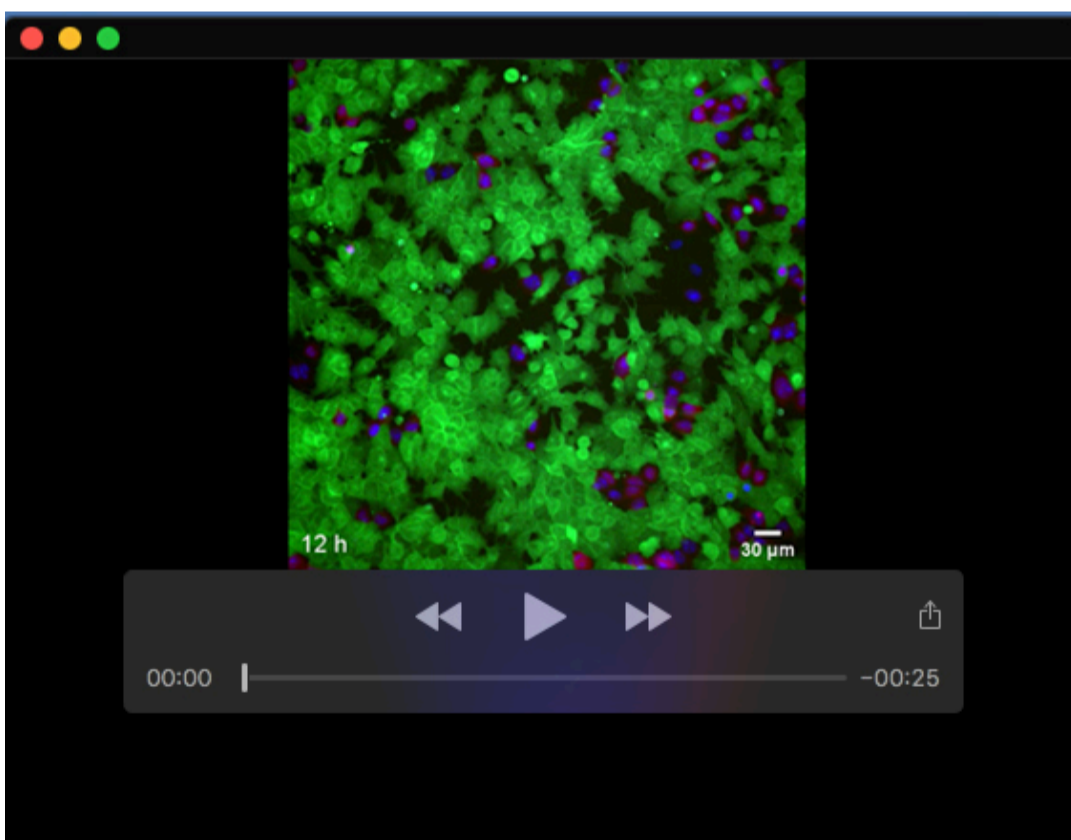


Fig. S21. Characterisation of neuronal differentiation stripe.(A) Immunofluorescence analysis of STN receiver cells co-cultured with either CmGP1GH1 sender cells or with E14GIP1 cytoplasmic EGFP-expressing control cells, illustrating that interaction with extracellular EGFP is required to drive neuronal differentiation in STN receiver cells. 4 fields of view are displayed per condition. Scale bar: 30µm. (B-C) Immunofluorescence analysis of kinetics of (B) 3xFlag-Neurog1 or (C) Tubb3 induction. Maximum intensity projections of 3 fields of view at low magnification are displayed to capture variability. Scale bar: 500µm.



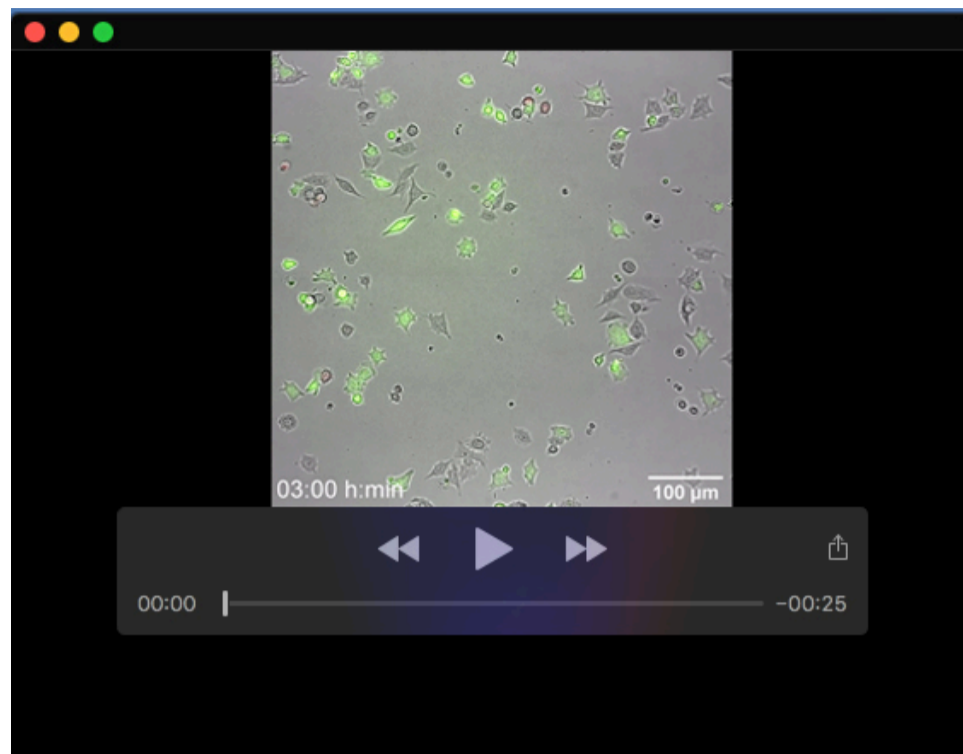
Movie 1. Time-lapse imaging of interactions between STC receiver and CmGP1GH1 sender cells.

Time-lapse imaging of STC clone A1 receiver cells cultured with CmGP1GH1 sender cells at a 1:1 ratio for 24 hours. Brightfield (grey), EGFP (green) and mCherry (red) images taken every 10 minutes over a 24 hour period. Immunofluorescence analysis of tagBFP (blue), EGFP (green) and mCherry (red) expression at the 24 hour timepoint is shown at the end of the movie. All images were acquired using a Nikon Ti-E microscope.



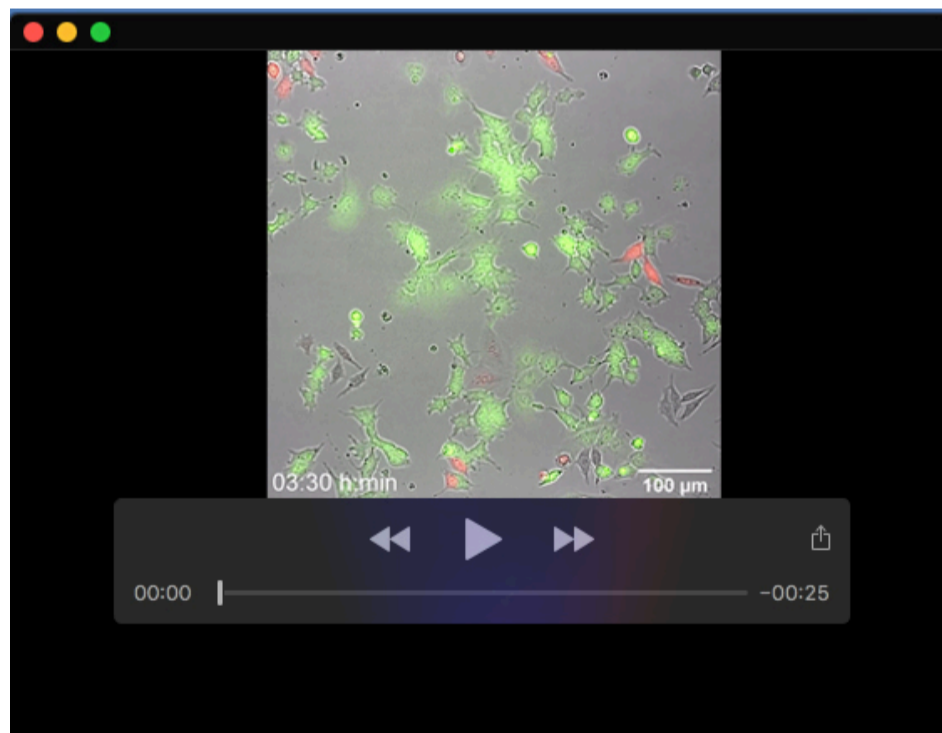
Movie 2. Kinetics of mCherry induction in STC receiver cells.

Time-lapse imaging of STC clone A1 receiver cells cultured with CmGP1GH1 sender cells at a 1:9 ratio at high density for 24 hours. tagBFP-3xNLS (blue), GFP (green) and mCherry (red) images taken every hour over a 24 hour period. Imaging was performed on a PerkinElmer Opera Phenix Plus microscope.



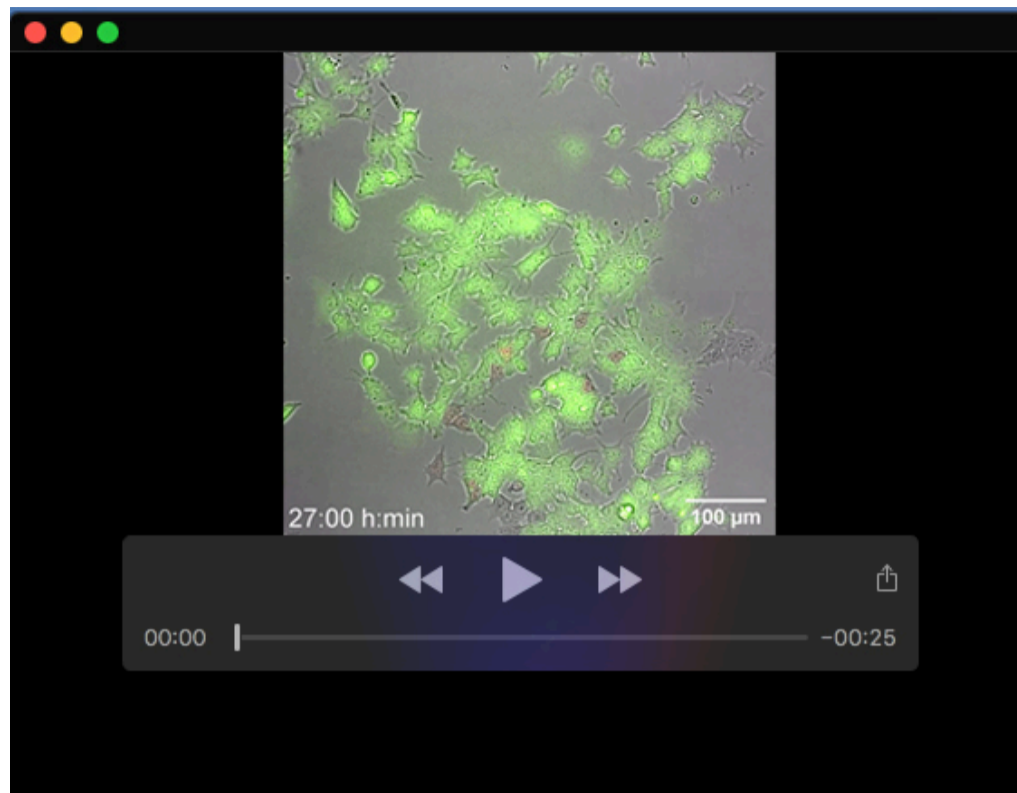
Movie 3. Time-lapse imaging of transient interactions between STC receiver and CmGP1GH1 sender cells.

Time-lapse imaging of STC clone A1 receiver cells cultured with CmGP1GH1 sender cells at a 1:1 ratio for 24 hours. Brightfield (grey), EGFP (green) and mCherry (red) images taken every 10 minutes over a 24 hour period. Immunofluorescence analysis of tagBFP (blue), EGFP (green) and mCherry (red) expression at the 24 hour timepoint is shown at the end of the movie. All images were acquired using a Nikon Ti-E microscope. Movies 1 and 3 display different fields of view from the same experiment.

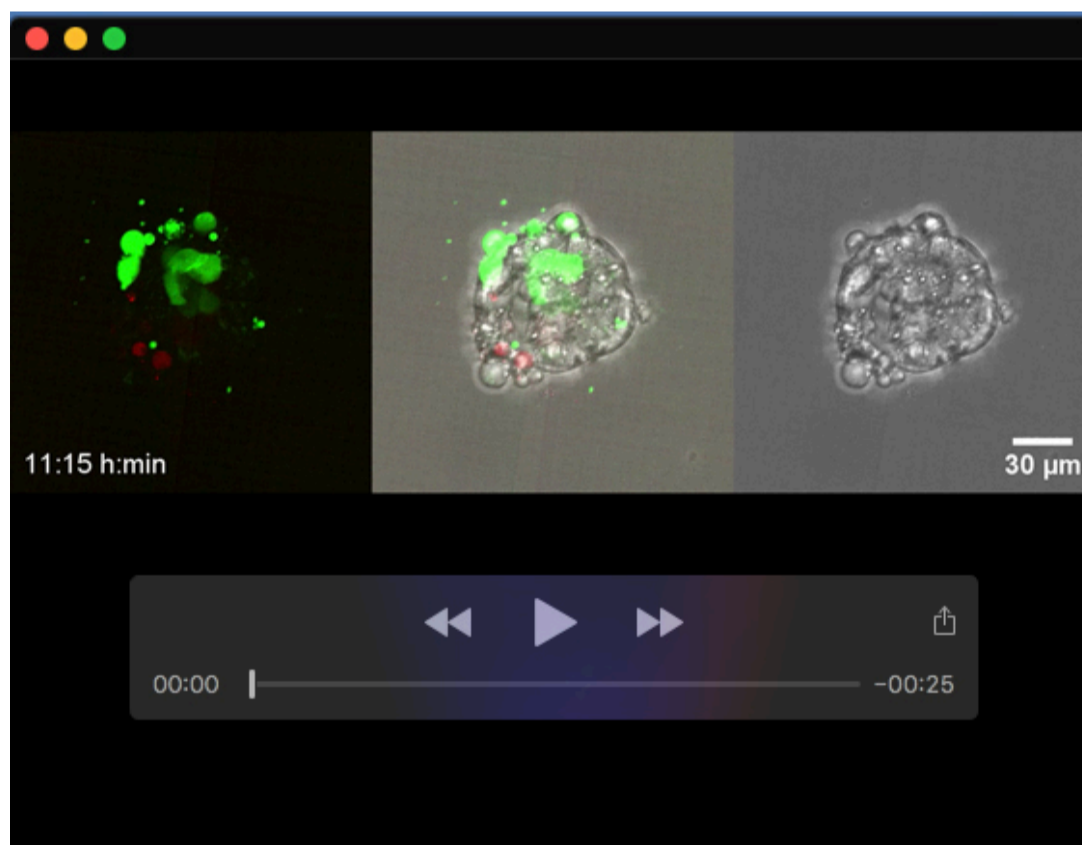


Movie 4. Kinetics of mCherry downregulation in STC receiver cells (0-24h).

Timelapse imaging of STC clone A1 receiver cells cultured with CmGP1GH1 sender cells at a 1:9 ratio for 24 hours, then treated with 1 μg/ml doxycycline (to inhibit mCherry transcription) and imaged for 24 hours. Brightfield (grey), EGFP (green) and mCherry (red) images taken every 10 minutes over a 24 hour period, using a Nikon Ti-E microscope.



Movie 5. Kinetics of mCherry downregulation in STC receiver cells (24-48h). Timelapse imaging of STC clone A1 receiver cells cultured with CmGP1GH1 sender cells at a 1:9 ratio for 24 hours, then treated with 1 μ g/ml doxycycline (to inhibit mCherry transcription) and imaged between 24 and 48 hours following addition of doxycycline. Brightfield (grey), EGFP (green) and mCherry (red) images taken every 10 minutes over a 24 hour period, using a Nikon Ti-E microscope.



Movie 6. Time-lapse imaging of morula to blastocyst transition following morula aggregation of STC receiver and CmGP1GH1 sender cells.

Time-lapse imaging of two wild-type morulae aggregated with STC clone A1 receiver cells and CmGP1GH1 sender cells. Brightfield (grey), EGFP (green) and mCherry (red) images taken every 30 minutes over a 27 hour 15 minute period. tagBFP-3xNLS (blue) was acquired for the first timepoint only, as sustained exposure to ultraviolet light results in death of chimaeric morulae. Filming started approximately 4 hours after morula aggregation.

As Movies 1, 3, 4 and 5 were acquired simultaneously and batch-processed, fluorescence intensities are directly comparable across these movies.